SANDIA REPORT
SAND2005-8032
Unlimited Release
Printed December 2005

Magnetostriction of Field Structured Magnetoelastomers

Dale L. Huber, James E. Martin, Robert A. Anderson, Douglas H. Read, Benjamin L. Frankamp

Prepared by
Sandia National Laboratories
Albuquerque, New Mexico 87185 and Livermore, California 94550

Sandia is a multiprogram laboratory operated by Sandia Corporation, a Lockheed Martin Company, for the United States Department of Energy's National Nuclear Security Administration under Contract DE-AC04-94AL85000.

Issued by Sandia National Laboratories, operated for the United States Department of Energy by Sandia Corporation.

Available to DOE and DOE contractors from
U.S. Department of Energy
Office of Scientific and Technical Information
P.O. Box 62
Oak Ridge, TN 37831

Telephone: (865)576-8401
Facsimile: (865)576-5728
E-Mail: reports@adonis.osti.gov
Online ordering: http://www.osti.gov/bridge

Available to the public from
U.S. Department of Commerce
National Technical Information Service
5285 Port Royal Rd
Springfield, VA 22161

Telephone: (800)553-6847
Facsimile: (703)605-6900
E-Mail: orders@ntis.fedworld.gov
Online order: http://www.ntis.gov/help/ordermethods.asp?loc=7-4-0#online

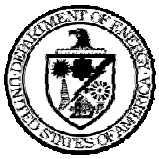

SAND2005-8032
Unlimited Release
December 2005

MAGNETOSTRICTION OF FIELD-STRUCTURED MAGNETOELASTOMERS

Dale L. Huber, James E. Martin, Robert A. Anderson, Douglas H. Read,
Benjamin L. Frankamp
Sandia National Laboratories
Albuquerque, New Mexico 87185, U.S.A.

Gerald L. Gulley[1]
[1]*Dominican University*
River Forest, IL 60305, U.S.A.

ABSTRACT

Field-structured magnetic particle composites are an important new class of materials that have great potential as both sensors and actuators. These materials are synthesized by suspending magnetic particles in a polymeric resin and subjecting these to magnetic fields while the resin polymerizes. If a simple uniaxial magnetic field is used, the particles will form chains, yielding composites whose magnetic susceptibility is enhanced along a single direction. A biaxial magnetic field, comprised of two orthogonal ac fields, forms particle sheets, yielding composites whose magnetic susceptibility is enhanced along two principal directions. A balanced triaxial magnetic field can be used to enhance the susceptibility in all directions, and biased heterodyned triaxial magnetic fields are especially effective for producing composites with a greatly enhanced susceptibility along a single axis. Magnetostriction is quadratic in the susceptibility, so increasing the composite susceptibility is important to developing actuators that function well at modest fields. To investigate magnetostriction in these field-structured composites we have constructed a sensitive, constant-stress apparatus capable of 1 ppm strain resolution. The sample geometry is designed to minimize demagnetizing field effects. With this apparatus we have demonstrated field-structured composites with nearly 10,000 ppm strain.

Executive Summary

The purpose of this project was to determine whether elastomeric composite materials can be synthesized in such a way as to have significant levels of magnetostriction, much greater than that possible with piezoelectric materials. In fact, it is possible, especially if the composites are synthesized in the presence of magnetic fields. At best, we have produced materials that exhibit roughly 100 times the strain of piezo materials.

Magnetostriction – roughly speaking the deformation of a material subjected to a uniform magnetic field - is a property one normally associates with solid magnetic materials, not elastomeric composites. When a field is applied to such a material it contracts along the field so as to increase the interactions between the magnetic spins. If one has such a magnetostrictive material in particulate form, then it is possible to make a soft composite material that will in some measure exhibit magnetostriction due to the magnetostriction of the constituent particles. This is not our approach, but such composites have been reported and have been found to have modest magnetostriction.

The composites we synthesize and study are made with Fe and Ni particles, materials which themselves exhibit negligible magnetostrictive strain. In the presence of a magnetic field these particles do acquire a magnetic moment, however, and it is the dipolar interactions between these magnetic moments that gives rise to magnetostriction of the composite itself. The interactions between dipoles is strongly dependent on the organization of the particles within the composite. We can create a variety of distinct composite structures by manipulating the particles with complex, dynamic magnetic fields before the elastomeric resin has fully polymerized, so a significant part of this project was spent on determining the structuring field that leads to optimal magnetostrictive composites.

A variety of interesting discoveries were made using an optical cantilever apparatus we designed to measure the contraction of prestrained magnetoelastomers in a highly uniform magnetic field produced by a Helmholtz coil. First, we discovered that the magnetostrictive strain increased linearly with the sample prestrain, regardless of the composite structure. Second, by controlling the composite structure we discovered we

could produce magnetoelastomers with ten times the contraction of random composites. Contractions of 10,000 ppm were observed in the best field-structured materials, compared to 100 ppm for piezoelectrics. The dependence of magnetostriction with composite structure was found to be in agreement with theoretical predictions we had made before this project. Third, through analysis and simulation we showed that these composites are subject to a hierarchy of structural phase transitions that occur as the magnetic field is increased. Detailed calculations show that these particle clumping transitions affect the magnetostriction, and even give rise to hysteresis of the sample strain. Finally, we discovered that the magnetostriction of these materials can lead to enormous magnetoresistance, far larger than ever observed on other materials. Our current record is a resistance change of $5x10^6$ % at a field of 0.1 T, an effect for which a patent is now being pursued.

This research has shown that these field-structured magnetoelastomers are viable as actuators and highly responsive magnetoresistive materials. The extreme magnetoresistance we have observed has already been demonstrated to have impact on chemical resistors we have developed in our lab: The response of these chemical sensors can be varied by a factor of 120,000 by applying a field of 0.1 T. These materials are ready for device development, so connections are now being sought with the robotics effort at Sandia. It would be an interesting next step to engineer a complete actuator component based on this effect.

[Intentionally Left Blank]

Table of Contents

FIGURES

Chapter 1

Martin, Anderson

THEORY AND SIMULATIONS

Introduction

There is a need for soft actuators that have a much larger strain response than piezoelectrics, and that can respond in microseconds. To meet these needs we are developing efficient Field-Structured Magnetostrictive Elastomers (FSMEs). [1-4] These are materials whose magnetic permeability is sensitive to tensile or compressive strains, as discussed below. Extant experimental studies of such materials have focused on the increase in the shear modulus due to the magnetic field. But these materials also contract in a magnetic field, and thus have the potential for many tensile actuator applications, for example as artificial muscles for robots. We wish to explore these materials as tensile actuators, in controlled stress experiments. The inverse magnetostriction effect is also useful, enabling stress/strain sensors based on permeability (or permittivity) changes. Related applications include magnetic- or electric-field-tunable capacitors for *RF* applications.

Magnetostriction refers to the tendency of magnetic materials to deform in a uniform magnetic field. In fact, there are two primary causes of deformation. First, a material will tend to elongate along the field to increase the penetration of the applied field into the body. The penetration of the applied field is opposed by the so-called demagnetizing field, [5] which is strongly dependent on the shape of the object, and decreases as the object elongates. Second, a material will tend to compress along the field to create a large microscopic, or local, field at each dipole site. This latter effect is magnetostriction. In our experiments the shape effect can usually be made negligible, so to a good approximation the *macroscopic* field in the elastomer *is* the applied field. [6]

To understand magnetostriction in composite materials, consider as an example a simple cubic lattice of *induced* magnetic dipoles subjected to an applied field that causes the dipoles to magnetize. Each dipole creates a small field of its own that is felt by all the other dipoles. The net effect is that the other dipoles enhance the "local" field at a dipole

site significantly - easily several times the applied field, which seems like cheating. [7] This enhancement is proportionately reflected in the magnetic susceptibility of the material. The net magnetic energy associated with an induced dipole goes down as the local field goes up, so any lattice distortion that would increase the local field creates a magnetostrictive stress. An elastic lattice with zero volume compressibility (Poisson ratio of 1/2) will increase the local field by compressing along the field direction and expanding in orthogonal directions. The stress is independent of the elastic properties of the lattice, but the strain is inversely proportional to the elastic modulus, so a soft lattice will exhibit a large strain, and a hard lattice will exhibit little strain.

Magnetostriction is usually discussed in connection with pure ferrous materials, the dipoles being the spins. In the composite materials we consider, each magnetic particle can be thought of as a dipole, and it is the interaction between these dipoles that gives rise to magnetostriction. [8] This effect does not obtain from magnetostrictive distortions of the particles themselves, but from particle polarization.

Theory of Magnetostriction

Deformations in an initially uniform magnetic field. When a magnetic particle composite is placed in an initially uniform magnetic field it may deform for a number of reasons. First, the individual particles can exhibit magnetostriction, causing a macroscopic deformation of the sample. This mechanism is negligible at the ~0.1 T fields we apply to our samples, and even the applied field did create appreciable stresses in the stiff ferrous particles, these would not appreciably transmit through the soft polymer matrix. Second, dipolar interactions between particles can cause magnetostriction of the sample. This is the effect we wish to isolate. Third, sample shape can create demagnetizing fields that can cause significant deformation. This is an effect we try to minimize in our experiments, but that can still be the dominant effect for some samples. Fourth, if ferrous pole pieces are used to direct the flux lines to the sample it is possible for image interactions to occur from the capping magnetic monopoles. This is not a factor in our apparatus, but has probably contributed to reports of "negative magnetostriction" in particle composites. Fifth, under special circumstances the field can exert a body torque on the sample, even when the field lines are directed

along the major axis of the sample. This torque can lead to large measured strains in our apparatus, but only for samples synthesized to minimize magnetostriction. Rather than embark on a full analysis of all of these effects at this point, we have chosen to describe each of these as required to interpret our experimental results.

Magnetostriction. Magnetostriction is a result of the tendency of the magnetized particles to move in such a way as to increase their magnetic moments. The typical tendency is for dipole pairs aligned with the applied field to approach each other, causing a contraction of the sample along the field, and dipole pairs perpendicular to the field to push each other way, reinforcing the contraction along the field, due to the fact that the Poisson ratio is close to 1/2 for these materials.

Self-consistent point dipole theory. In a recent theoretical paper it has been shown that composites of magnetizable particles in an elastic continuum have the potential to exhibit large magnetostrictive stresses and strains, provided the particles can be suitably arranged. [9] This paper treats composites that have *at most* one unique axis, taken to be the z-axis, along which the field is applied. For example, a composite consisting of chains formed by a uniaxial structuring field will have its unique axis parallel to the chains. A composite structured into sheets by a biaxial field (see below) will have its unique axis normal to the sheets, and a composite structured by a triaxial field (below) may not have a unique axis, nor will a random composite. The goal of this paper is to predict the stresses that the field will induce in the composite in the directions parallel and perpendicular to the applied field. The principal conclusion is that it is possible to use fields to create particle composites that have significantly enhanced or suppressed magnetostriction relative to random particle composites.

Because this paper has motivated the experimental work described herein, it is helpful to give the predictions. We do so in terms of magnetic variables, since the original paper is written in the language of electrostatics. The case of magnetostriction is slightly simpler, because the susceptibility of the continuous, polymer phase will normally be very close to zero, and thus the permeability of the polymer phase will be nearly that of free space, μ_0.

In the self-consistent local field approximation the magnetostrictive stresses parallel

(*z* axis) and perpendicular (*x* axis) to the applied field are

$$\sigma_z = -\frac{1}{2}\mu_{eff}\mu_0 H_0^2(1+\gamma_{zz}) \qquad (1)$$
$$\sigma_x = +\frac{1}{2}\mu_{eff}\mu_0 H_0^2(1-\gamma_{zx}).$$

Here μ_{eff} is the effective *relative* composite permeability (dimensionless) $\mu_{eff} = \left[1+2\beta(\phi+\psi_2)\right]/\left[1-\beta(\phi-2\psi_2)\right]$, which depends on the relative particle permeability μ_p through the contrast factor $\beta = (\mu_p - 1)/(\mu_p + 2)$, and depends on the composite structure through the parameter ψ_2 discussed below, and the particle volume fraction ϕ. The magnetostriction coefficients are defined by the strain derivatives $\gamma_{zi} = -\mu_{eff}^{-1}\partial\mu_{eff,z}/\partial\varepsilon_i,\ i = x,y,z$. A calculation gives

$$\gamma_{zi} = \frac{(\mu_{eff}-1)(\mu_{eff}+2)}{3\mu_{eff}} - \lambda_i\frac{(\mu_{eff}-1)^2}{\mu_{eff}} \qquad (2)$$

where $\lambda_z = \frac{-2}{\pi\sqrt{3}} + \frac{2}{7}\frac{(3\psi_2-\psi_4)}{\phi}$ and $\lambda_x = \frac{1}{\pi\sqrt{3}} + \frac{4}{7}\frac{(3\psi_2-\psi_4)}{\phi}$. An incompressible composite will have Poisson ratio of 1/2, so a field-induced compression along the *z*-axis must be accompanied by a volume-conserving expansion in the *x*,*y* directions. The measured stress will thus be $\sigma_{meas} = \sigma_z - \sigma_x$.

Magnetostriction of particle composites depends on the structural parameters ψ_2 and ψ_4, and is notably independent of the particle size. These parameters are given in terms of the *k*-th Legendre polynomial $P_k(x)$ by

$$\psi_k = -\sum_{j\neq i}\left(\frac{a}{r_{ij}}\right)^3 P_k\left(\cos\theta_{ij}\right) \qquad (3)$$

where r_{ij} is the distance between a pair of particles in the composite, and θ_{ij} is the angle

of their line of centers to the direction of the applied field. These sums are taken over a spherical cavity centered on the i-th particle, then averaged over a statistical number of particles.

Predictions for simulated structures. To evaluate these structural parameters we must have a model of structure. We have developed a Brownian Dynamics simulation that enables us to model structure in 1-, 2-, and 3-dimensional fields for composites containing 10,000 particles. A detailed description of these simulations can be found in reference. [10]

From these simulated structures we have obtained the structural parameters for composites formed in uniaxial and biaxial fields, as well as for random composites. In the reduced stress units, $\sigma'_{meas} = \sigma_{meas} / \frac{1}{2} \mu_{eff} \mu_0 H_0^2$, where the stress is normalized by the energy density of the field, we have predicted that the reduced stress of a random 10 vol.% composite should be -2.7, the minus sign denoting a compressive stress. For a uniaxial composite the reduced stress is enhanced several-fold, -6.9, whereas for a biaxial composite with the field directed normal to the sheets the reduced stress is slightly suppressed, -2.5. At higher particle loadings the stresses are larger, but the predicted trends are similar. The maximum stress we computed was for the magnetic ground state structure, the body center tetragonal lattice. A 10 vol.% composite containing aligned bct domains would have a reduced stress of -9.4.

Unfortunately, it is not possible for us to make magnetostriction predictions for samples structured in triaxial magnetic fields, because the mean-field approximation of our magnetostriction theory becomes poor in this case. In essence, the mean field theory predicts that the sum of the inverse composite susceptibilities taken along three principal directions is invariant to structuring. [11] Triaxial composites violate this sum rule, due to the pure many-body nature of the interactions in this case. We have discussed this point in detail elsewhere. [12]

Chapter 2

Martin, Anderson

SYNTHESIS AND PROCESSING

Motivation. The goal of synthesis is to produce materials with optimal magnetostriction. As the above theoretical discussion indicates, this is roughly equivalent to finding a method of *athermally* organizing the dense, micron-size particles into structures that maximize their effective permeability. The innovation of triaxial magnetic field structuring has made the optimization of athermal composites possible, and we have described synthesis in triaxial magnetic fields in detail elsewhere. [12] Here we would only like to give a brief description of the synthesis methods we have used, the motivation for using these, and the resulting susceptibility enhancements achieved.

Materials. The magnetostrictive coefficient is independent of particle size, provided this is much larger than a single magnetic domain, typically tens of nanometers. Multidomain particles can be magnetically "soft", meaning the remanent magnetization is negligible, or "hard", meaning the remanence is significant, such as in permanent magnet materials. We prefer to use soft magnetic particles, as these eliminate remanent strain.

The susceptibility of the material of which the particles are made is not terribly important. When a field is applied to a soft magnetic particle the resultant magnetization is the product of the particle susceptibility times the field. One might assume the particle susceptibility is equal to the susceptibility of the material of which it is composed, but this is only true when the material susceptibility is quite small - too small to be of interest here. In fact, the particle susceptibility is practically independent of the material susceptibility and is mostly a function of the particle shape. Material susceptibilities are commonly in the range of 10^2-10^5 but the susceptibility of a sphere is limited to 3 (MKS), [13] because its magnetization creates a demagnetizing field that opposes the applied field. Thus high susceptibility materials are of no obvious benefit.

To achieve large magnetostriction the saturation magnetization of the particles should be as large as possible. FSMEs contain nearly contacting particles aligned with the applied field. In the particle gaps the fields can become exceedingly large (~100x the

applied field) causing magnetic saturation of the proximal parts of the particles, which limits their mutual attraction. To avoid this it is desirable to choose particles with high saturation magnetization, such as Fe, which has a moment of ~2.2 Bohr magnetons per atom, giving a saturation magnetization of 2.1 T. (Fe also has little remanence.) We use 3-5 micron carbonyl iron particles, obtained from Lord Corporation, curing these in the silicone polymer, Gelest Optical Encapsulant 41. To minimize demagnetizing field effects, the samples are cast as long solid rectangles, of dimensions 3.25x3.25x50.0 mm, unless otherwise specified.

Using magnetic fields to create structure. More than merely being a practical approach, magnetic fields are an ideal way of creating structure, since they naturally lead to structures that optimize the composite permeability in a carefully annealed thermal system - one in which particle diffusion insures that a free energy minimum is attained in the applied field. This is an obvious point: in an applied field the ground state particle structure is that which minimizes the net magnetostatic energy, and at low fields this energy is negative and proportional to the composite effective susceptibility. The suspension will therefore evolve to maximize its permeability, and so it would seem that a simple uniaxial magnetic field would be optimal for structuring particle composites.

Composites with such *annealed disorder* are not practically achievable in the laboratory, because this would require that the dipolar interactions generate particle forces comparable to the thermal fluctuations that give rise to diffusion. If the applied field is turned down so as to achieve this condition, the particles will simply sediment. To eliminate the effect of gravity, significant fields must be used (0.01-0.02 T). In such fields the dipolar interactions completely dominate thermal fluctuations, so the structures that form are an example of *quenched disorder*. We have shown that *heterodyned* triaxial magnetic fields can be used to create structures with quenched disorder that mimic those having annealed disorder, and have demonstrated through permeability measurements that composites structured by heterodyning have optimal magnetic properties. [12]

Field structuring. The FSMEs investigated in this paper were made by exposing a suspension of 3-5 μm Fe or 4-7 μm Ni particles in a silicone to magnetic fields while the

resin gels. The samples are then post-cured at 70°C for four hours. The structuring fields are created by a resonant triaxial Helmholtz coil of our own design. This computer-controlled magnet and its associated tunable capacitor bank are described elsewhere. [12]

A variety of structures can be created by dynamic magnetic fields. A uniaxial magnetic field, created by a Helmholtz coil or by two parallel plate magnets, causes the particles to form chains. But a biaxial field, created by applying two orthogonal ac fields. leads to composites having a layered structure, the particle sheets forming in the field plane. In this case the ac frequencies should be high enough that rotating particle chains do not form and in practice we use frequencies in the range of 100-1000 Hz. In the special case of equal component frequencies we set their phase difference to 90° to create a rotating field. Finally, a triaxial magnetic field can be created by combining three orthogonal magnetic fields, at least two of which are ac. Composites formed in triaxial fields can have a variety of structures [10, 12], but the important point is that triaxial fields can be used to highly optimize the properties of particle composites and this deserves further discussion.

Triaxial fields. Particle interactions in triaxial fields are complicated, and are treated in detail in [10], but a qualitative discussion here should serve as a practical guide as to their effects. The magnetic interactions between particles are largely due to their dipole moments. At low fields the dipole moment is proportional to the local field, which is comprised of two contributions: the applied field and the field due to all the other dipoles. In a *balanced* triaxial field (i.e. all rms field component amplitudes equal) the time-average interaction between the moments induced by the applied field is zero, so the only nonvanishing interaction is due to the fields produced by the other dipoles. Thus the interaction is solely due to many-body effects, so that the interaction between any two particles is strongly dependent on the positions of the other particles.

A triaxial field has three components, each of which has an amplitude and frequency, for a total of six parameters. In a balanced triaxial field the root-mean-square (rms) amplitudes are equal, which reduces the field parameters to four. Within reasonable limits the field amplitude only determines the time scale of particle motions, and because this is not germane to the structures produced, we really only have to worry

about the three field frequencies. At reasonable high field frequencies (> 100 Hz), it is only the beat frequencies between the fields that are important, and there are only two such difference frequencies, and thus only two parameters.

We will use the term triaxial field to refer to the case where the two beat frequencies are so large that the particle suspension cannot follow the beats. The term 2-d heterodyning will refer to the case where the particle suspension can follow only one beat frequency (e.g. component frequencies of 0 Hz, 200 Hz, 201 Hz), and 3-d heterodyning to refer to the case where the suspension can follow both beat frequencies (e.g. 200 Hz, 201 Hz, 202 Hz). Heterodyning creates interesting suspension dynamics that are described in a recent paper [12].

Composite susceptibilities. An interesting aspect of magnetic particle composites that is not always appreciated is just how small their susceptibilities are compared to that of the material of which their constituent particles are composed. One sometimes sees a sort of "rule of mixing" assumption, where the susceptibility of the composite is taken to be the product of the volume fraction of the particle phase times the susceptibility of the material of which the particles are made, but in fact this assumption can be very poor, because the susceptibility of a single particle is much more a function of the shape and orientation of the particle than of the material of which it is composed. For example, the susceptibility of a spherical particle is just $\chi_p = 3\beta = 3(\mu_p - 1)/(\mu_p + 2)$. For a material of high relative permeability μ_p, such as Fe or Ni, the particle susceptibility approaches 3. The Maxwell-Garnet prediction for the susceptibility of a random composite is then just $\chi_{eff} = 3\phi/(1-\phi)$. For small volume fractions this gives a specific susceptibility χ_{eff}/ϕ close to 3. The specific susceptibility can be thought of as the effective susceptibility of a typical particle in the composite.

The effectiveness of field structuring can be judged from measurements [12] on a set of Ni particle samples made at a loading of ϕ=6.8 vol.%. Because the particles are not spherical, the specific susceptibility χ_{eff}/ϕ=7.1 of a random composite was found to exceed the Maxwell-Garnet prediction of roughly 3. A composite structured by a uniaxial magnetic field was found to have an enhanced specific susceptibility of 17.2

along the structuring, or z axis, and 5.7 normal to this. A composite structured by a biaxial field had χ_{eff}/ϕ=4.9 along the z axis, and 14.7 in the *x*-*y* plane. Finally, a composite formed in a 3-d heterodyned field with the z-axis field component biased by +25% gave χ_{eff}/ϕ=23.1 along the z axis and 10.3 normal to this. Thus biased heterodyning permits the formation of anisotropic composites whose susceptibilities exceed those created by a simple unaxial field. This large susceptibility should lead to greater magnetostriction.

Chapter 3

Martin, Anderson, Read, Gulley

MEASUREMENTS

Optical cantilever apparatus. The reduction of demagnetizing fields is a principal difficulty in designing an apparatus to measure magnetostriction. These fields are created by the magnetization of the sample itself and oppose the applied field, seriously reducing the field in the sample. The magnitude of demagnetizing fields is strongly dependent on the shape of the magnetic sample. In order for the applied field to penetrate the sample the field must be applied along a long axis of the solid, e.g. in the plane of a sheet or parallel to a long cylinder. An optical cantilever apparatus readily accommodates long thin samples, and enables the samples to be pre-stressed, which is important to the magnitude of the effect. The completed apparatus, Fig. 1, consists of the magnetoelastomer suspended from a cantilever. The FSME is centered in Helmholtz coil and is pre-stressed by adding weights to the cantilever, so measurements are made at constant strain. A mirror on the cantilever deflects a laser beam, which hits a 640x480 CCD array positioned 6 m away. A small beam spot is created by imaging onto the CCD a 50 μm aperture positioned a few cm in front of the laser. This apparatus has ~50 nm displacement resolution, which for a 50 mm sample is ~1 ppm strain resolution.

The Helmholtz coil is designed for high field homogeneity and low power dissipation. Field homogeneity was optimized by a careful selection of the coil spacing, and power dissipation was minimized by making the coil cross section as thick as practical. The coil pair resistance is 2.2 Ohm and each coil is 400 turns of 1 mm square wire. Two Kepco bipolar current supplies (36V-12A) connected in parallel supply currents as large as 18 A to the coil, generating fields up to ~1200 Oe.

Salient aspects of the data. Let us now examine some typical response data, to appreciate the salient aspects of response in these materials in the configuration we have described. The term response will be used to refer to the observed contraction or elongation of the magnetoelastomer in a magnetic field. Response is generally a combination of effects, but when the response is essentially due to magnetostriction, or

when the magnetostrictive contribution to the response is extracted from the raw data, we will refer to this as magnetostriction.

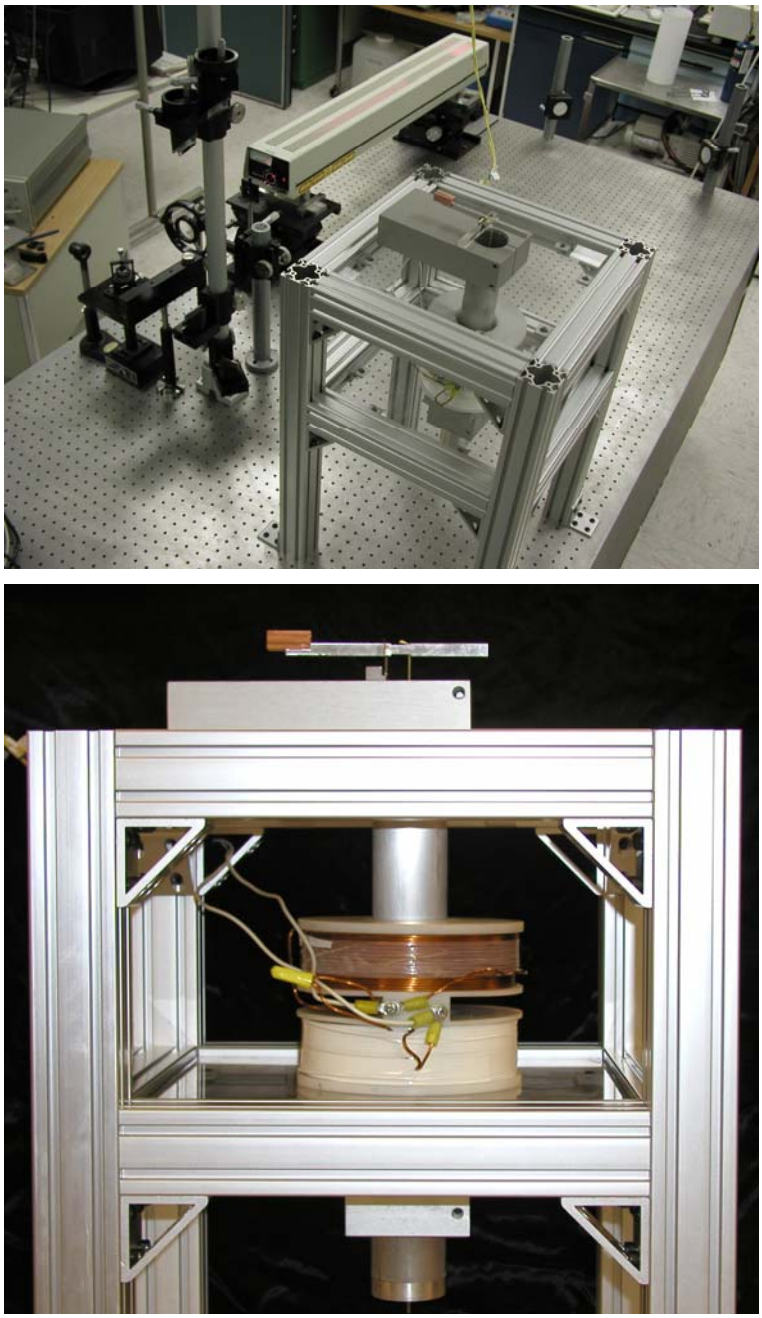

Figure 1. (left) Optical cantilever apparatus. (right) Cantilever and the Helmholtz coil. Coil is elevated above the stainless steel table to eliminate magnet image dipoles.

Saturation. We will start with the simplest case, that of samples of Fe particles chained in a uniaxial magnetic field, with the chains parallel to the long axis of the

sample. At low fields the magnetostriction is observed to be proportional to the energy density of the field, as expected, Fig. 2. But at high fields the magnetostriction reaches a limiting value as the Fe saturates, Fig. 3a. This high field data can be fit by the remarkably simple expression

$$\gamma = \frac{\alpha W}{1 + W / W_{ch}} \tag{4}$$

where $W=BH$ is the twice the field energy density and W_{ch} is the *characteristic* value of this, at which the sample strain is 1/2 the maximum attainable. For composites having large susceptibilities one would expect α to be relatively large. At constant susceptibility W_{ch} will increase with the saturation magnetization of the particles.

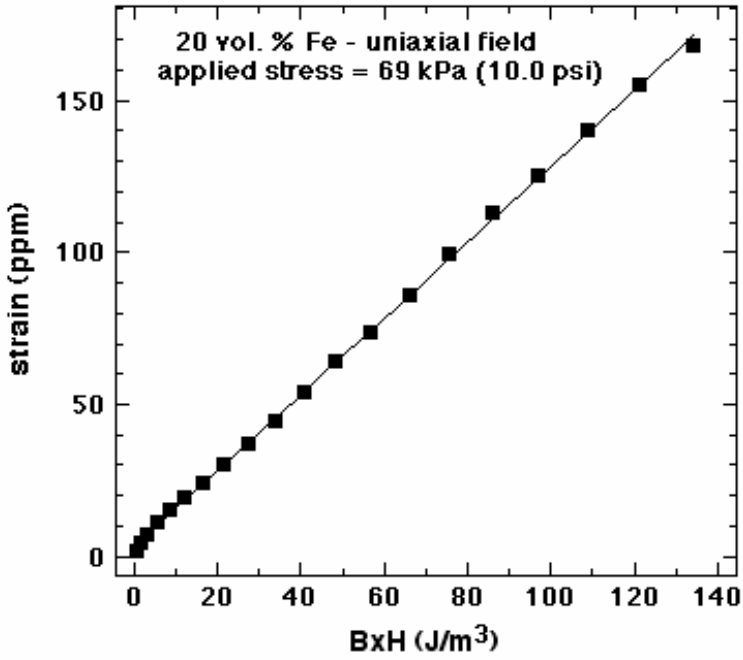

Figure 2. At low fields the strain is proportional to the energy density of the field. These data are for a sample structured by a uniaxial magnetic field.

If this relation is an accurate description of the data, then a plot of W/γ vs W should give a straight line. Data for a 10 vol.% uniaxial sample show that this is indeed the case, Fig. 3(bottom), giving α=1.18 ppm/Pa and W_{ch}=8.35 kPa. In a saturating field the strain will approach $\gamma_{max}=\alpha W_{ch}$, which in this case is 9,800 ppm. This strain is five times

greater than that obtained for terfenol-D.

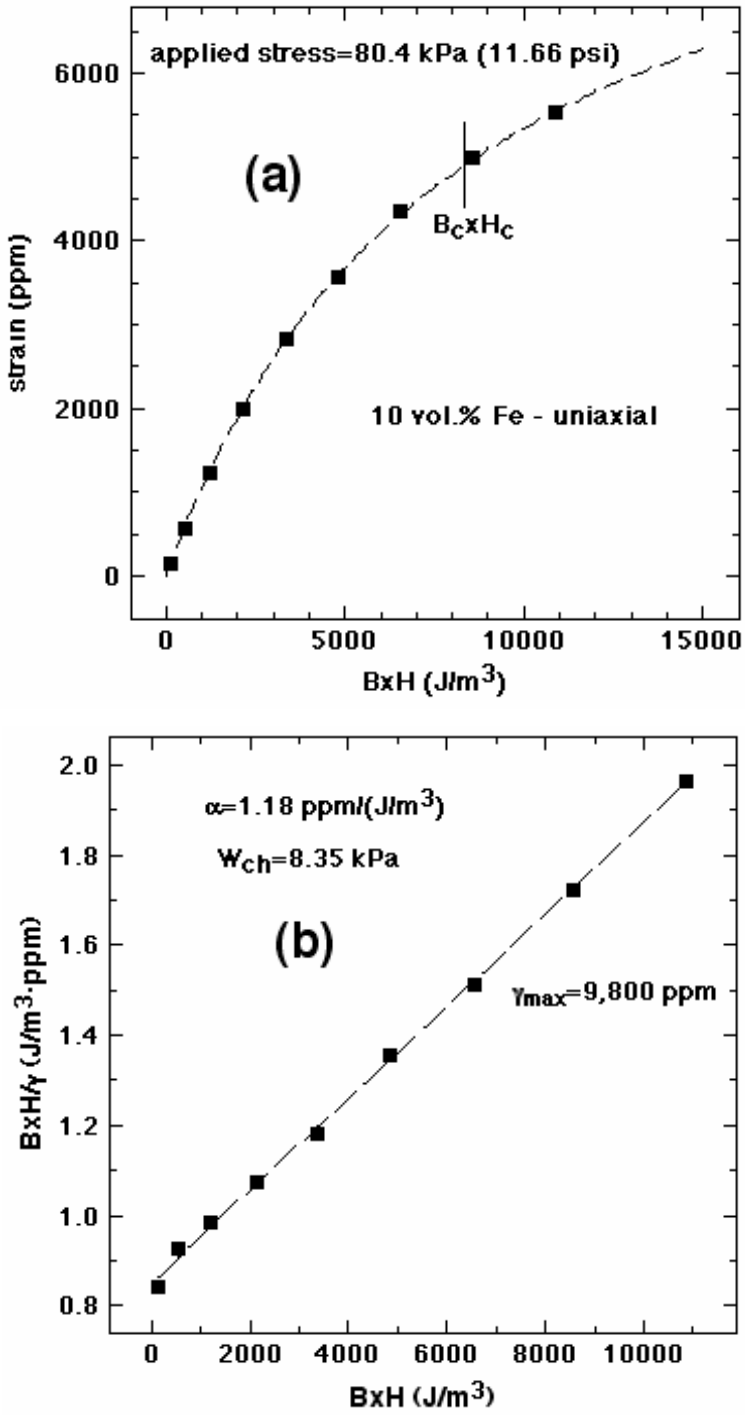

Figure 3. (top) Response data for a 10 vol.% Fe composite shows the effect of magnetic saturation. (bottom) This linear plot shows that Eq. 4 is an accurate description of the data. From this plot a saturation strain of 9,800 ppm is obtained.

Prestress. It is clear that in order for a chain of hard spheres to contract there must be gaps between the particles. So it is not surprising that there should be some dependence of magnetostriction on sample prestress or prestrain. The low field data in Fig. 4 were taken at three widely different prestresses, and show a nonmonotonic dependence of the observed strain on prestress. In this case the elastic modulus of the sample is 1.7 MPa, so the sample prestrain varied from 7400 ppm to 61,000 ppm. The prestrain is thus much greater than that needed to create gaps large enough to close. This is a complicated aspect of these materials that we will discuss below.

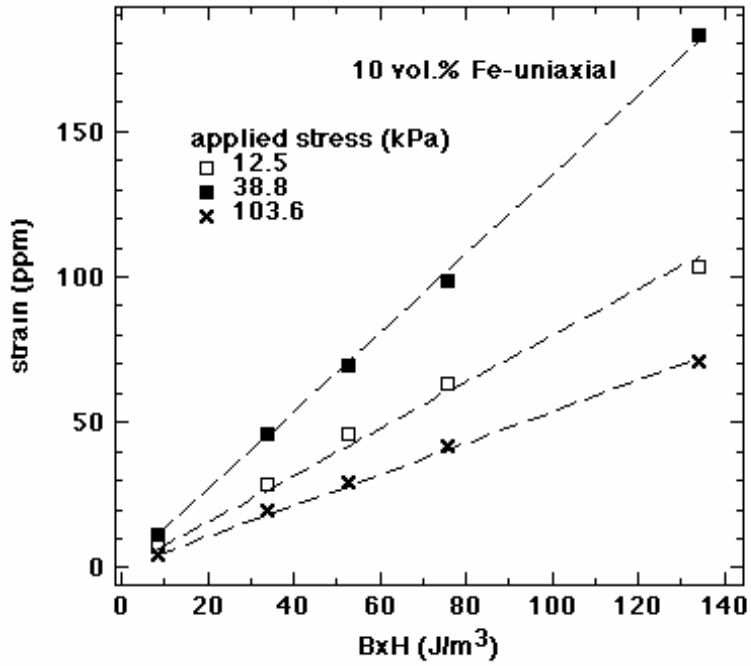

Figure 4. Measurements of the response of a uniaxial Fe composite show a dependence on prestress. In fact, the response increases linearly with prestress for stresses below a yield stress. Note the especially low response at the highest applied stress.

Particles. The linear theory of magnetostriction shows that the stress depends on the particle susceptibility, and this should be very similar for Ni or Fe powders. Experiments, however, show that Fe composites have six times greater magnetostriction than Ni composites (data for 20 vol.% composites). Measurements of the susceptibility of these composites show very similar values, so this difference is unexpected. We believe that it is due to poor adhesion of the Ni particles to the polymer, which causes severe field-induced clumping transitions in the strained Ni composites.

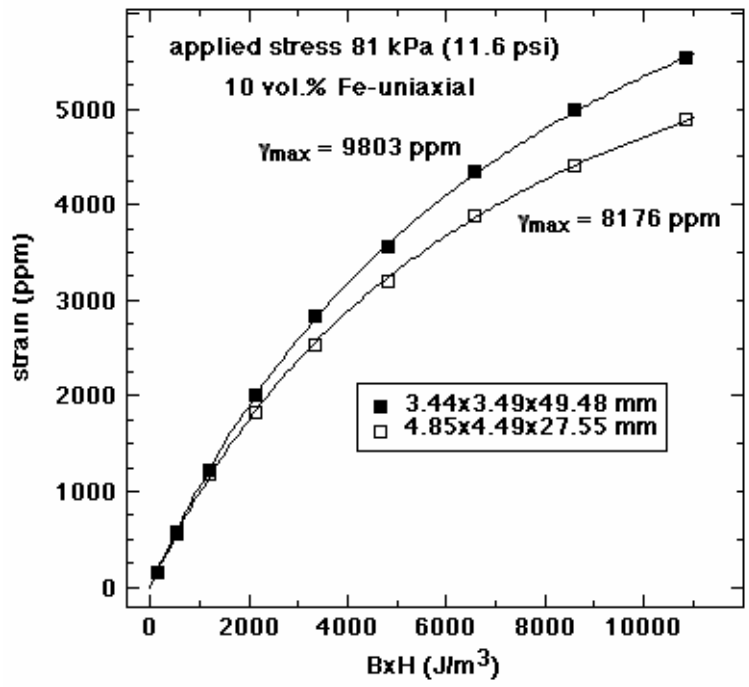

Figure 5. Measurements on samples of aspect ratios 14.3 and 5.9 show how the sample shape can influence the response. Higher aspect ratio samples have greater response, as expected.

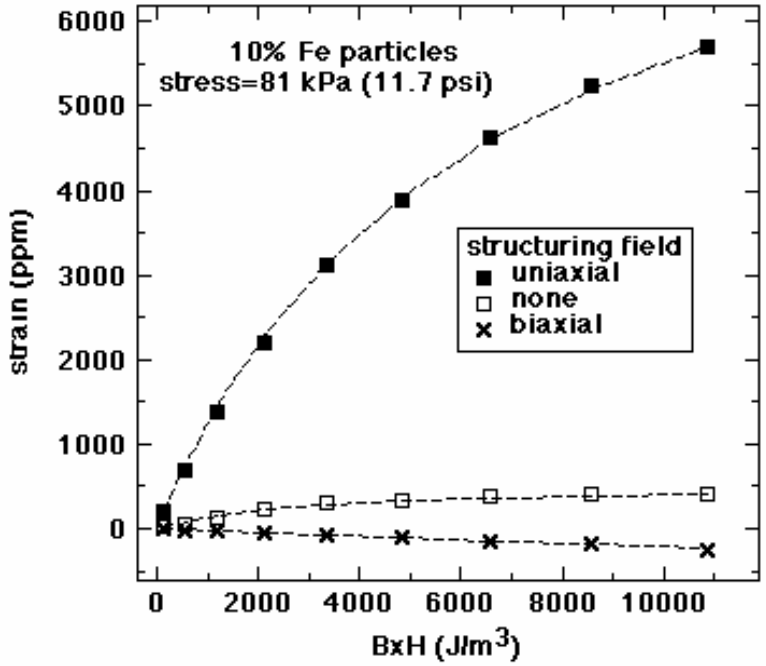

Figure 6. The structure of the particle agglomerates has an enormous impact on the response, with biaxial composites exhibiting a negative response.

Shape. The observed response can also depend on the sample shape. In Fig. 5 measurements on a sample with an aspect ratio of 14.3 are compared to those on a sample of aspect ratio 5.9. The high aspect ratio sample has significantly greater response, due to the reduced effect of demagnetization fields. Accounting for demagnetization field effects is thus an important aspect of this work.

Structure. The structure of the particle agglomerates within the composite have an enormous influence on the response, Fig. 6. An unstructured sample has much smaller magnetostriction than a sample structured by a uniaxial field, and a sample structured by a biaxial field normal to the long axis of the sample even exhibits a negative response. Some samples exhibit even more complex behavior, with an observed positive response at low fields and a negative response at high fields. But whether or not this mixed behavior occurs is also dependent on the prestress.

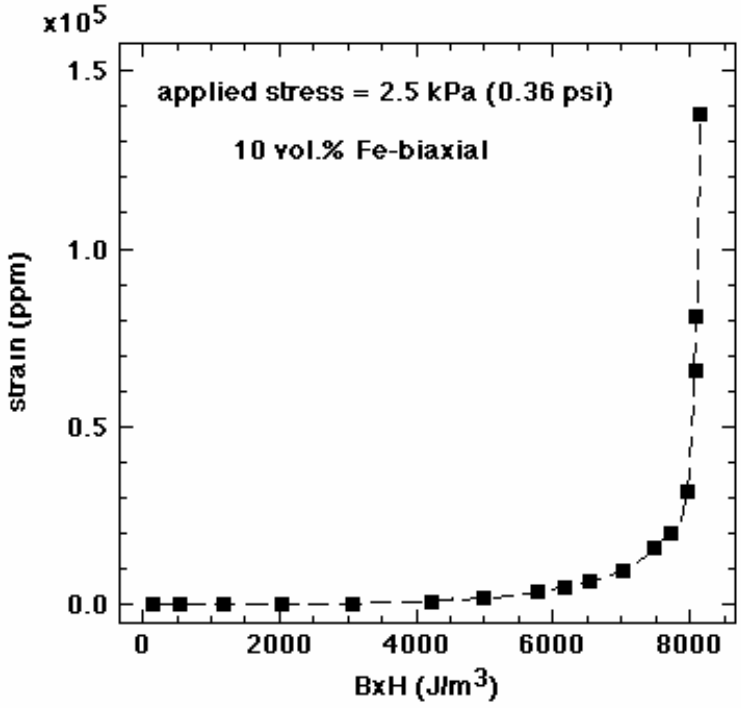

Figure 7. Biaxial composites made at small particle loadings are found to have an anomalously large response at small applied stresses.

Extraordinary response. A few samples were found to exhibit an extraordinary response, Fig. 7. This extraordinary response occurs at lower particle loadings, low

applied stresses, and high fields. It only occurs for samples structured by a biaxial field.

There are quite a few effects for which an explanation is needed. We will start by considering demagnetization field effects as an understanding of these is essential to the interpretation all of the response data.

Chapter 4

Martin

DEMAGNETIZING FIELD STRESSES

The stress on a magnetic prolate spheroid due to its demagnetizing field arises because an elongation of the sample will decrease its demagnetizing field, thus increasing its internal field and magnetic moment. Our sample geometry is that of a solid rectangle, so this computation does not exactly correspond to experiment, but is nonetheless a good approximation. In fact, the reason we use the prolate spheroid geometry is that the field inside a prolate spheroid is uniform when placed in an initially uniform field. This makes possible an analytical solution to internal field, which can be formulated in terms of a demagnetization factor that is *independent* of the material susceptibility. The field inside a solid rectangular object is not uniform, and does not admit to an analytical solution. A demagnetization factor can be defined for the average internal field, but then this depends in a complex way on the material susceptibility.

Consider a prolate spheroid of aspect ratio $g>1$ with its long axis aligned with the field, which we take to be along the z axis. For this case the demagnetization factor n is

$$n = \frac{1}{g^2-1}\left[\frac{g}{2\sqrt{g^2-1}}\ln\left(\frac{g+\sqrt{g^2-1}}{g-\sqrt{g^2-1}}\right)-1\right]$$
$$\cong \left[\ln(2g)-1\right]/g^2 \quad \text{for } g >> 1. \tag{5}$$

If an external field is applied to an FSC, the internal field will be quite non-uniform, due to the discrete particles. Here it will be adequate to treat the composite as a continuum solid, so the "macroscopic" internal field is uniform throughout the material. If the applied field is low enough that this magnetic solid is far from saturation, then we can assume the composite susceptibility χ is independent of field. The internal field is then $\mathbf{H}_{\text{int}} = \mathbf{H}_0 - n\mathbf{M} = \mathbf{H}_0 - n\chi\mathbf{H}_{\text{int}}$ and

$$\mathbf{H}_{\text{int}} = \mathbf{H}_0 / (1 + n\chi) \tag{6}$$

The energy of a linear magnetic material of moment **m** in an applied field $\mathbf{H}_0$ is $U = -\frac{1}{2}\mu_0 \mathbf{m} \cdot \mathbf{H}_0$. This expression includes the work done by the perfect power supply used to keep the applied magnetic field constant. The applied field will thus cause a force $\mathbf{F} = -\frac{\partial U}{\partial Z}\hat{\mathbf{z}}$, where Z is the length of the solid. A positive force indicates an elongational stress. In terms of the sample moment $\mathbf{m} = V\mathbf{M}$ the force is $F = +\frac{1}{2}\mu_0 H_0 V \frac{\partial M}{\partial Z}\hat{\mathbf{z}}$, where $V = \frac{\pi}{6}\rho^2 Z$ is the sample volume and the sample magnetization is $\mathbf{M} = \chi_c \mathbf{H}_{\text{int}}$. Using Eq. 6 for the internal field gives

$$\mathbf{F} = \frac{1}{2}\frac{\mu_0 H_0^2 V}{(1+n\chi)^2}\left[\frac{\partial \chi_c}{\partial Z} - \chi^2 \frac{\partial n}{\partial Z}\right] \tag{7}$$

The volume of a prolate spheroid of minor diameter ρ is $V = \frac{1}{6}\pi\rho^2 Z$ so $\rho = \sqrt{6V/\pi Z}$ and $g = Z^{3/2}/\sqrt{6V/\pi}$.

Large aspect ratio samples. For samples having a large aspect ratio it is simple to obtain an analytical result for the demagnetizing stress. In this approximation, and for an incompressible spheroid, $\frac{\partial n_a}{\partial Z} = \frac{-3}{\rho g^3}\left(\ln 2g - 3/2\right)$. Substituting this equation into Eq. 7 gives for the measured stress

$$\sigma_{meas} = \frac{\sigma_{mag}}{\left(1+n\chi\right)^2} + \frac{\mu_0 \chi^2 H_0^2}{\left(1+n\chi\right)^2}\frac{\ln 2g - 3/2}{g^2} \tag{8}$$

where the magnetostrictive stress is $\sigma_{mag} = \frac{1}{3}\mu_0 H_0^2 \frac{\partial \chi}{\partial \gamma}$ and γ is the strain. This

expression can be used to correct experimental data taken at low applied fields for the demagnetizing field strain, with the result

$$\gamma_{mag} = \left\{ \gamma_{meas} - \frac{\mu_0 M^2}{E}\left[n - 1/2g^2\right] \right\} \times \left(\frac{H_0}{H_0 - nM} \right)^2 \qquad (9)$$

where $\mathbf{M} = \chi \mathbf{H}_{\text{int}}$ and E is the tensile modulus.

Saturation. At magnetic fields large enough that the linear susceptibility approximation fails, the calculation of the stress becomes more complex. Define the non-linear susceptibility $\chi(H_{\text{int}}) = M / H_{\text{int}}$. Then the internal field can be written as $\mathbf{H}_{\text{int}} = \mathbf{H}_0 / \left[1 + n\chi(H_{\text{int}})\right]$. For composites the susceptibility is small, perhaps no larger than 5, and for long prolate ellipsoids the demagnetization factor is small as well, so the product $n\chi$ is small. With little error we can use the approximation $\mathbf{H}_{\text{int}} = \mathbf{H}_0 / \left[1 + n\chi(H_0)\right]$. For a change in the sample magnetization at constant applied field the force is still $F = +\frac{1}{2}\mu_0 H_0 V \frac{\partial M}{\partial Z}$ ẑ. Using these expressions we can show that Eq. 9 is approximately correct even for saturating fields.

Small aspect ratio samples. For samples with a small aspect ratio, say g<4, Eq. 9 is a really poor approximation, as Fig. 8a shows. On the other hand, differentiating the exact form, Eq. 5, of the demagnetizing factor n with respect to g would just create a mess. A 0good approximation to the exact derivative dn/dg, taken numerically, is all that is really needed. Balancing accuracy against simplicity we came up with

$$\frac{dn}{dg} \approx -\frac{2n}{g} + \frac{1}{g^3}\left[1 - \frac{7}{8}\ln\left(1 + g^2\right)/g^2\right]. \qquad (10)$$

This expression becomes exact for large g and is never off by more than ~1.4%, as shown in Fig. 8b. The formula for the effect of demagnetizing fields on the measured strain is

$$\gamma_{mag} = \left\{ \gamma_{meas} - \frac{\mu_0 M^2}{E} \left[n - \frac{1}{2g^2} \left[1 - \frac{7}{8} \ln\left(1 + g^2\right) / g^2 \right] \right] \right\} \times \left(\frac{H_0}{H_0 - nM} \right)^2 \qquad (11)$$

This expression will give dramatically different results for the estimated magnetostriction for short, thick samples. To correct the sample strains in a controlled stress experiment one can simply divide Eq. 11 by the composite tensile modulus *E*.

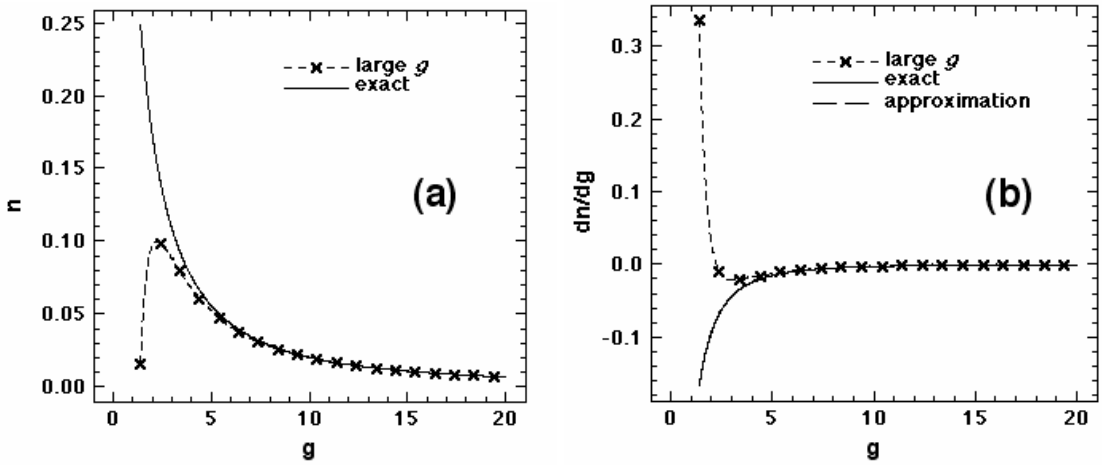

Figure 8. (a) Approximate and exact forms of the demagnetization factor are compared. (b) The approximate and exact derivatives differ substantially for aspect ratios less than 5.

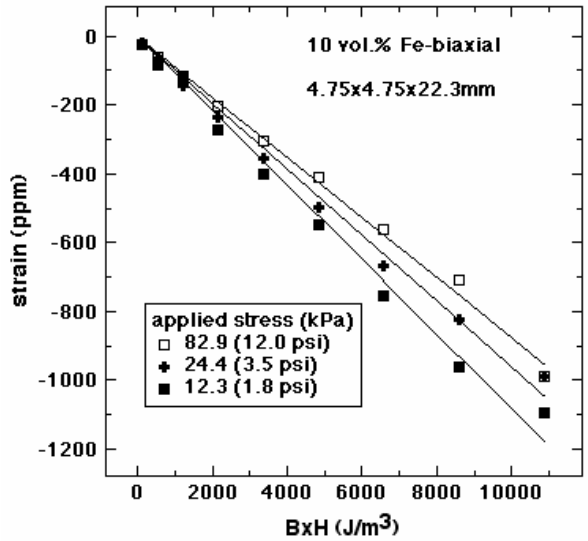

Figure 9. Demagnetizing field strain is found to be essentially independent of the applied stress.

A key prediction of Eq. 11 is that the demagnetizing field strain (or stress) is

independent of the sample preload. Experimental data in support of this are shown in Fig. 9 for a 10 vol.% biaxial composite with an aspect ratio of 4.7. Here the observed response is entirely negative (elongation), being dominated by demagnetization fields. Because magnetostriction does depend on the sample preload, the combination of the two effects can lead to complicated trends.

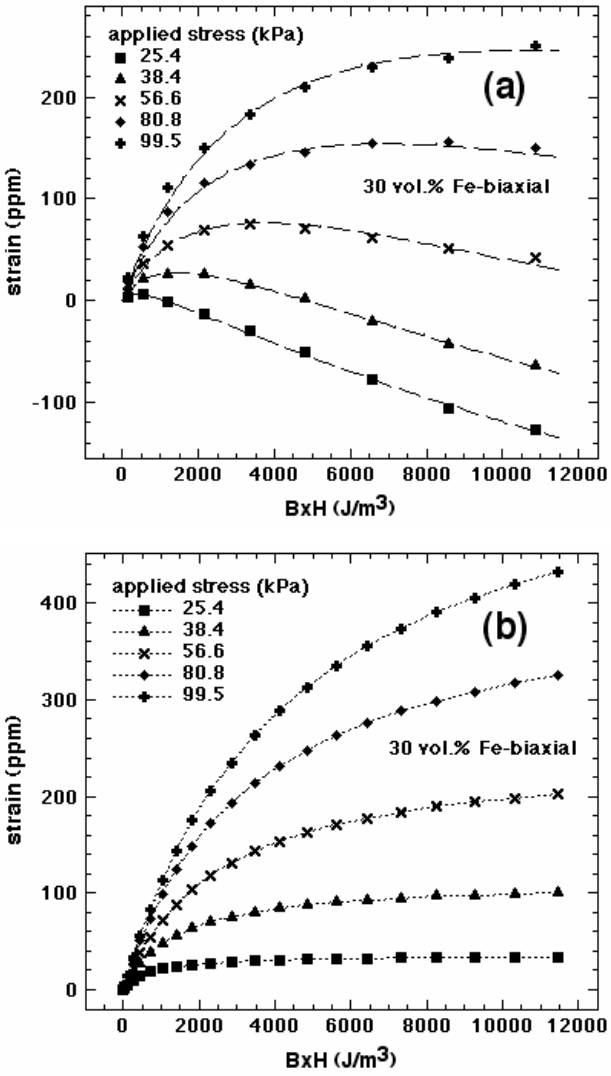

Figure 10. (a) For a 30 vol.% biaxial field-structured composite the response data depend nonmonotonically on the field, with both negative and positive responses. (b) The magnetostriction extracted from the response data is positive and monotonic.

An example. A biaxial, 30 vol.% Fe particle composite is an ideal example of the importance of demagnetization field corrections, since it should exhibit small magnetostriction and thus the demagnetization fields should produce a significant

contribution to the response. The data for this sample, Fig. 10a, show a complex behavior with both negative and positive responses obtained at some sample preloads. The modulus for this composite is 7.5 MPa, so the range of sample prestrains is from 3400 - 13300 ppm.

To correct this response data for demagnetizing field effects requires an expression for the sample magnetization. In an earlier paper [11] we studied the magnetization behavior of field-structured particle composites and found that the expression

$$M = \frac{\chi H}{\sqrt{1+\left(\chi H / \phi M_{sat}\right)^2}} \qquad (12)$$

is quite accurate. Here ϕ is the volume fraction of particles, χ is the composite susceptibility, and M_{sat} is the saturation magnetization of the particle material. M_{sat} for Fe is 1.72×10^6 A/m. The composite susceptibility we obtain from earlier experiments, [11] and along the applied field χ is 3.03 for a 30 vol.% biaxial composite.

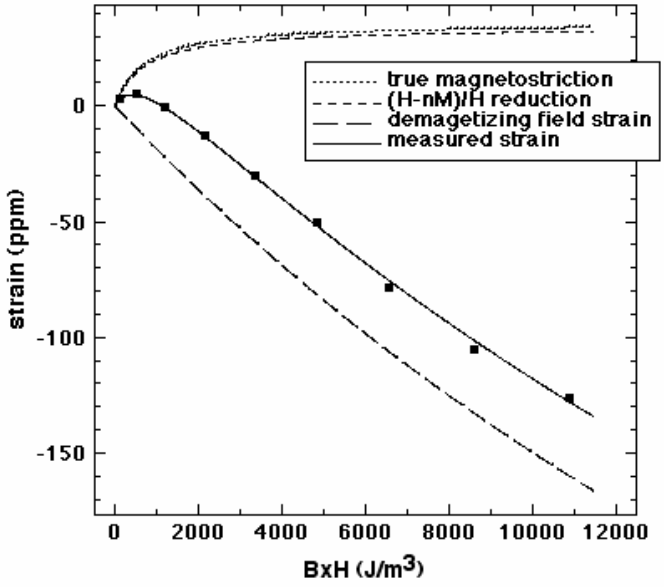

Figure 11. The magnetostriction effect can be extracted from the response data by modeling and subtracting the effect of demagnetizing fields.

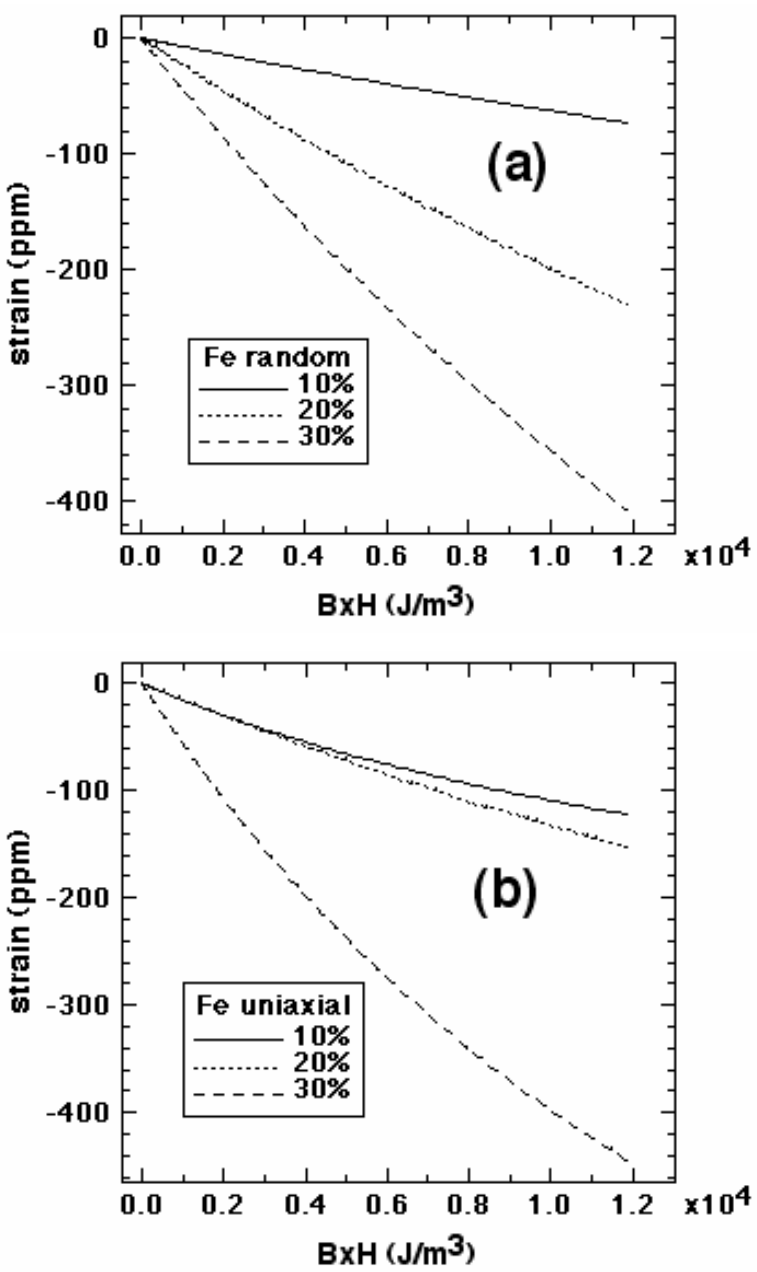

Figure 12. Modeling the demagnetization field strain for random (a) and uniaxial (b) composites shows that the effect becomes increasingly significant as the particle loading increases.

We first examine the response at the lowest preload, Fig. 11, since this is mostly due to demagnetization fields. This curve is fit to the sum of two functions, Eq. 4, whose two parameters we seek, and Eq. 11, whose parameters are known. Some adjustment to the sample aspect ratio is also required, as the samples are solid rectangles, not prolate spheroids. The result is that the demagnetization strain is 27 ppm at this preload. The

fits to all of the data sets were made with exactly the same demagnetization response, and the extracted magnetostriction curves are in Fig. 10b. From this we see that the magnetostrictive response is really quite poor for this sample, as predicted by theory. We also observe an increase in the magnetostriction with increasing preload.

Finally, it is of interest to examine the dependence of the demagnetization strain on particle loading for the aspect ratios of our standard samples. This shown in Fig. 12 for both random and uniaxial composites, using the measured tensile modulus and composite susceptibility. For the uniaxial samples the demagnetization field correction becomes significant at 30 vol.%.

Chapter 5

Martin, Read, Gulley

EXTRAORDINARY RESPONSE

Some of the samples we synthesized to test our understanding of magnetostriction in field-structured composites exhibited an extraordinary positive response at low preloads and high fields. This surprised us because this effect only occurred for samples we expected to have minimal magnetostriction. This extraordinary response only occurs when the transverse susceptibility (i.e. normal to the long axis) of the magnetoelastomer significantly exceeds the longitudinal susceptibility.

Susceptibility anisotropy. For most samples the field exerts a stabilizing torque, since a magnetic material will tend to align along its long axis. The cause of the extraordinary response is a destabilizing torque, due to an inverse susceptibility anisotropy in some samples. The parallel and perpendicular sample susceptibilities, including the effect of demagnetizing fields, are

$$\chi_{\parallel} = \frac{\chi_{c,\parallel}}{1+n_{\parallel}\chi_{c,\parallel}} \quad , \quad \chi_{\perp} = \frac{\chi_{c,\perp}}{1+n_{\perp}\chi_{c,\perp}} , \tag{13}$$

in terms of the susceptibilities intrinsic to the composite itself, $\chi_{c,\parallel}$ and $\chi_{c,\perp}$. In the absence of an applied stress the sample will align along the axis of greatest susceptibility. The magnetic field is applied along the longitudinal axis, but if the perpendicular susceptibility is larger, i.e. $\chi_{\perp} > \chi_{\parallel}$, the field will exert a destabilizing torque on the sample.

The question arises as to whether it is possible for this destabilizing torque to arise in a long thin FSC. Consider the worst case, a long cylindrical sample. For this the demagnetization factors are very close to $n_{\parallel} = 0$, $n_{\perp} = 1/2$. For a 10 vol.% sample made of particle sheets we have shown [11] that the composite susceptibility normal to the sheets is 0.335 (MKS) and in the plane of the sheets it is 1.593. If the sheets are formed

normal to the cylindrical axis, the sample susceptibility is $\chi_\perp = 1.593/(1+0.5\times 1.593) = 0.8875$ which is much greater than the longitudinal susceptibility of 0.335. Such a sample will have a destabilizing torque, provided the applied stress is small enough.

At higher particle concentrations a destabilizing torque will not occur. For example, for a 20 vol.% composite of particle sheets the susceptibility normal to the sheets is 1.380 (MKS) and in the plane of the sheets it is 2.750. If the sheets are again formed normal to the cylindrical axis, the sample susceptibility is $\chi_\perp = 2.750/(1+0.5\times 2.750) = 1.158$ which is now lower than the longitudinal susceptibility of 1.380, so the torque will be stabilizing, even at zero applied stress.

Torque balance. The magnetic torque on the sample can be computed by from considering the magnetostatic energy of a sample inclined at an angle θ to the applied field. The magnetostatic energy is $U = -\frac{1}{2}\mu_0 \mathbf{m}\cdot\mathbf{H}_0$ where **m** is the sample moment. Let our Cartesian coordinates (x, y) be such that the applied field is in the y direction. The coordinates (x', y'), are defined such that the sample is along the y' direction. The sample moment is then $\mathbf{m} = vH_0(\chi_\parallel \cos\theta\hat{\mathbf{y}}' - \chi_\perp \sin\theta\hat{\mathbf{x}}')$, where v is the sample volume. The energy is thus $U = -\frac{1}{2}vH_0^2(\chi_\parallel \cos^2\theta + \chi_\perp \sin^2\theta)$ and the magnetic torque is

$$\tau_m = \mu_0 v H_0^2 \cos\theta \sin\theta \left(\chi_\perp - \chi_\parallel\right). \tag{14}$$

A positive, destabilizing torque occurs when the transverse susceptibility exceeds the longitudinal. The stress applied to the sample exerts the negative torque $\tau_s = -Fl\sin\theta$, where l is the sample length. Balancing the mechanical and magnetic torques gives the equilibrium angle

$$\cos\theta = \frac{\sigma}{\mu_0 H_0^2\left(\chi_\perp - \chi_\parallel\right)} \tag{15}$$

in terms of the sample stress σ. When this expression gives a positive value of $\cos\theta$ that is less than unity, an instability will occur. This condition occurs with large fields and small applied stresses. The sample strain is just 1-$\cos\theta$.

For the 10 vol.% sample of sheets, $\chi_{\perp} - \chi_{\parallel} = 0.553$. At an applied stress of 3.45 kPa (0.5 psi) the critical field will be 70.5 kA/m (883 Oe). Larger fields will show a clear instability, as the data in Fig. 7 demonstrate.

Chapter 6

Martin, Read, Gulley

EXPERIMENTAL RESULTS

In these controlled stress experiments the strain is directly measured, but in addition there are a number of computed quantities that are of interest. These include the maximum strain at saturation, the characteristic field product BH (twice the field energy density), the magnetic field contribution to the stress and modulus, the work performed, and the energy efficiency.

Before giving these factors it is worth noting that the self-consistent point dipole model actually overestimates magnetostriction. Consider the 10 vol.% composite structured by a uniaxial field, for which the predicted stress is $6.9 \times \frac{1}{2} \mu_{eff} \mu_0 H_0^2$. Experiments show that the effective relative permeability for this composite is $\mu_{eff} = 2.36$ and the tensile modulus is 1.7 MPa (245 psi). Using these parameters we predict a strain of $\gamma(ppm) = (4.8 m^3/J) B \times H$, where B is the magnetic induction field created by the magnet in the absence of the sample. Experimental data at low fields and optimal sample preload give $\gamma(ppm) = (1.2 m^3/J) B \times H$, so the real material falls well short of expectations. We believe the discrepancy is related to the fact that the observed magnetostriction is dependent on preload, and the reasons for this are complex, as discussed briefly below.

Saturation strain and characteristic field product. The maximum strain at magnetic saturation and the characteristic field product are obtained from fitting to Eq. 4, as described above. For the 10 vol.% chain sample the result is in Fig. 13a. Here it is seen that the greatest saturation strain occurs at an applied stress of ~80 kPa, corresponding to an applied tensile strain of 4.7%. At this preload the characteristic field product $B \times H$ is 6.4 kPa, so the composite reaches half its saturation strain at a field of ~72 kA/m (900 Oe). A field of this magnitude is easily achieved with an open-air Helmholtz coil, making these materials a practical choice for actuator applications.

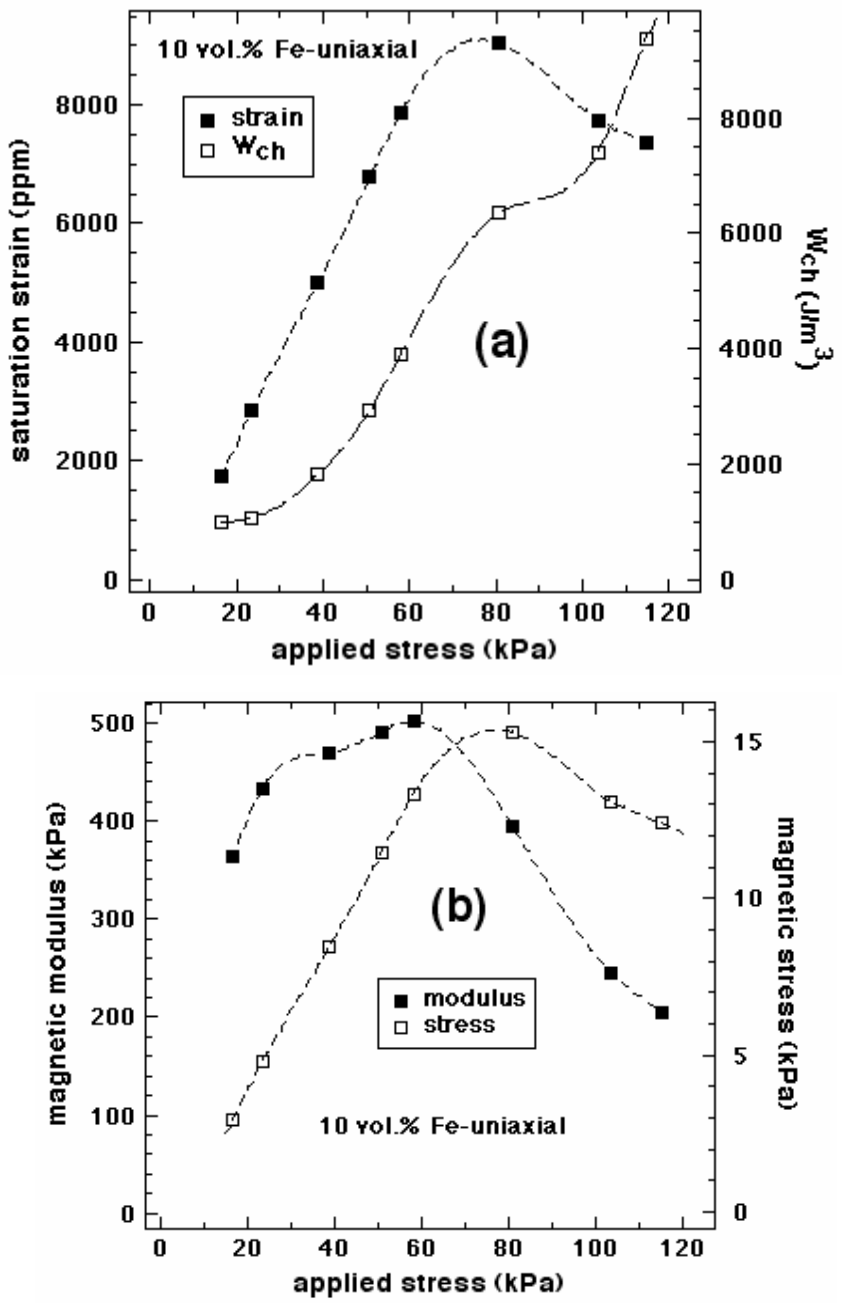

Figure 13. (a) The saturation strain is shown to approach 10,000 ppm for a 10. vol.% Fe composite. The characteristic field products, Eq. 4, are well within the range of open air coils. (b) The magnetic modulus is as large as 500 kPa, but the magnetic stress reaches only 15 kPa.

Magnetic modulus and stress. Because measurements at low applied stresses show a linear dependence of the sample strain on the applied stress, invoking a magnetic tensile modulus E_m should be a useful way to describe the data. For a sample under constant stress, the effect of the magnetic field is to change the strain alone. This strain change is

$\Delta\gamma = \sigma[1/E_0 - 1/(E_0 + E_m)]$, so the magnetic modulus is

$$E_m = \frac{\Delta\gamma E_0^2}{\sigma - \Delta\gamma E_0}. \qquad (16)$$

where E_0 is the tensile modulus in the absence of an applied field. The magnetic modulus for the 10 vol.% Fe chain composite is given in Fig. 13b, using the measured tensile modulus of 1.7 MPa (245 psi). E_m increases with magnetic field and can be as large as 0.4 MPa at modest fields. Fig. 13b shows a pronounced yield behavior, and the yield stress is found to increase with magnetic field, so it would be careless to use the magnetic modulus to compute stresses and strain without taking this yield behavior into account.

When the magnetic field is turned on, the sample contracts, so part of the stress initially supported by the elastomer is taken up by the magnetic interactions between the particles. This magnetic stress load is

$$\sigma_m = \sigma E_m/(E_0 + E_m) = \Delta\gamma E_0, \qquad (17)$$

a formula which is intuitive, since a force added to a harmonic well merely generates a displaced harmonic well with the same stiffness. The data in Fig. 13b show that a magnetic stress of 15 kPa can be obtained at a particle loading of 10 vol. %.

It is interesting to look at the work done per unit volume of sample during this strain. This "work density" is the product of the strain and the applied stress. For the 10 vol.% Fe sample this work density is u=9800ppmx80.4kPa=0.8kPa at magnetic saturation.

Particle loading. As the particle loading increases, the sample response decreases, Fig. 14a, but the magnetic stress increases, Fig. 14 b, because of the increase in the composite tensile modulus. The work density increases with particle loading, Fig. 15a, reaching a value of over 1 kPa at an applied strain of ~2% for a particle loading of 45 vol.%. The magnetic modulus, Fig. 15b, increases sharply with concentration, peaking at over 2 MPa

at 45 vol.%, compared to the zero field tensile modulus of 10.8 MPa.

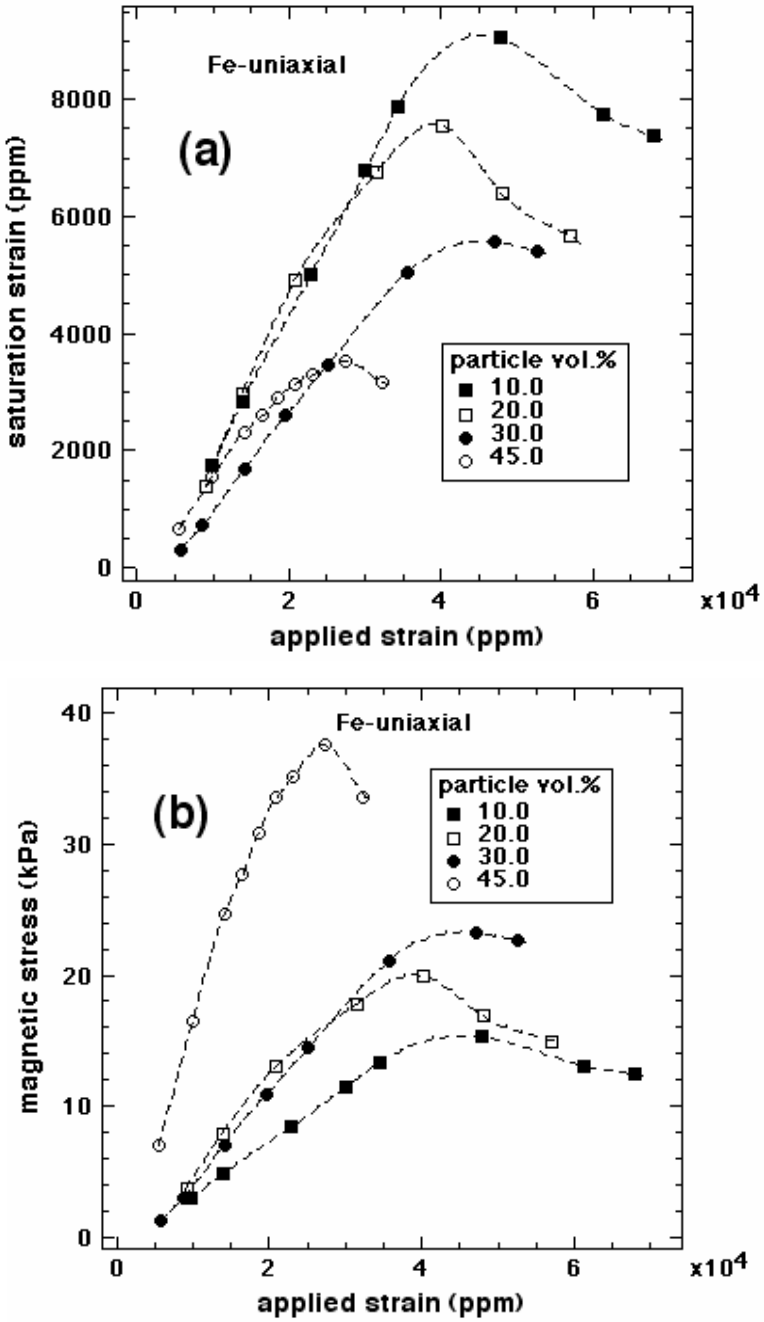

Figure 14. The saturation strain (a) and stress (b) as a function of applied strain for uniaxial composites of a range of particle loadings.

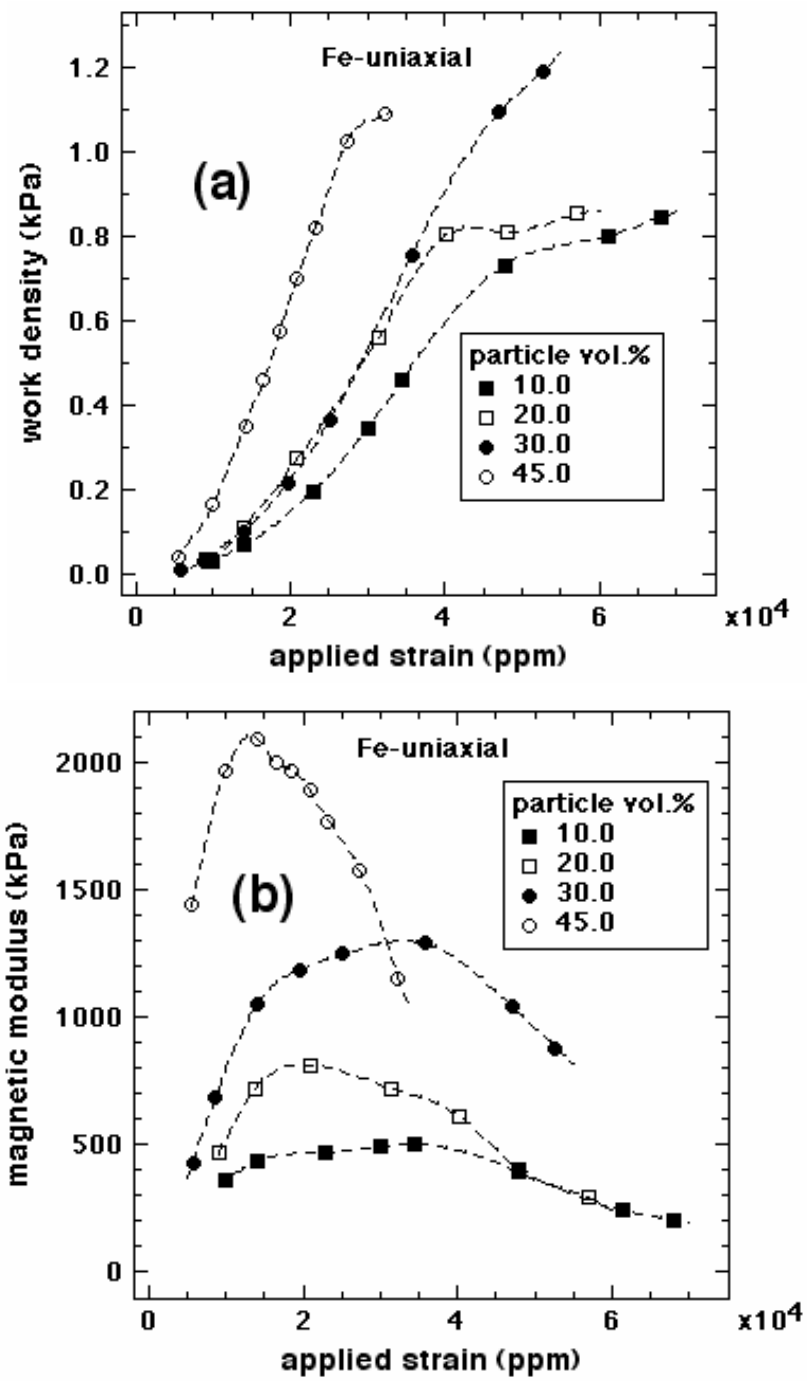

Figure 15. The work density (a) and magnetic modulus (b) as a function of applied strain for uniaxial composites of a range of particle loadings.

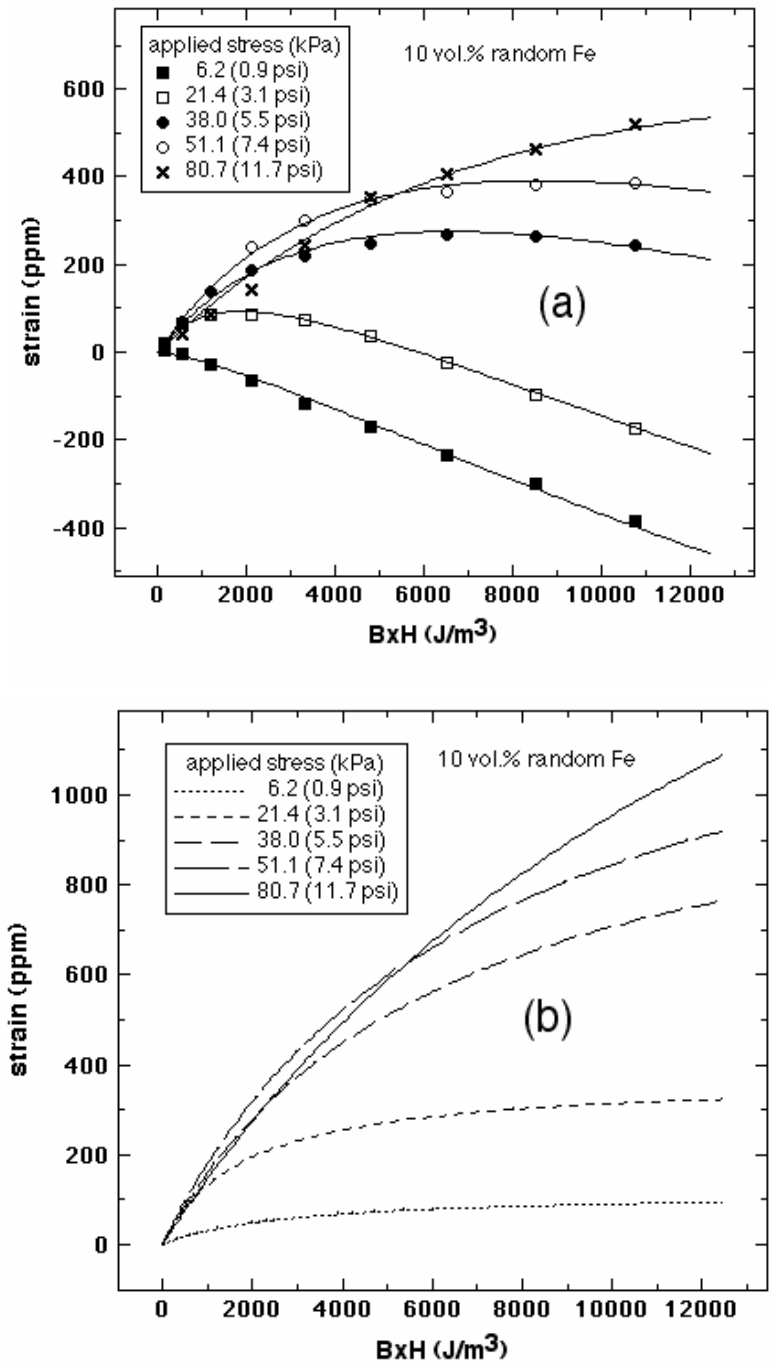

Figure 16. Response (a) and magnetostriction data (b) for a 10 vol.% Fe composite.

Structure. It is of some interest to compare the magnetostriction of random composites to uniaxial and biaxial field-structured composites. In Fig. 16 are shown the response and magnetostriction data for a random 10 vol.% Fe composite. These data were corrected for demagnetizing fields as described above. Comparing these data to the 10 vol.%

uniaxial data, Fig. 5, we see that there is a difference of about a factor of 5 in the magnetostrictive strain. We are unable to provide data for a biaxial sample at this particle loading because of the torque instability exhibited by this sample.

At 30 vol.% the torque instability does not exist, and comparing data taken at the same applied stress show that the magnetostrictive strain of the biaxial sample is roughly 6.6 times smaller. The tensile modulus of the biaxial composite, 7.5 MPa, is larger than that of the uniaxial composite, 4.2 MPa, so the measured magnetic stress ratio (see Eq. 17) is 6.6x4.2/7.5=3.7. The theoretical magnetic stress ratio, based on simulated 30 vol.% structures, is 4.4, which is in reasonable agreement with the observations. In the linear regime the biaxial composite strain response is $\gamma(ppm) = (0.13m^3/J)B \times H$ and the uniaxial composite obeys $\gamma(ppm) = (0.66m^3/J)B \times H$ at an applied stress of 100 kPa. Accounting for the modulus difference gives a magnetic stress ratio of 3.

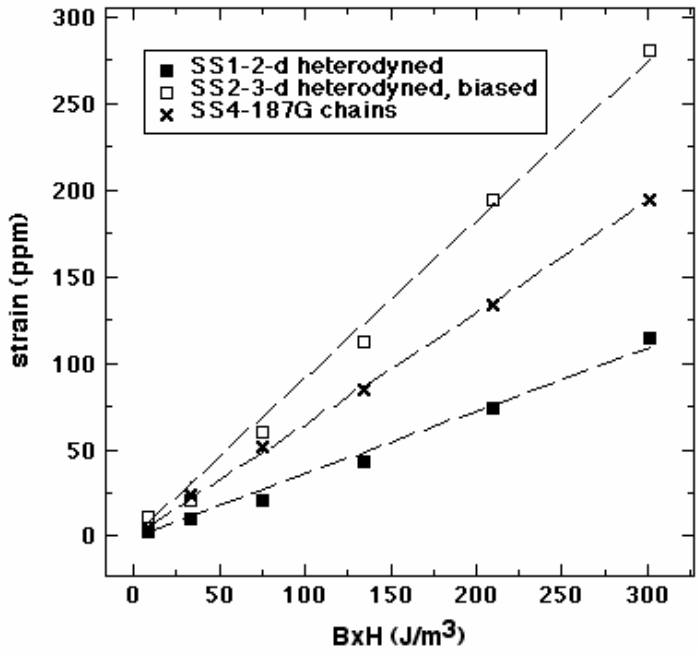

Figure 17. Biased heterodyning leads to composites with greater magnetostriction than those synthesized in a simple uniaxial field.

Triaxial composites. As mentioned above, we have been successful in using triaxial magnetic fields to enhance the susceptibility of particle composites, [12] and according to the self-consistent point dipole theory given above this enhancement should increase the magnetostriction of these materials. To test this hypothesis we made samples with

several triaxial field conditions, including two- and three-dimensional heterodyning. Because the uniform field region of our triaxial magnet is small, we had to reduce the length of our samples, which reduced their aspect ratio. For comparison, a uniaxial composite of the same size, 3.3x3.3x24mm was made. Key results of this study are shown in Fig. 17. As expected, the balanced triaxial field with 2-d heterodyning reduced the magnetostriction relative to the uniaxial sample. But the biased 3-d heterodyned composite showed a significant increase in magnetostriction, consistent with its larger susceptibility. We cannot make a detailed comparison to theory, as our mean-field approach is not valid for composites made in triaxial fields. [12]

Chapter 7

Martin, Anderson

MAGNETIC-FIELD-DRIVEN INSTABILITIES IN SINGLE CHAINS

A remaining issue is why the observed strain depends on the sample preload, when the preloads are clearly sufficient to accommodate a much greater contraction without the particles contacting. This is a complex effect that we believe has to do with field-induced particle clumping transitions. The possibility of clumping was discussed in our paper on electro- and magnetostriction, but here we would like to develop that idea quantitatively. This is a complex topic that at this time is not fully resolved, so in this chapter we wish only to summarize a few basic issues for a single chain.

The elementary physical idea is that of a soft mode in a chain of particles. There are two forces on a particle in a long chain of particles subjected to a longitudinal magnetic field: an attractive dipolar interaction with the other particles in the chain, and an elastic interaction with the gel that tends to localize the particle at the mid point between the vicinal particles. Each of these potentials has a curvature, and when the sum of these curvatures is zero the force on the particle is zero and the chain become unstable to fluctuations.

In the interest of simplicity we will consider a simpler instability: that of a single particle in an elongated chain with all of the other particles held fixed. All of the particles are initially equally spaced and we calculate the force on one single particle displaced a distance ε from the midpoint between its neighbors. If the displacement is positive and the force is negative, or vice versa, then the midpoint is a stable position.

The chain is taken to be aligned along the z axis. Each dipole of moment $\mathbf{m} = m\hat{\mathbf{z}}$ produces a field that along the chain axis is $\mathbf{H}_m = \frac{1}{2\pi r^3} m\hat{\mathbf{z}}$. A self-consistent point dipole calculation shows that the moment of each dipole is $m = v\chi_p H_0 /(1-\chi_p \zeta(3)/6\delta^3)$ where H_0 is the magnitude of the applied field, $v = \frac{\pi}{6} d^3$ is the particle volume, ζ(x) is the Reimann zeta function, and the *elongation* δ=1+γ where γ is the chain strain (at δ=1 the particles just contact.) The particle susceptibility is 3β where β is the permeability

contrast factor defined above. The dimagnetophoretic force on a particle is given by the well-known expression $\mathbf{F} = \mu_0 \mathbf{m} \cdot \nabla \mathbf{H}_{loc}$, which reduces to $\mathbf{F} = \mu_0 m (\partial H_{loc} / \partial z) \hat{\mathbf{z}}$ for an enchained particle, with $\mathbf{H}_{loc}$ the local field.

To compute the force on a particle we need to know the gradient of the local field. This local field is the sum of the applied field plus contributions from all of the other dipoles. From symmetry the local field is an even function and can thus be expressed as a series of the square of the particle displacement. To first order in ε^2 the result is

$$\mathbf{H}_{loc}(\varepsilon) = \frac{\mathbf{H}_0}{1 - \dfrac{\chi_p \zeta(3)}{6\delta^3}} \left[1 + \frac{\chi_p \zeta(5)}{\delta^5 d^2} \varepsilon^2 \right] \tag{18}$$

The force on a particle is thus

$$\mathbf{F} = +\zeta(5) \frac{\pi d}{3\delta^5} \frac{\mu_0 \chi_p^2 H_0^2}{\left[1 - \dfrac{\chi_p \zeta(3)}{6\delta^3} \right]^2} \varepsilon \hat{\mathbf{z}} \tag{19}$$

and we note that this magnetic force is always destabilizing.

The force on a single particle embedded in a gel and displaced in the z direction is $\mathbf{F}_g = -3\pi d G \hat{\mathbf{z}}$, where G is the gel modulus. For a particle in a chain, G will have to be renormalized due to debonding of the gel from the particle in the particle gap region, so G may be regarded as an effective parameter. In this view of the gel each particle is localized as if by a cantilever spring. Elastic interactions between particles are not included, so we simply call this the cantilever model.

The stability criterion is obtained by comparing forces. The single particle becomes unstable when

$$\frac{\zeta(5)}{\delta^5} \frac{\mu_0 \beta^2 H_0^2}{\left[1 - \beta \zeta(3) / 2\delta^3 \right]^2} \geq \frac{G}{n}. \tag{20}$$

The factor n=1 for the single particle fluctuation with the rest of the particles constrained. For the physically more realistic case of unconstrained particles, the soft mode will exhibit itself as a clumping of particles into dimers. Without giving the details, the instability transition is given by Eq. 20, with n=2.

Consider the application of a field to a chain that is prestrained. As the field is ramped up, the particles suddenly dimerize. At a higher field the dimers form tetramers, and at a yet higher field the tetramers form octamers and so forth, so that there is a non-ending succession of clumping transitions, each with its own stability condition. As the field is ramped back down, there is a succession of declumping transitions. But each of these transitions occurs at a lower field than the corresponding clumping transition. For example, a tedious calculation shows that the declumping transition for dimers is

$$\frac{31}{32}\frac{\zeta(5)}{\delta^5}\frac{\mu_0\beta^2H_0^2}{\left\{1-\beta\zeta(3)/2\delta^3\left[1+\frac{6}{\zeta(3)}\left(\frac{\delta-1}{\delta}\right)^2\right]\right\}^2}\le\frac{G}{n}. \qquad (21)$$

De-clumping thus occurs at a smaller field, and the chain is hysteretic.

Stress calculation. Before giving simulation results we must discuss the problem of stress calculation for the cantilever model. In general, the stress in a chain of particles is computed across any particular plane by simply summing the force of interaction between each particle on one side of the plane with all of the other particles on the other side. The force of interaction between the two semi-chains is then normalized by the area associated with the single chain to generate a stress. This computational prescription seems simple enough, but in the cantilever model the force on a particle due to the gel is not a pairwise interaction. How then does this gel force contribute to the stress?

To compute the gel stress we must account for the fact that the gel itself provides the support for the cantilevers. To model this we imagine that the cantilevers are connected to the nodes of a chain of springs, as depicted in Fig. 18. Each of the n Hookean springs has a force constant K and thus in the unperturbed state the tension in

each spring is Kl_0, where l_0 is the unperturbed spring length. Now suppose the particle attached to the cantilever attached to node m+1 is displaced by a force F applied along the chain direction. The effect of this cantilever force is to alter the tension in the springs above and below this node. The tension change in each spring contributes to the magnetic stress in a plane that bisects that spring.

The computation of the change in the spring tension is straightforward. Let x and y denote the spring length below and above node m+1, respectively. The total chain length, which is fixed, is then $L = nl_0 = mx + (n-m)y$. A force balance gives $F = K(x-y)$. Combining these two equations and solving then gives $y = l_0 - \frac{m}{n}\frac{F}{K}$. The tension of the springs above node m+1 change by $-\frac{m}{n}F$ and below node m+1 they change by $+\frac{n-m}{n}F$. Two points are noteworthy. First, the tension change in each spring is independent of the initial (zero field) spring tension. Second, this tension change depends on the position of the particle to which the force is applied, which is an unusual aspect of the cantilever model. The gel contribution to the stress across a plane that intersects spring m, which connects nodes m and m+1, is

$$\sigma_{gel} = \sum_{j=1}^{m} -\frac{j-1}{n-1}F_j + \sum_{j=m+1}^{n} \frac{n-j}{n-1}F_j . \qquad (22)$$

The remaining stress contributions are from the dipolar and hard sphere interactions between particles separated by the stress plane. The sum of these terms gives a sample magnetic stress that is independent of the location of the stress plane, which is an important check on Eq. 22.

Simulations. The implications of this cantilever model of magnetostriction are interesting. To explore the predicted instabilities a dynamics simulation was written that included, in addition to the magnetic and gel forces, both hard sphere interactions and viscoelastic dissipation in the gel, the latter of which serve to damp phonons that would arise from the clumping instabilities. Typical results of this simulation are shown in

stress versus elongation data in Fig. 18. Upon extension a series of de-clumping transitions are observed, until at full elongation the chain consists of equally spaced particles. Clumping transitions occur at lower elongations upon contraction, as expected, causing true hysteresis in the stress curves (the contraction stress is lower, so we have not created a perpetual motion machine of the first kind.) Two points are important. First, because of the energy dissipation it is not possible to obtain the stress from a strain derivative of the dielectric constant. Second, the stress still decays monotonically with the strain, unlike the experimental data, so this single chain model does not explain the preload dependence of our measured magnetostriction. Current work is focused on understanding collections of interacting chains. These calculations show some promise of explaining the preload dependence.

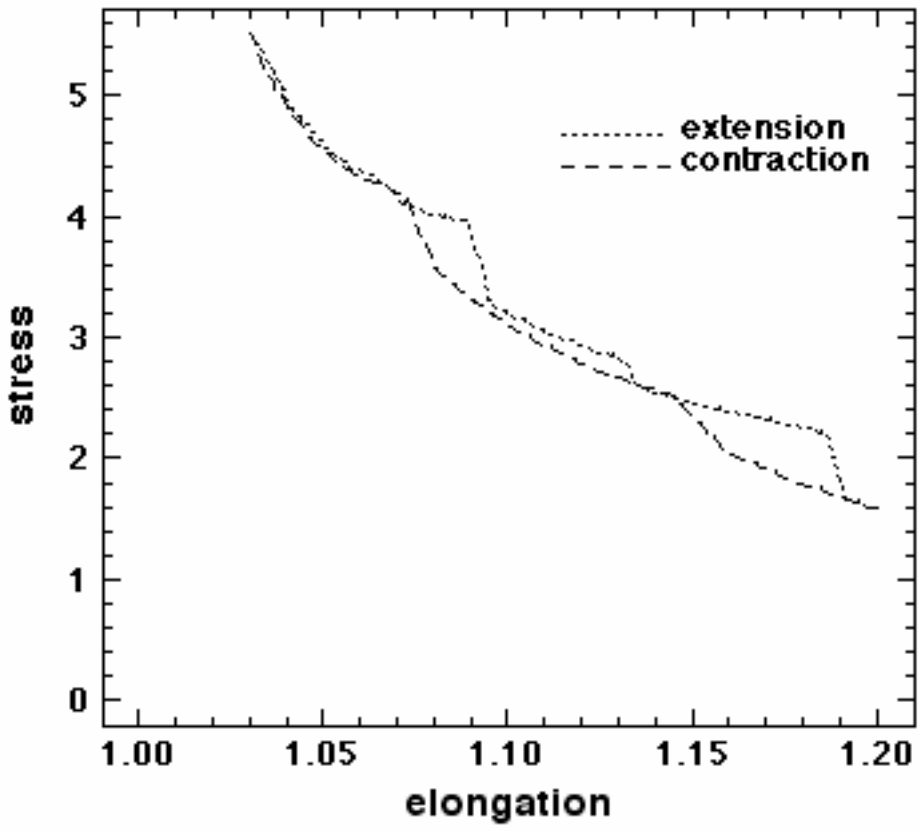

Figure 18. Simulation of the cantilever model shows abrupt changes in the stress that are due to clumping transitions.

Chapter 8

Anderson, Martin

INSTABILITIES IN INTERACTING CHAINS

Introduction

Our experimental observations of magnetostrictive effects, in elastomers containing field-structured chains of roughly spherical magnetic particles, presents us with several unexpected results. One major surprise is that the magnetically-induced contractions increase when tensile prestrain is increased, typically varying in direct proportionality with the prestrain. Modeling a single chain produced field-driven clumping instabilities, but did not manage to reproduce the prestrain dependence of magnetostriction. This raises the possibility that the prestrain dependence is actually due to chain interactions. In fact, this is quite an interesting and subtle subject, since the clumping instabilities *within* a chain generate interactions *between* chains. The reason for this is that the field due to a long single chain of dipoles falls off exponentially fast with the distance from the chain. When this transverse distance exceeds the interparticle spacing the field from the chain can be ignored. But when a field is applied to a chain the particles undergo the clumping instabilities described above, and this causes the field due to this chain to increase dramatically: The exponential fall-off still occurs, but the interaction length scale becomes the average distance between the clumps. This is how the clumping instability induces interactions. To explore the effect of multiple-chain interactions we developed the analytic and numerical analyses discussed here.

In what follows, we assume: (a) monodisperse spheres of magnetic material are embedded in a non-magnetic elastomeric matrix, (b) the magnetic material has high permeability and is magnetically soft (β=1 polarization limit), (c) all spheres are structured into long chains, parallel to the z axis, with the spheres in each chain in contact when the matrix is not mechanically strained, and (d) test samples are much longer (in the z direction) than their width, so that the depolarization contribution to the induced strain can be ignored.

Magnetostriction without clumping

It is informative to calculate the magnitude of the magnetostriction when the spheres are not allowed to form clumps. In this case the sphere-to-sphere spacing in a stretched matrix becomes $(1+\gamma)d$, where γ is the applied tensile strain and d is the sphere diameter. In the β=1 limit the magnetic field along a chain axis at a distance s from a polarized sphere of moment m is $(1/4)(m/m_0)(d/s)^3$, where m_0 is the moment acquired by an isolated sphere in a uniform magnetic field H_0. The local field, including the field arising from all other dipoles of moment m in a long chain is therefore

$$H_{local}/H_0 = m/m_0 = [1+(1/2)\zeta(3)(m/m_0)(1+\gamma)^{-3}], \qquad (23)$$

from which

$$m/m_0 = [1-(1/2)\zeta(3)(1+\gamma)^{-3}]^{-1} = [1-0.601028(1+\gamma)^{-3}]^{-1}. \qquad (24)$$

For samples loaded with 10% or less spheres by volume, the field contributions from neighboring chains (presumed to be uniformly spaced in the x-y plane) is small and has been ignored. Under this circumstance, at zero strain the ratio m/m_0 is 2.5064.

The free energy associated with a polarized sphere in a uniform applied magnetic field of strength H_0 is $-(1/2)\mu_0 m H_0$, where $\mu_0=4\pi*10^{-7}$ Wb/(A m) is the permeability of free space, $m=3v_s H_{local}$, and v_s is the sphere volume. The magnetic free energy per unit sample volume, U_{mag}, is therefore $-(3/2)\phi\mu_0[1-(1/2)\zeta(3)(1+\gamma)^{-3}]^{-1}H_0^2 = -(3/2)\phi[1-(1/2)\zeta(3)(1+\gamma)^{-3}]^{-1}B_0^2/\mu_0$, where ϕ is the volume fraction occupied by the spheres. From evaluating the numerical quantities, we find

$$U_{mag} = -1.19366*10^6\ \phi\,[1-0.601028(1+\gamma)^{-3}]^{-1}\ B_0^2. \qquad (25)$$

With ϕ=0.1 and B_0=1200 gauss (0.12 T), U_{mag} = -1719 J m^{-3} $[1-0.601028(1+\gamma)^{-3}]^{-1}$. At zero strain the energy reduction is 4308 J m^{-3}. The magnetic contribution to the stress can be found by differentiating Eq. 25 with respect to strain, with the result

$$\sigma_{mag} = -2.15227*10^6\ \phi\,(1+\gamma)^{-4}\,[1-0.601028(1+\gamma)^{-3}]^{-2}\,B_0^2. \qquad (26)$$

By using the above ϕ and B_0, σ_{mag} = -3099 Pa $(1+\gamma)^{-4}[1-0.601028(1+\gamma)^{-3}]^{-2}$. Results from evaluating Eq. 26 at various applied prestrains, γ_0, are listed in **Table I**.

Table I: Predicted magnetic compressive stress and contractile strain

10 vol % of β=1 spheres, no sphere clumping, B_0=1200 gauss

Applied prestrain(%)	Magnetic stress: psi & (Pa)	Predicted contraction with sample modulus E=150 psi (1.034 MPa): from comparing σ_{mag} and E from minimization of free energy	
0	2.824 (19470)	1.88 %	-----
2	2.208 (15230)	1.47 %	1.84 %
4	1.772 (12220)	1.18 %	1.37 %
6	1.451 (10000)	0.97 %	1.08 %
8	1.208 (8330)	0.81 %	0.87 %

This table also shows the predicted contraction, γ_0-γ, determined simply by comparing the magnetic stress with a typical experimentally measured modulus, E, of 150 psi ($1.034*10^6$ Pa). The larger contraction found by minimizing the net free energy reflects the increase in contractive force as the spheres move closer to each other.

From either of these calculations, a roughly 50% reduction in magnetostriction is expected as the prestrain is increased from 2% to 8%. We also note that the magnitude of the predicted contraction is roughly consistent with our observation of contractions of the order of 1% under experimental conditions comparable to the parameters used in these calculations.

Magnetostriction with clumping

The above analysis fails to explain our experimental observation of increased magnetically induced contractions in pre-strained samples. Clearly, a major contribution to these magnetostrictive effects is missing from our simple calculations. Thus, we expect that particle-clumping may be playing a significant role, so a computational model has been developed to explore some of these effects.

In the model described below, we relax the condition that the sphere spacing in the chains follows the tensile strain of the matrix, thereby allowing spheres to clump. But we still require that the overall length of the particle chains is consistent with the applied strain, and the present version of the model requires that all sphere clumps be of the same length. Thus, if the clumps are *k* spheres in length, the gaps between the clumps must be *k* times larger than the inter-sphere gaps if the spheres were evenly spaced.

Mean moment. As was implied in the derivation of Eq. 25, the magnetic contribution to the free energy, U_{mag}, obeys the formula

$$U_{mag} = - (3/2)\phi \, (\overline{m}/m_0) B_0^2 / \mu_0, \qquad (27)$$

where $\overline{m}$ is the mean moment of spheres in the chains. Thus, the mean normalized moment $\overline{m}/m_0$ was needed, as a function of applied strain and clump length. Obtaining the moments self-consistently required iterative numerical calculations that included three-dimensional summations of, in some cases, tens of millions of dipolar fields. The requirement that all clumps were the same length allowed all clumps, and in effect all chains, to be treated as identical, which greatly improved the computational economy. Nevertheless, these calculations were sufficiently costly of computational time that finding minimal free energies relied on the use of pre-computed $\overline{m}/m_0$ tables.

In our calculations of $\overline{m}/m_0$, the chains of magnetic spheres are arranged on a square lattice with a chain spacing consistent with a volume fraction of 10%. When tensile strain is applied along the chain axes, the chain spacing is reduced to maintain constant volume fraction.

At finite applied strains, the arrangement of the inter-clump gaps in each chain presents further choices. We investigated two high-symmetry options, in which (a) the gaps in neighboring chains are aligned with the gaps in the central chain and (b) the gaps in neighboring chains are either aligned with gaps in the central chain or are displaced along the z axis to be aligned with the midpoints of clumps in the central chain. In option (b), alignment with gaps or clump midpoints was alternated checkerboard-fashion, an arrangement we will call z-staggered inter-clump gaps. Because substantial electric

fields arise from the ends of the clumps, these two arrangements give markedly different strain and clump-length dependences of the mean moments. The results of option (b), shown in Fig. 19, were applied to our free-energy minimization routines. Option (a) calculations, which yielded a significantly less dramatic dependence on clump length, have not been applied to the model.

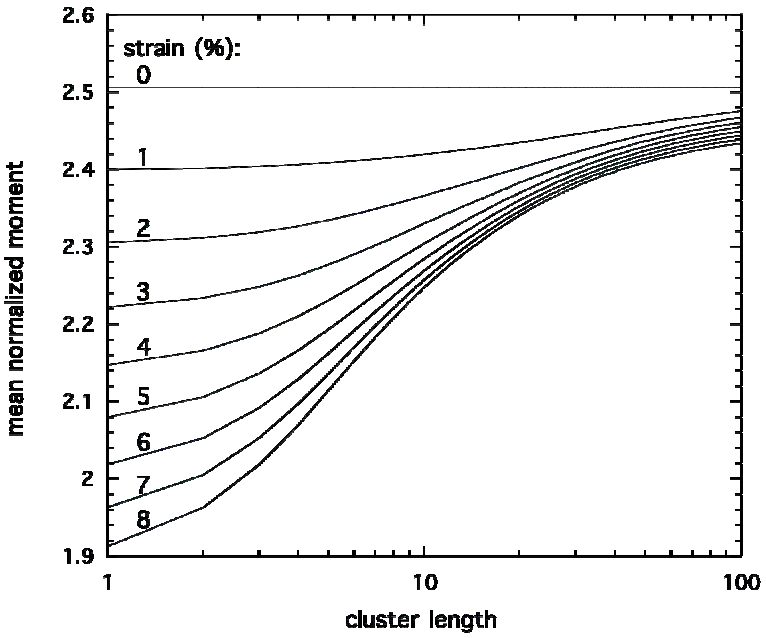

Figure 19. Mean normalized moment $\overline{m}/m_0$ as a function of applied strain and clump length. Volume fraction of magnetic spheres was 10% and chains were arranged on a square lattice with z-staggered inter-clump gaps. Moments were computed for all clump lengths of 10 or less; for longer clump lengths, ten specific lengths approximately equally spaced on the logarithmic axis were computed, and values for clump lengths lying between these were obtained through parabolic interpolation

A further z-position issue arose from the periodic, Bessel-function axial-field component from a line of evenly-spaced dipoles. This field contribution affected the computed mean moment at a ±0.3% level at 20 vol% particle loading, an amount that is quite noticeable because *changes* in the mean moment are the important quantity. At the 10 vol% particle loading invoked in our modeling, the greater chain spacing allowed this field contribution to decay to around ±0.004%, but we still needed to remove it to reduce chaos when minimum-energy conditions were sought. Our first-order nulling scheme

was, in effect, to average the results from the dipole-field summations when the neighboring chains were displaced vertically by plus and minus 0.25 d. This procedure removed all noticeable oscillatory beats in the magnetic energy as a function of clump length.

Mechanical energy contributions. If not for the possibility of particle clumping, the elastic energy density would simply be $U_{\text{elastic}} = \gamma^2 E$. When a constant force (stress=σ_0) is applied, the prestrain satisfies $\gamma_0 = \sigma_0 E$. The energy-density contribution from work done against this constant force (for example, by a change in sample length from magnetostrictive contraction) is given by $U_{\text{stress}} = (\gamma_0 - \gamma)\gamma_0 E$. These two contributions can be combined to give a mechanical energy density $U_{\text{mech}} = (\gamma^2 - \gamma_0\gamma + \gamma_0^2)E$. For convenience the elastic energy due to the prestrain alone can be subtracted, simplifying the mechanical energy density to the formula

$$U_{\text{mech}} = (\gamma_0 - \gamma)^2 E, \qquad (28)$$

where $\gamma_0 - \gamma$ is the contractile strain.

No obviously correct way to model the elastic-energy consequences of particle clumping is evident, therefore we consider two different models. In the first of these models, the spheres in each chain are presumed to be linked together with simple springs that exert no force when the spheres are in contact. A parameter is needed to control the magnitude of the inter-particle forces from these springs, and it is intuitive to specify the fraction, f, of the net modulus of a sample that arises from these springs. In the second model considered the spheres are viewed as individually attached to cantilever springs whose "fixed" ends ride along with the strained elastomeric matrix. The controlling parameter in this case, also denoted f, will be normalized so that a clumping of all spheres into pairs has the same energy cost in either mechanism. In either model the elastic matrix is presumed to be uniformly strained, independent of particle clumping.

In the chain-springs model (m1), clumps of length k have the effect of reducing the number of springs that must be stretched to $1/k$ the total number of springs, but the

inter-clump gaps become k times larger. This results in an elastic-energy clumping cost that is linear in k. By using Eq. 28 the net mechanical energy can be written

$$U_{\text{mech, m1}} = [\,(\gamma_0-\gamma)^2 + f\,(\text{k-1})\,\gamma^2\,]\,E\,. \qquad (29)$$

The matrix modulus receives no contribution from the chains in the cantilever-springs model (m2), but particle clumping causes the springs attached to each sphere to be deformed according to the series $\gamma d[1,3,5,\ldots,(k\text{-}1)]$, for clumps of even length k, and by $\gamma d[0,2,4,\ldots,(k\text{-}1)]$ for clumps of odd length. These series represent only half of a clump because the spring deformation is symmetrical about the clump center. The elastic energy from these deformations varies the mean square of the deformations, or as $\gamma^2[1^2+3^2+5^2+\ldots+(k\text{-}1)^2]/k$ in the case of even k. For either even or odd lengths, the sums in the square brackets, after normalization to k, equal $(k^2\text{-}1)/6$. The net mechanical energy can then be written as (the factor 2/3 equates the elastic energy costs of dimerization in either model)

$$U_{\text{mech, m2}} = [\,(\gamma_0-\gamma)^2 + (2/3)\,f\,(k^2\text{-}1)\,\gamma^2\,]\,E\,. \qquad (30)$$

In this version the elastic energy cost of forming clumps is not linear in the clump length, but approaches a quadratic dependence on the clump length at large k.

Free-energy minimization. Our software automated the search for minimal-energy conditions, where the energy is defined as the sum of U_{mag} from Eq. 27 and U_{mech} from either Eq. 29 or Eq. 30. After the parameter f was input, one has the option of either selecting values of clump length or allowing an automated search for the clump length that minimized the energy (see Fig. 20). In either case, finding the minimal-energy sample contraction (which depended on the two main parameters, clump length and f) was automated. The strain was resolved to 0.001%, with $\overline{m}/m_0$ values at each strain being extracted from the much coarser tabulated values by an interpolation scheme that maintained continuity in both the values and their first derivative with strain. Having a

continuous first derivative was crucial in preventing results from the automated contraction scan from becoming pinned at strains used to prepare the $\overline{m}/m_0$ table.

Figure 21 shows the predicted magnetostrictive effects, under the assumption that the energy-minimizing clump lengths shown in Fig. 20 pertain. We have determined in Chapter 7 that the sphere clumping process is encumbered with hysteresis, and this argues against such clump lengths actually being realized with high precision.

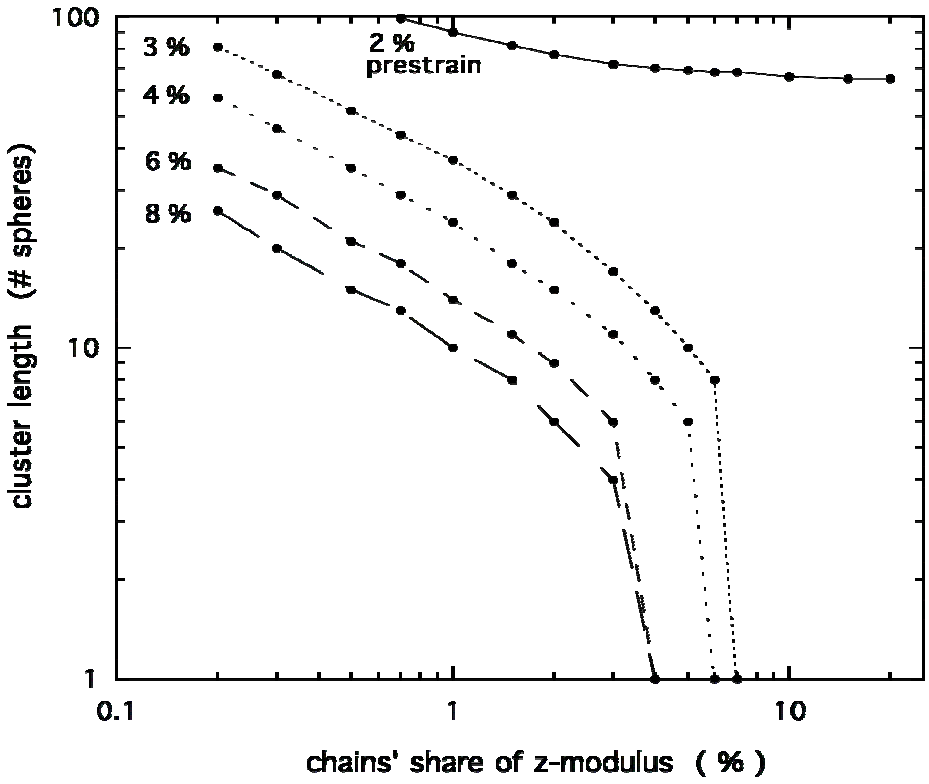

Figure 20. Clump lengths that minimize the free energy, in the chain-springs model, as a function of the chains' share of the z-axis modulus. Volume fraction of magnetic spheres was 10% and chains were arranged on a square lattice with z-staggered inter-clump gaps. The sample modulus was 150 psi (1.034 MPa) and the magnetic field was 1200 gauss.

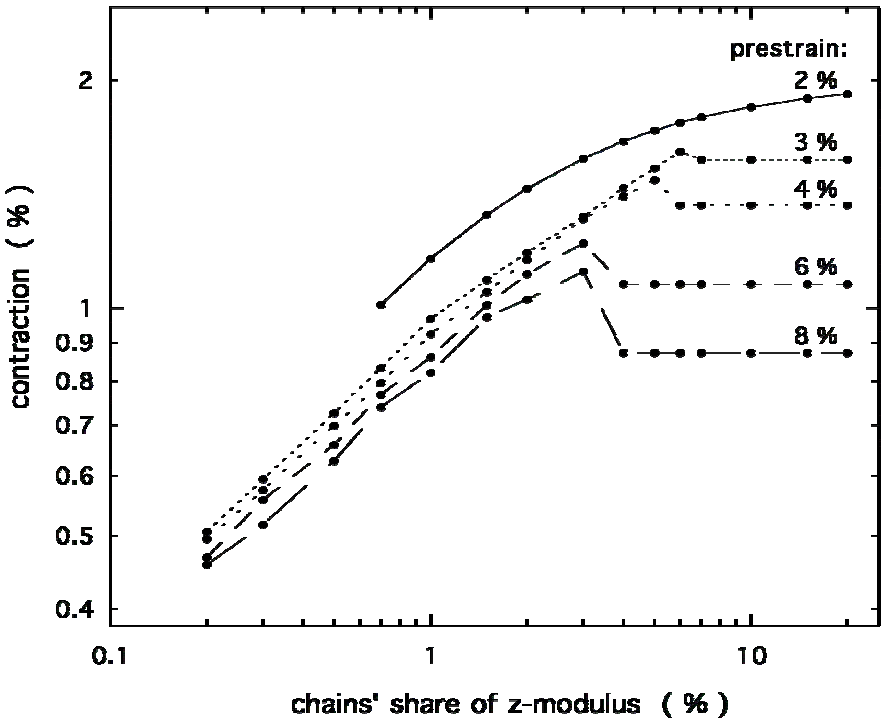

Figure 21. Computed magnetostrictive contraction at clump lengths that minimize the free energy, in the chain-springs model. Physical parameters were as indicated for Fig. 20.

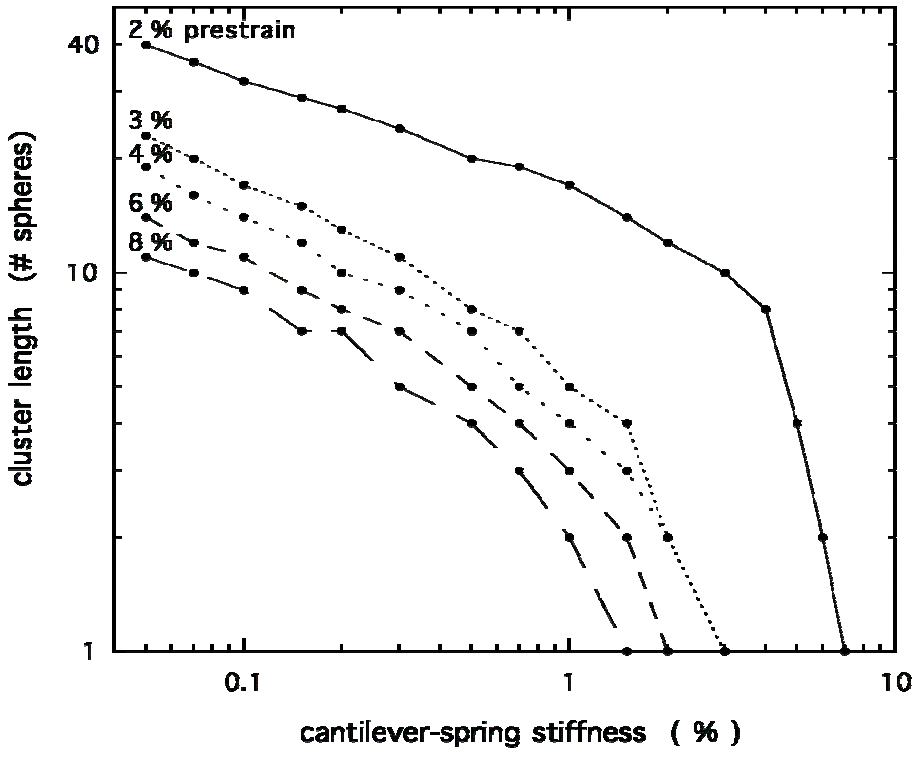

Figure 22. Cluster lengths that minimize the free energy, in the cantilever-springs model, as a function of the cantilever stiffness. The cantilever stiffness is normalized to give the same elastic energy cost of forming dimers in either model. Physical parameters were as indicated for Fig. 20.

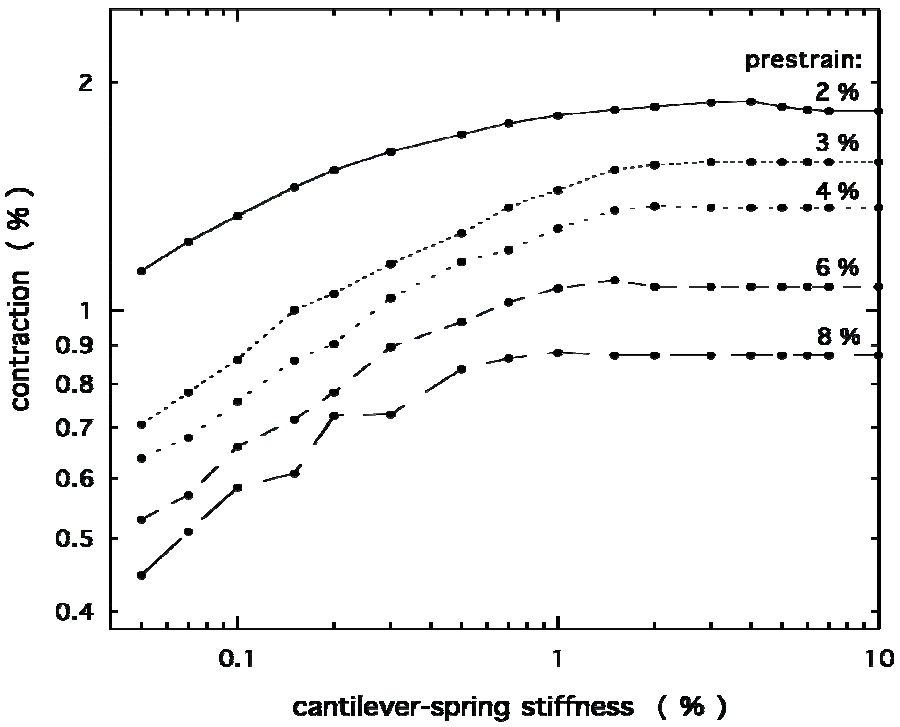

Figure 23. Computed magnetostrictive contraction at clump lengths that minimize the free energy, in the cantilever-springs model. Physical parameters were as indicated for Fig. 20.

Figures 22&23 demonstrate the sensitivity of predictions, of clump size and magnetostrictive effects, to the modeled elastic coupling between enchained spheres. The tendency of sphere clumping to reduce the inverse relation between prestrain and contraction appears to be much less noticeable in the cantilever-springs model, where the elastic energy cost of large clumps rises quadratically, rather than linearly, with the clump length

Discussion

These modeling efforts have not explained our experimental findings of direct variations between magnetostrictive contractions and prestrain, although the inverse variation has been greatly reduced compared to one's naïve expectation. Figure 24 helps to illustrate the complicated relationship between clump length and magnetostrictive contraction. The large dots mark the clump lengths, and corresponding contractions, that would minimize the free energy. It is interesting to note that the predicted contractions would

change to a direct variation with prestrain, were the clump lengths somehow held at 15 spheres for example, beyond the crossing of the curves. Perhaps this curious effect points toward an explanation.

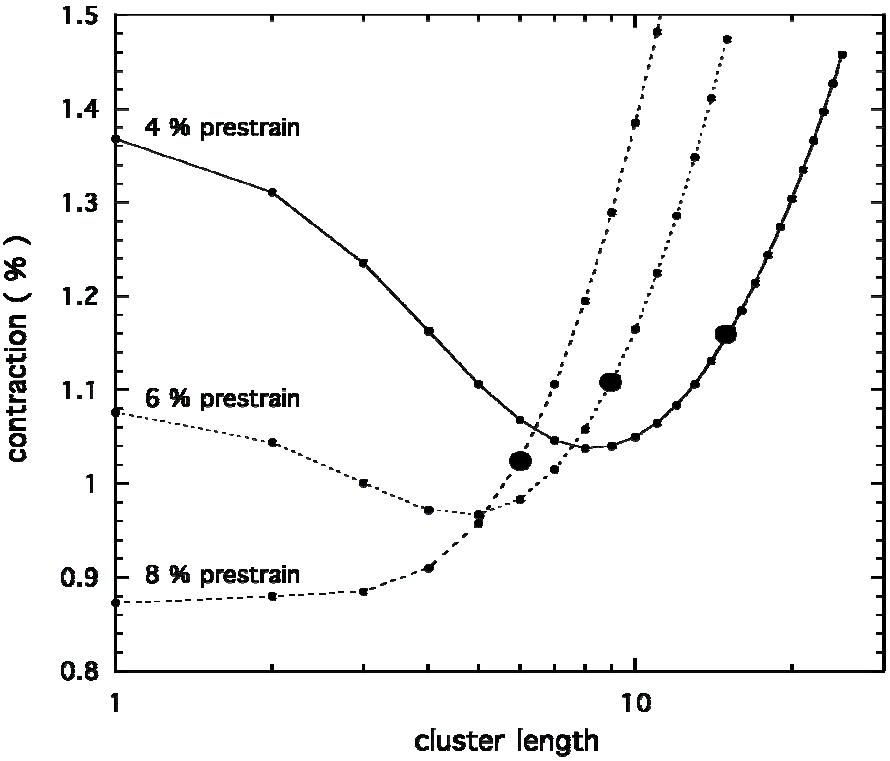

Figure 24. Contractile strain that minimizes the free energy, in the chain-springs model, as a function of clump length. The chains' share of the z-axis modulus was 2%. Large dots mark the minimal-energy clump lengths. Physical parameters were as indicated for Fig. 20.

..

Chapter 9

Martin, Read, Williamson

EXTREME MAGNETORESISTANCE

Introduction

We have shown that field-structured composites (FSCs) of electrically conducting magnetic particles, e.g. Au-plated Ni particles, in a polymer matrix have considerable interest as sensors. [14,15] In particular, as pressure sensors FSCs have shown reversible ~12 decade electrical conductivity changes with strains of only 6%. This is a gauge factor (relative resistance change per unit strain) of 10^{14}, which is ~10^{11} times better than previously known piezoresistive materials. Combining this large piezoresistance with the exceptional magnetoresistance we have observed should lead to exceptional magnetoresistance effects. Measurements we have made indicate that this is indeed the case, even at applied magnetic flux densities less than 0.1T, which are easily achieved with open air copper coils. Here we report on magnetoelastomer composites made with 3-5 micron carbonyl Fe particles coated with Au.

Results

Magnetostriction. A composite of 10. vol.% Au-plated carbonyl Fe particles in a silicone prepolymer (Gelest Optical encapsulant 41) was structured a uniaxial magnetic induction field of 0.08T and cured at 55°C. This sample was molded into a solid rectangle of dimensions 4.9x4.9x27.6mm. The mechanical response of this sample was assessed by constant stress measurements in an optical cantilever apparatus. These response curves are shown in Fig. 25 for samples containing plated and unplated particles. The composite containing the plated particles has a much smaller response, only about 500 ppm strain at an induction field of 0.12 T. This reduced response appears to be primarily due to poor adhesion of the polymer to the plated particles, and partly due to the lower magnetic susceptibility of the Au-plated Fe composite. For example, our

experiments have shown that Ni particle FSCs of Ni particles have only 16% of the magnetostriction of Fe FSCs, even though the magnetic susceptibilities of these composites are nearly identical. Adhesion mitigates against the field-driven particle clumping instabilities that reduce magnetostriction.

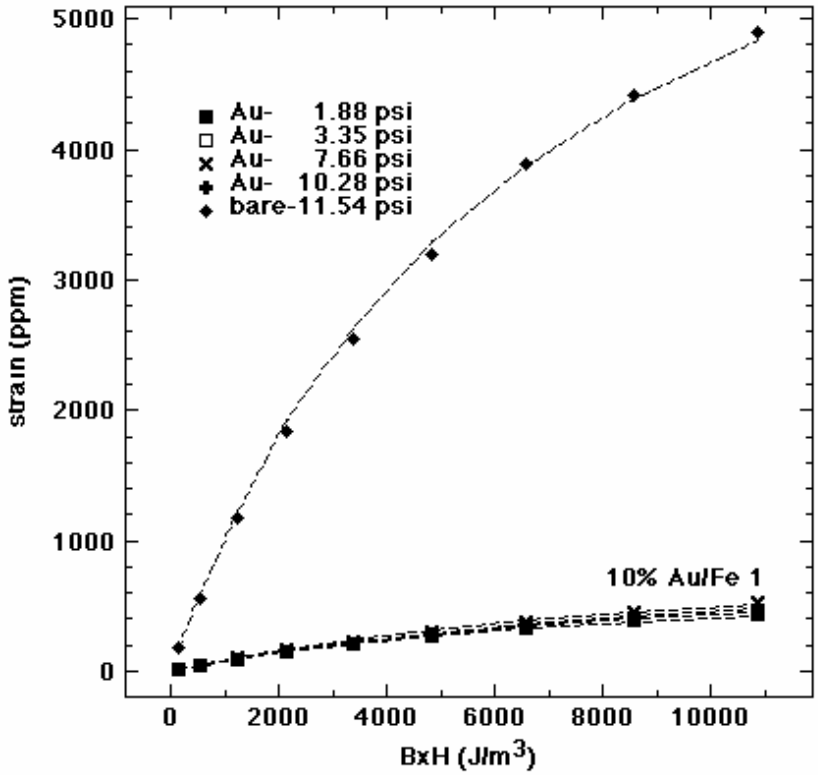

Figure 25. Response curves for Au-plated and unplated Fe particle composites shows that the plated particles give much less response.

Magnetoresisitance. A stress of 35.5 kPa was applied to the Au/Fe particle sample. This stress was chosen to reduce the electrical conductivity of the composite. A field of 0.08 T was then applied to the composite, producing a 300 ppm strain. The magnetoresistance data in Fig. 26 show an extreme effect, roughly 4.7 million percent, the largest value ever observed at this field for any material.

Magnetoresistive materials are usually used for sensing magnetic fields, such as in reading magnetic memory. For these composite materials to be useful for field variations over such small length scales would require a reduction of the particle size. Fortunately, the synthesis of magnetically soft, superparmagnetic nanoparticles is now routine.

Strongly magnetic Fe nanoparticles, with saturation magnetism rivaling that of bulk Fe have now been made, and we have shown that these can be used to create nanocomposites with susceptibilities ten times greater than can be achieved with the carbonyl Fe particles used in this study. Such composites should have very large magnetostriction at small applied fields. If these Fe particles can be coated with Au without significant agglomeration, then these would likely bring the extreme magnetoresistance we have observed into the nanoscale.

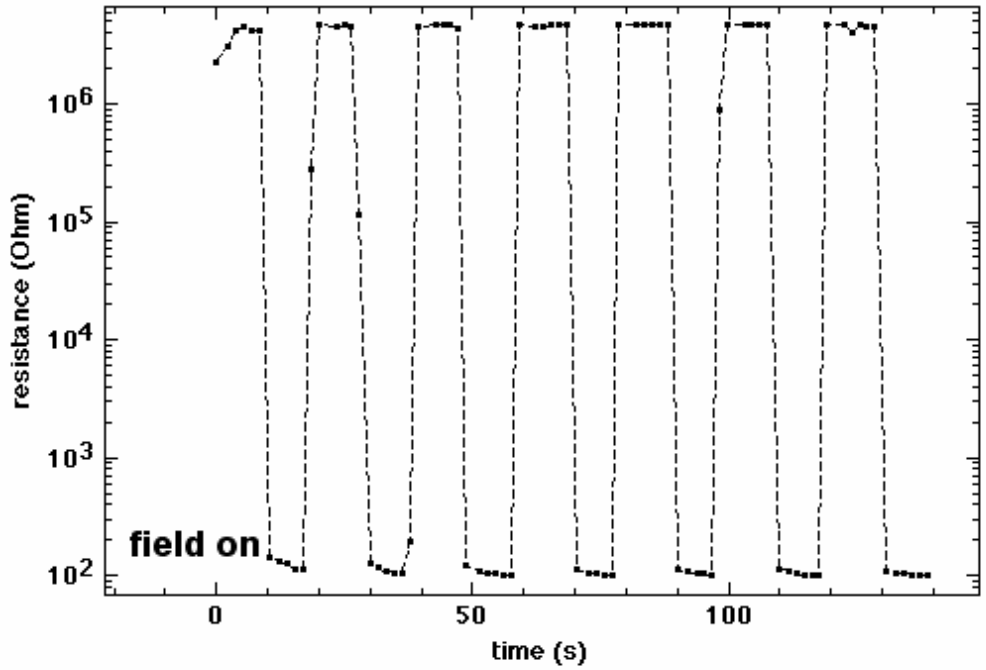

Figure 26. Magnetoresistance data for the Au-plated composite shows nearly five decades of response at a field of ~0.08 T.

The extreme magnetoresistance of FSCs could have other technological implications, such as the ability to use magnetic fields to control the response range of sensors. For example, applying a magnetic field to a chemiresistor would tend to increase the concentration at which it finally transitioned to an insulator, and thus broaden its sensing range.

Chapter 10

Anderson, Martin

SIMULATING PARTICLE CLUMPING IN A MAGNETOELASTOMER

Introduction

In this chapter we consider the behavior, when a uniform magnetic field is applied, of an idealized elastomeric solid that contains an array of parallel chains of magnetic particles. We imagine that these chains extend the length of the solid and that the particles in each chain are in contact with each other in the absence of applied mechanical strain. When such a sample is stretched, we imagine that the particle coordinates are uniformly deformed, resulting in gaps of roughly equal length between formerly contacting particles in each chain.

In the computations reported here, a model 3-D elastomeric solid was held at constant macroscopic tensile strain along the axis defined by the chains. The purpose of these computations was to examine the practicality of determining the equilibrium positions of the embedded particles by means of finite-difference particle-trajectory simulations. We did not attempt to quantitatively emulate the mechanical and magnetic properties of our test samples.

These simulations tracked a large number of particles, and we found that the computational progress toward equilibrium was very slow and showed a rate that fell roughly inversely with the accumulated number of trajectory iterations. Nevertheless, the behavior of this computation was interesting and potentially informative.

Contractile forces in a pre-stretched, magnetic-particle containing elastomer, when a uniform magnetic field is applied, can be viewed as arising from two sources: (1) interactions between magnetically polarized particles embedded in the sample's elastic matrix, and (2) elastic tension in the matrix. The first of these contributions is readily appreciated, but the second contribution, perhaps unexpectedly, also responds to the application of the magnetic field as follows:

When a uniform magnetic field is applied to such a pre-stretched sample,

magnetic forces are generated which each particle in each chain to be attracted to its two neighboring particles. But the forces on a given particle would typically not be perfectly balanced, and small variations in particle spacing, for example, would cause a force imbalance that would grow as pairs of particles became drawn together. If magnetic forces were sufficiently large to overcome the elastic opposition to this small-scale deformation, the process would be expected to result in lengthening particle clumps in each chain. As these clumps lengthened and the gaps between consecutive particle clumps in a chain became fewer, at a fixed macroscopic strain the matrix material in the vicinity of these gaps would become increasingly stretched. Thus, particle clumping could effectively raise the elastic tension in a sample if the sample were held at constant macroscopic strain.

In what follows, we assume: (a) monodisperse spheres of magnetic material are embedded in a non-magnetic elastomeric matrix, (b) the magnetic material has high permeability and is magnetically soft (β=1 polarization limit), and (c) all spheres are structured into long chains, parallel to the z axis, with the spheres in each chain coming into contact when the matrix is not strained.

Model Magnetoelastomer

The model material in our computations contained 5000 monodisperse, unit-diameter spheres of magnetic material that were arranged into 100 individual z-oriented chains, each containing 50 spheres that were in contact in the absence of strain. These particle chains formed a uniformly spaced 10 by 10 square lattice in the x-y plane. Uniform gaps were opened between the particles in a chain when a z-axis tensile strain, 10% in these calculations, was applied. The spacing between stretched chains was consistent with the chosen 20% volume fraction of the spheres. In the absence of magnetic interactions, corresponding particles in the different chains would have resided at the same z-coordinate.

Mechanical interactions. The mechanical properties of our model material were determined by two sets of linear springs. Interparticle forces arising from the elastic

matrix were modeled with springs that linked each sphere to the two adjacent spheres within a chain, and to its four lateral neighbors which were the corresponding spheres in the four nearest neighboring chains. The intra-chain springs generated no force when spheres were exactly in contact, and the inter-chain springs generated no force when the connected particles had identical z coordinates. Note that because lateral cyclic boundary conditions were not applied, particles in chains residing at the lateral boundaries of the model solid were connected with only two or three spheres in neighboring chains.

At the top and bottom ends of each chain, springs having a force constant twice as large as those within the chain were extended beyond the ends of the chains and anchored at upper and lower fixed planes normal to the z axis. The spacing between these planes was set to give a 10% z-axis macroscopic strain. During the course of computations, the z-axis forces that would have been needed to hold the model material at the fixed tensile strain were obtained, at both the top and bottom boundaries, by summing the deformations of the chain-end springs.

A realistic emulation of the mechanical properties of real elastomers, in which the ratio of Young's modulus and shear modulus would be very close to 3:1, was not intentionally incorporated in these simulations. We simply desired a lateral mechanical interaction that would attempt to align the small-scale particle displacements of adjacent chains. Accordingly, the chain-axis springs and transverse springs were assigned arbitrary force constants of 1.0 and 0.2. With these values, the transverse springs had about 60% greater stiffness than would have been consistent with a 3:1 ratio of Young's and shear moduli, but we also ran a simulation in which the transverse-spring interaction was set to zero.

In order to avoid severe interpenetration of adjacent spheres in a chain, a fast-rising repulsive force, corresponding to a spring constant 400 times larger than that of the chain-axis springs, was generated whenever the difference in sphere coordinates became less than unity. This interaction succeeded in preventing sphere interferences greater than a few percent of the sphere diameter.

Magnetic interactions. Each of the dipoles experienced magnetic forces from all other dipoles. These forces were summed from pair-wise dipolar interactions, where both

moments of a pair were treated as independent vectors. But only the projection of the vector force along the z axis was retained.

Note that the demagnetizing field arising at the top and bottom ends of the model elastomer was not compensated by placing capping monopoles at the chain ends or by invoking a cyclic boundary condition there. Thus, the magnetic interactions between the dipoles tended to deform the particle coordinates toward the vertical midplane. This tendency is evident in Figure 27, and this effect stretched the springs at the ends of each chain and increased the calculated chain tension at the chosen macroscopic strain.

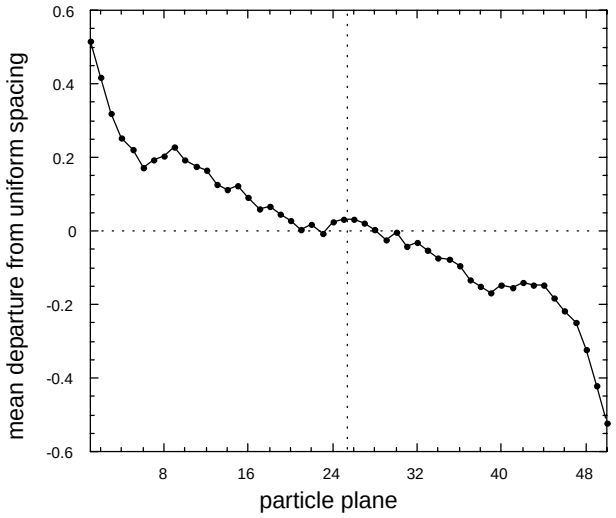

Figure 27. Mean departures, at 800 iterations, of horizontal planes of spheres from their z-positions in the absence of magnetic interactions. Both ends of the model sample are contracted toward the vertical mid-plane. Departures are normalized to sphere diameter.

Self-consistent dipole moments: Each sphere experienced not only the applied magnetic field, but also the fields arising from the moments of all other spheres. In the computations reported here, each dipole moment was calculated from the net field at its location. These calculations were iterated to convergence.

Simulation Method

Physical units. For the purposes of this computation, the applied field, the permeability of free space, and the sphere diameters were all effectively set to unity. And, as was

mentioned, the mechanical force constants were also arbitrarily set. The chosen numerical quantities, however, resulted in comparable mechanical and dipolar forces.

At the outset of a simulation, the coordinates of each of the spheres were determined according to the chosen sphere volume fraction and macroscopic strains. A small random fluctuation, 0.5% of a sphere diameter, was imposed on the z-axis (vertical) coordinates. The initial moments were then found by cycling ten times through a self-consistent calculation of each dipole's moment. At this point, the residual errors in the moments had fallen to a few parts per million.

Main computation. The major segment of a computation consisted of a large number of iterations, each having two tasks. In the first of these, the z-position of each of the 5000 spheres was incremented linearly proportional to the sum of the mechanical and magnetic forces acting on it from all other spheres. This process was analogous to a trajectory simulation with equal time steps and linear frictional drag. The proportionality constant used had been pre-determined, by trial and error, to be near the limit of computation stability. The second task was to re-compute the dipole moments from the local fields by cycling once through the dipoles once, in order to maintain near self-consistency.

Results and Discussion

Transverse springs present. Figure 28 displays the roughly logarithmic growth of tension as a function of the number of computational iterations. This slow evolution predicts that a great number of iterations would be necessary to approach an equilibrium particle configuration. However, this simulated behavior may shed some light on the behavior of actual test samples, if the mechanical response of the samples were limited by viscoelastic behavior. By interpreting the computational iterations as fixed intervals of time, the horizontal axis might be analogous to elapsed time. These results would then predict that particle clumping obeys logarithmic kinetics.

Sections near the center of the solid, showing the evolution of a plane of spheres over the duration of a simulation, are shown in Figure 29. The steady coarsening of the particle clumps in each chain is evident. Note that the gap positions can, in some cases,

be followed from one panel to the next. The tendency for adjacent gaps to be diagonally offset is also apparent.

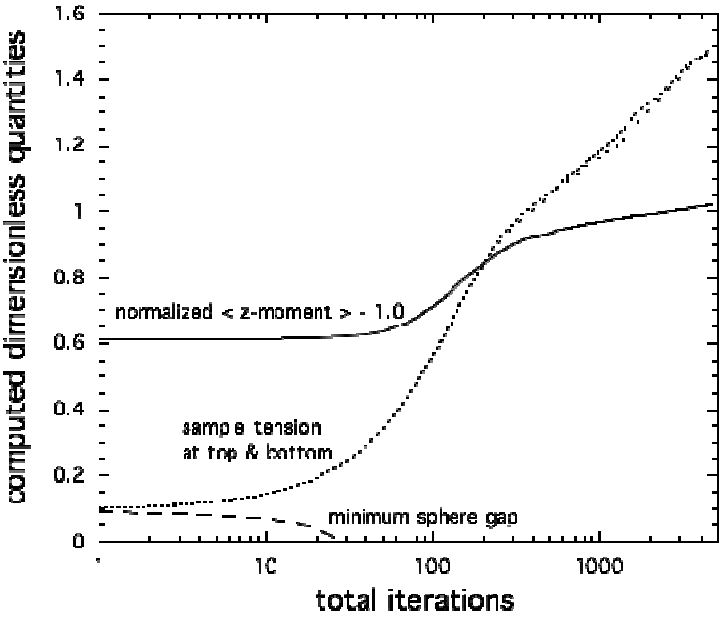

Figure 28. Evolution of the mean z-moment (normalized to the moment of an isolated sphere) and the tension at top and bottom ends of the model elastomer, during the coarse of a computation. Sphere volume fraction was 20% and fixed z-axis strain was 10%.

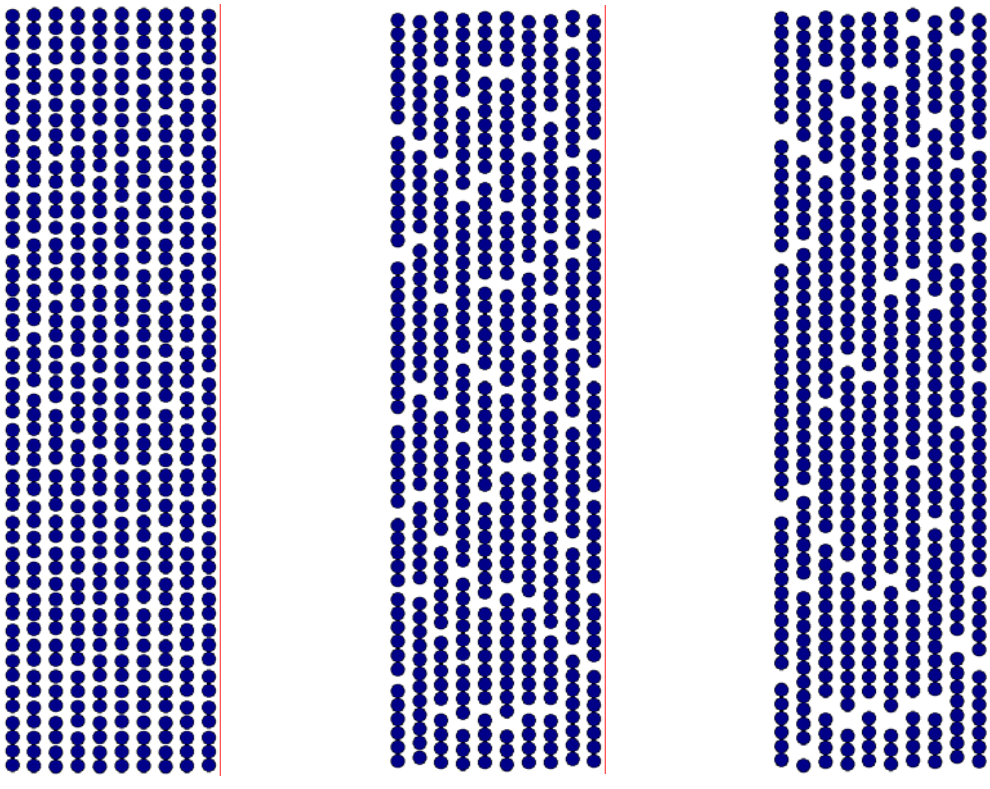

100 iterations 800 iterations 4600 iterations

Figure 29. Evolution of clumping in a ten-chain simulation.

Transverse springs absent: We repeated the simulation, from an identical starting condition, with the transverse mechanical interaction turned off. Figure 30 displays results that can be compared with those in Fig. 28. The mean moment becomes larger, but the growth of tension becomes suppressed compared with the Fig. 28 results.

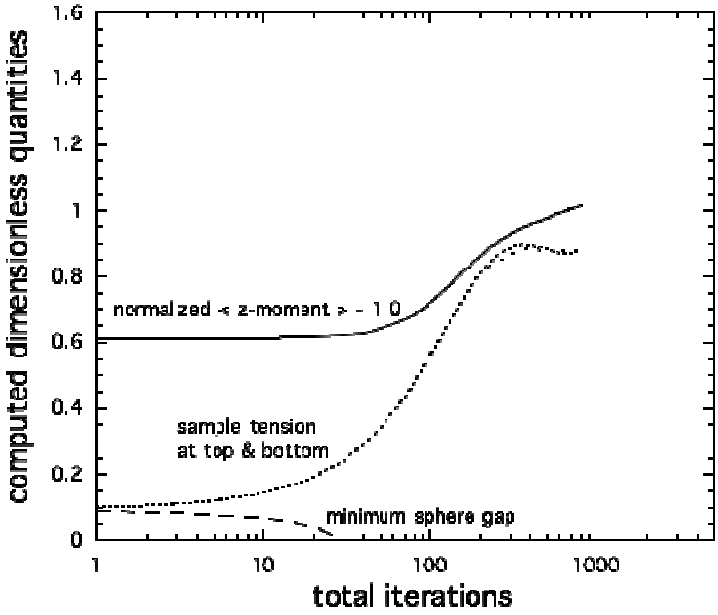

Figure 30. Evolution of the mean z-moment and the tension at top and bottom ends, in the absence of transverse mechanical interactions. This simulation was started identically with the simulation of Fig. 28.

Figure 31 indicates another surprising consequence of omitting the transverse mechanical interaction. The particle clumping is seemingly not greatly affected at 800 iterations, but the particles at the top and bottom ends appear to have a larger variation in vertical positions.

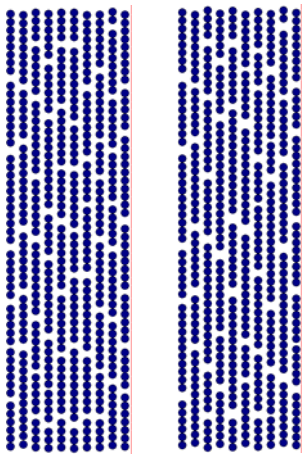

Figure 31. Plane of spheres sectioned in same vertical planes as shown in Fig. 29. These two views compare the clumping structure at 800 iterations with the transverse-spring constant set at 0.2 (left panel) and 0.0 (right panel).

It would be of interest to repeat these computations using real magnetic and mechanical units, and to explore the parameter space.

Chapter 11

Huber, Frankamp

IRON NANOPARTICLES

Introduction

Iron has a number of properties that make it particularly useful as a nanoparticle. Iron is cheap and plentiful, it is environmentally benign, and has no human toxicity except in extreme doses. Its magnetic properties are also very useful. Iron has the highest room temperature saturation magnetization of any element, and its cubic crystalline structure makes it a soft magnetic material. The high saturation magnetization means that an iron nanoparticle can possess a very large magnetic moment, while the fact that it is a soft magnet means that a fairly large nanoparticle (with a correspondingly large moment) can still have a superparamagnetic blocking temperature at a relatively low temperature. The magnetic softness of iron nanoparticles can, however, be overcome if necessary. For magnetic storage applications, where a hard magnet is desirable, iron rods can be used. The shape anisotropy of the nanorods makes them extremely hard. In either case, the high magnetic moment of iron is a huge advantage.

Iron has one major weakness that impacts its usefulness in nanoparticle form, its reactivity. Iron is very reactive towards both water and the oxygen in air. This reactivity manifests itself slowly in large iron structures as rusting, but in nanoparticles can occur rapidly and spectacularly. This has effectively limited the use of iron nanoparticles to inert or reducing environments unless they are pretreated to passivate them towards oxidation.

This section outlines the synthetic approach used to create composite materials containing both micron sized iron particles and superparamagnetic nanoparticles dispersed in the elastomeric polymer. The previously described study of magnetostriction in micron sized magnetic particles prompted an investigation of similar behavior using magnetic nanoparticles to essentially modulate the susceptibility of the polymer medium. To this end, magnetic nanoparticles, both iron and iron oxide, were prepared and analyzed as possible candidates.

Synthesis and characterization of Iron Particles

The most popular chemical decomposition method is the thermal decomposition of iron pentacarbonyl. This method has long been used to make micron-scale iron particles, often called carbonyl iron (these are in fact the type of particles used in the previously discussed micron scale iron composites). The advantage of the decomposition of this species is that its decomposition yield only iron and carbon monoxide, which leaves as a gas. There are no ions or other impurities to be contaminate the product (if the iron pentacarbonyl was pure). Iron pentacarbonyl is also very soluble in organic solvents, which is useful as one will not easily yield metallic iron nanoparticles in an aqueous environment. Iron pentacarbonyl also decomposes at modest temperatures, with the rate becoming appreciable around 100°C and being quite fast around 200°C (at this temperature a typical decomposition reaction can be complete in under an hour). Precise control of particle size is rather difficult in these types of systems, owing to the extraordinarily complex kinetics of the decomposition of iron pentacarbonyl. The decomposition rate, and even the mechanism and kinetic order of the decomposition, are highly dependant upon the reaction conditions. The decomposition is self catalyzed, as well as being catalyzed by numerous other species, so as concentrations change through the course of the reaction, the reaction rate can change greatly. The first literature reports of the formation of iron nanoparticles through iron pentacarbonyl used a variety of polymers as both catalyst and surfactant.[16, 17] A number of other surfactants have been used for this type of reaction, but the essence of the reaction has changes little. The iron carbonyl, an appropriate high boiling point solvent, and the surfactant are placed in a vessel under an inert atmosphere and heated. The carbon monoxide must be allowed to

vent for the reaction to continue to completion, so an oil bubbler is often used as a one way valve.

We have developed a unique method for forming iron nanoparticles from the iron pentacarbonyl decomposition reaction. We utilize a beta-diketone surfactant that binds the particles weakly enough that it does not significantly perturb the magnetic properties of the iron, but strongly enough to prevent agglomeration. This process is illustrated in Figure 33, and the resultant materials are shown in Figure 34

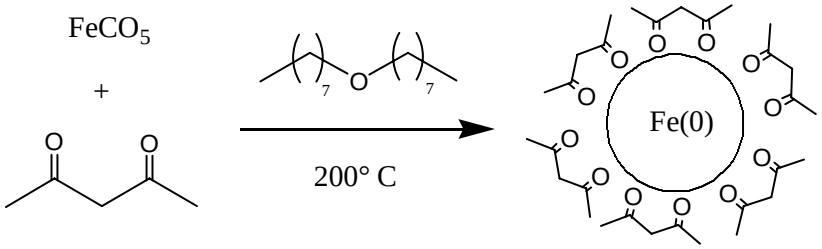

Figure 33. Iron nanoparticle formation using thermal decomposition of iron pentacarbonyl, and our unique surfactant, pentanedione (a beta-diketone).

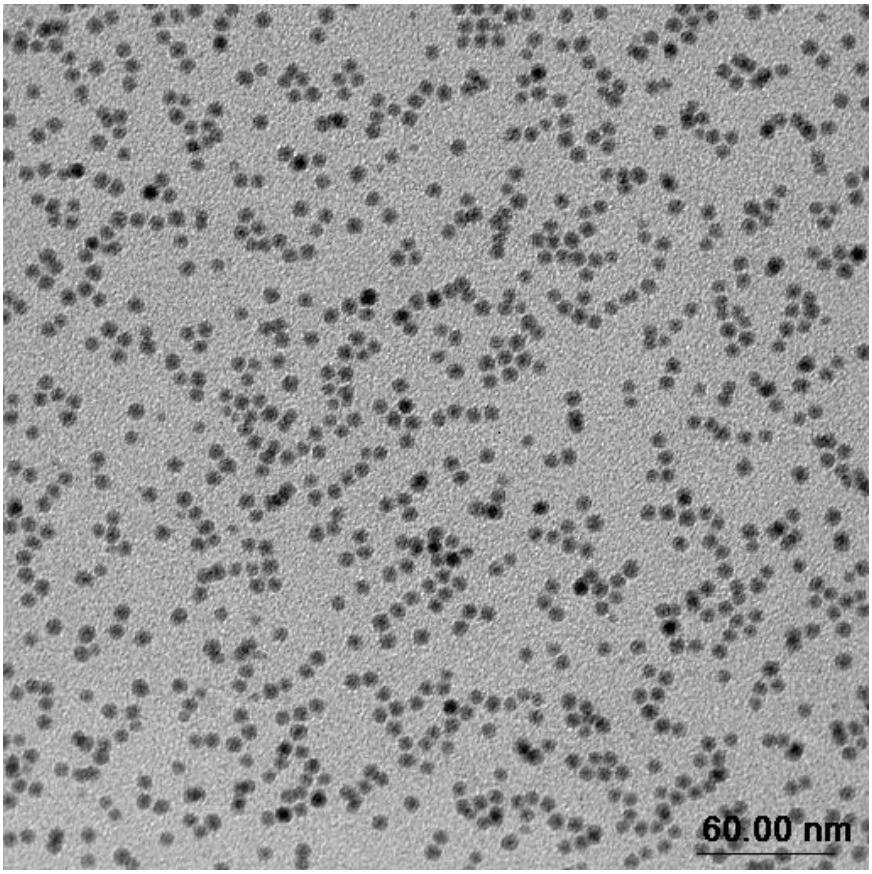

Figure 34. Representative TEM of Fe nanoparticles prepared using thermal decomposition of iron pentacarbonyl.

Iron nanoparticles are extraordinarily reactive, most notably being pyrophoric. It is important to keep this in mind whenever handling iron nanoparticles both for safety reasons and to maintain the nanoparticles' integrity. There are a number of ways to mitigate the extreme reactivity that iron nanoparticles have towards oxidizing agents, including gently oxidizing the surface. By exposing the surface of the particles to a weak oxidizer, or a very dilute strong oxidizer, the particles can be passivated. At ambient temperatures, the oxidation of iron nanoparticles typically produces magnetite, which is a strongly adherent layer that can passivate the particles towards further oxidation. While rapid oxidation produces heat that can lead to delamination of the oxide and wholesale

oxidation in a potentially spectacular reaction, the slow, gentle oxidation of the surface only can protect the core and maintain it as iron. An example of this is shown in Figure 5. Species that have been used successfully for this passivation include: low partial pressures of oxygen, carboxylic acids, and alcohols. While oxidizing the surface may leave the core unchanged, it will still enormously change the properties of the nanoparticle. The chemical properties are obviously greatly altered as are magnetic properties due to the very large fraction of the volume that is contained in the outer layers of the particle. These are also issues for the other methods of preventing oxidation, coating with oxidation resistant coatings, and alloying. Alloying will naturally make an entirely different material, such as iron platinum alloys that are still highly magnetic, but are indefinitely stable in air. Even coating particles has a surprisingly strong effect on the magnetic properties of the particles, generally greatly weakening them. This has been shown by a number of researchers to occur when gold coating iron nanoparticles.

We conducted our own investigations of methods of passivation including gold coating and preoxidizing the nanoparticles (see Figure 35). While both of these methods were successful in preserving an iron core, the did so at extreme detriment to the magnetic properties of the nanoparticles. The gold coated particles were so weakly magnetic that it was difficult to determine a precise value, and the oxidized particles were reduces to only about 60 emu/g. For this reason, this approach was not used for the production of composite materials, though research is ongoing.

We chose instead to attempt to imbed iron nanoparticles into a silicone encapsulent under inert conditions. The silicone would then act as an oxygen barrier for the small amount

of time they would need to be handled in air. This approach met with some immediate difficulty when a commercial encapsulant was used.

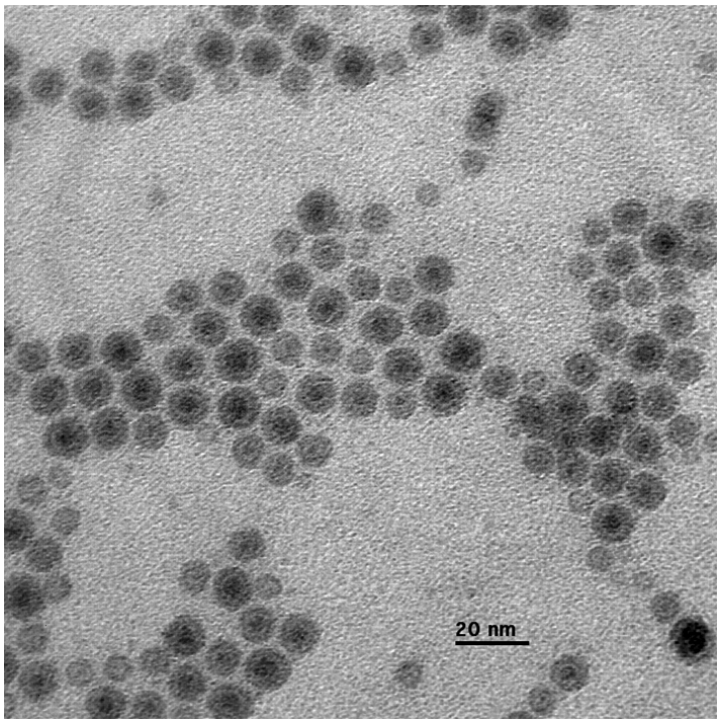

Figure 35. Gently oxidized iron nanoparticles show clear evidence of an oxide layer and a darker iron core.

Commercial silicones universally contain additives to control the cure and final properties of the cured material. These additives and their concentrations are closely guarded trade secrets. One common additive is a thermally unstable cure inhibitor. High purity silicones are often cured through the hydrosylilation reaction shown in Figure 36, which is a reaction that readily occurs at room temperature. To maximize working time at room temperatures, cure inhibitors are added to one of the precursors. Fast cure is desirable, however at a slightly elevated temperature, so cure inhibitors that quickly decompose at these elevated temperatures are generally employed. One common class of thermally unstable cure inhibitors are organic peroxides. These organic peroxides produce oxygen during their decomposition which would be expected to severely harm the magnetic properties of our iron nanoparticles. This was observed in every

commercial preparation attempted, so the decision was made to prepare our own, unadulterated, formulation.

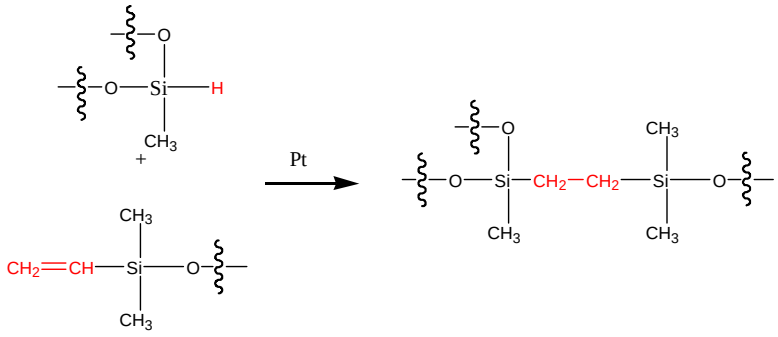

Figure 36. Platinum catalyzed hydrosilation reaction is utilized in bother commercial silicone encapuslants, and our custom formulations.

Formulating this silicone system was not easy, but we were able to devise a method that contained only three components: a vinyl polymer, a silane crosslinker, and a platinum catalyst (in a minute quantity of solvent). We established protocols for systems that cured from anywhere between 5 minutes and 5 hours. We decided that to facilitate handling and degassing, a minimum of 20 minutes was required, but closer to an hour was ideal. The problem arose when adding iron nanoparticles to the mixture. The nanoparticles interact with the platinum catalyst in some way that deactivates them towards the hydrosilation reaction. For example, a system that reliably cured in 20 minutes, when used in the presence of iron nanoparticles the sample failed to set, even after many days. The use of additional catalyst proved effective only when extreme quantities were used, and it was unpredictable and uncontrollable. In light of these difficulties we shifted our focus to more chemically stable magnetite nanoparticles.

Chapter 12

Frankamp, Huber

MAGNETITE NANOPARTICLES

Synthesis and Characterization of Magnetite Nanoparticles

Magnetite nanoparticles were prepared using two different methods. The first method involves the decomposition of iron oleate at high temperature (Figure 37).[18]

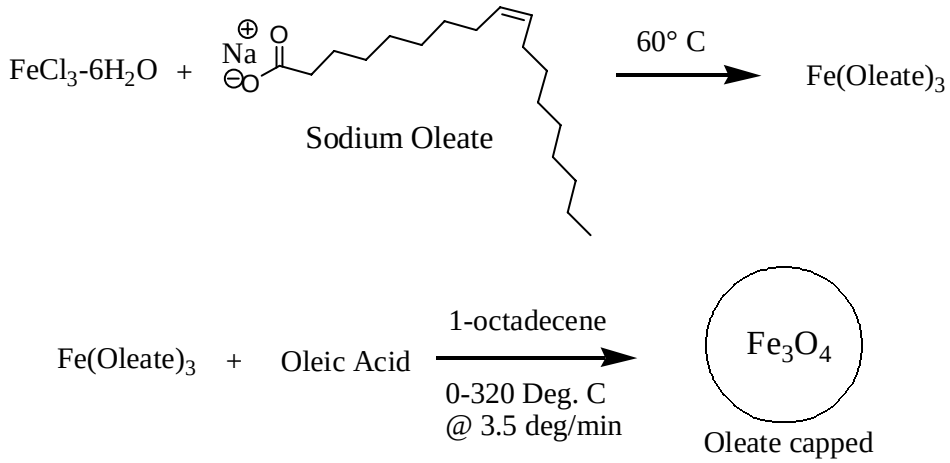

Figure 37. Synthesis of magnetite nanoparticle using Hyeon method.

This method was investigated based on the author's claim of scalability, 40 gram's of final product, and monodispersity, in theory eliminating the need for size selective precipitation to narrow the distribution of nanoparticle size. During this investigation we developed a method to synthesize the sodium oleate compound used in the first step as it is not widely available commercially (Figure 38).

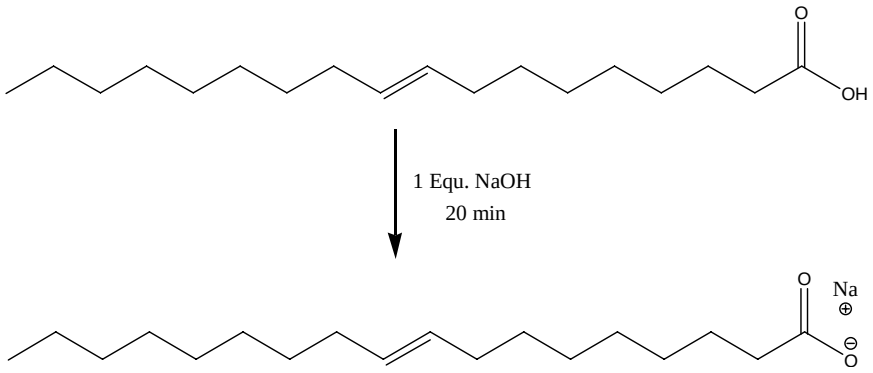

Figure 38. Soponification of oleic acid to sodium oleate using NaOH.

Essentially soponification, the transformation from oleic acid to sodium oleate, was carried out by drop wise addition of one molar equivalent of 3 M methanol solution of NaOH to a rapidly stirring solution of oleic acid. The oleic acid was dissolved in acetone. A white precipitate forms immediately as the carboxylic acid forms a salt complex with incoming sodium ions. The solution was allowed to stir for 20 minutes, followed by filtration and drying under vacuum. On average, the yield of this reaction was better than 95%.

Once we synthesized a sufficient stockpile of the sodium oleate compound the formation of the iron complex proceeded smoothly at 70° C, resulting in a viscous, deep red oil. The remaining challenge was to control the rate of heating, as the preparation method calls for a steady increase of 3-3.5° C per minute up to a final temperature of 320° C. This presented a challenge because our thermocouple controlled hot plate was insufficient to bring the required mass of solvent and precursor to the desired final temperature, soaking out at ~ 270° C. To overcome this obstacle we used a heating mantle and variable transformer which easily provided the energy needed to reach 320° C. Unfortunately, the rate of heating was difficult to regulate. We decided to manually ramp the power settings to bring us to the desired temperature in the appropriate amount of time. Several batches of nanoparticles were prepared using this method and a representative TEM is shown in Figure 39.

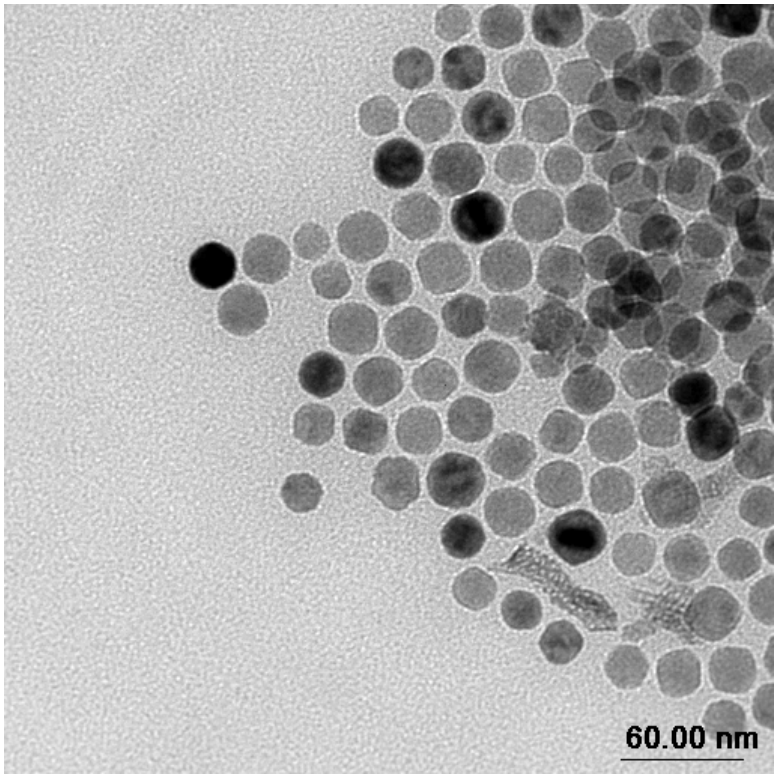

Figure 39. Representative TEM of magnetite nanoparticles formed using iron oleate precursor.

It is clear from the TEM that the size distribution is not uniform as predicted form the literature. In addition, we were never able to reproduce the quantity of nanoparticle reported in the reference 1. Furthermore, the particles produced using this method was not easy to purify often resulting in a 'goo' rather than a particulate powder.

Given these synthetic challenges we decided to investigate a more straight forward method of magnetite formation using the coprecipitation of ferric chloride and ferrous chloride in the presence of ammonium hydroxide. [19] The general synthetic scheme for this coprecipitation method is outlined in Figure 40.

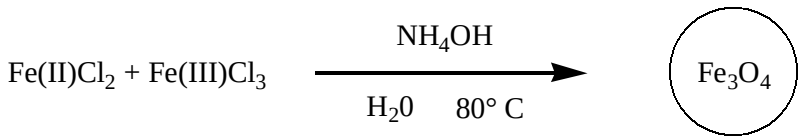

Figure 40. General synthetic scheme for the preparation of magnetite from the coprecipitation of iron (II) and iron (III) chloride with ammonium hydroxide.

Characterization

In general a 1:2 (Fe(II) to Fe(III)) molar ration of iron salts where taken up into water and sparged with nitrogen gas for 30 minutes as the temperature stabilized at the desired temperature. To this solution the ammonium hydroxide was added drop wise through an addition funnel with vigorous magnetic stirring. There are several advantages to this preparation method. The first is the ease of synthesis, no controlled heating required, and the relatively benign starting materials. Secondly, this preparation method can be used to produce large quantities of magnetite. We were able to produce enough material to prepare all subsequent magnetostriction samples from the *same* batch of nanoparticle. Finally, it is very easy to purify and, if need be, can be functionalized to change the surface chemistry of the particles. The drawback is a more polydisperse sample than the previously discussed Hyeon preparatory method. A representative TEM is shown in Figure 41 with selected area electron diffraction (SAED) data shown in Figure 42. The SAED data is summarized in Table 2 and strongly indicates the presence of cubic magnetite.

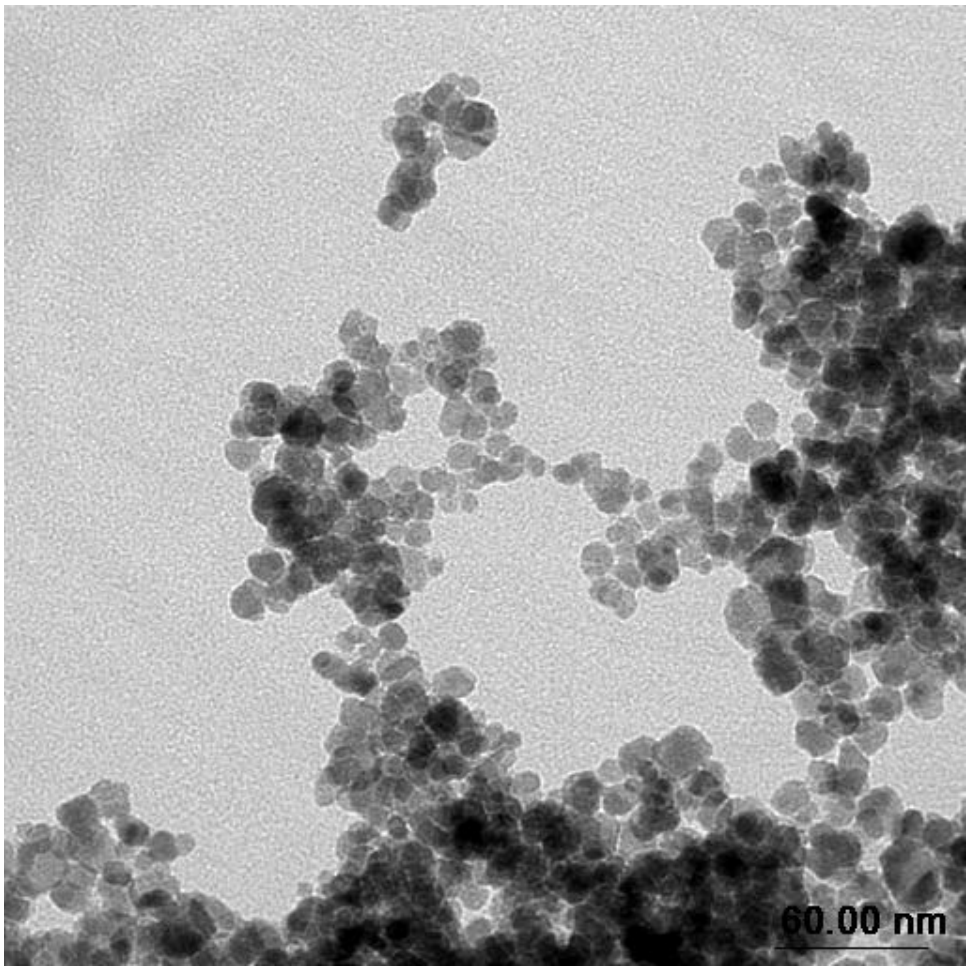

Figure 41. Representative TEM image for coprecipitation synthesis of magnetite.

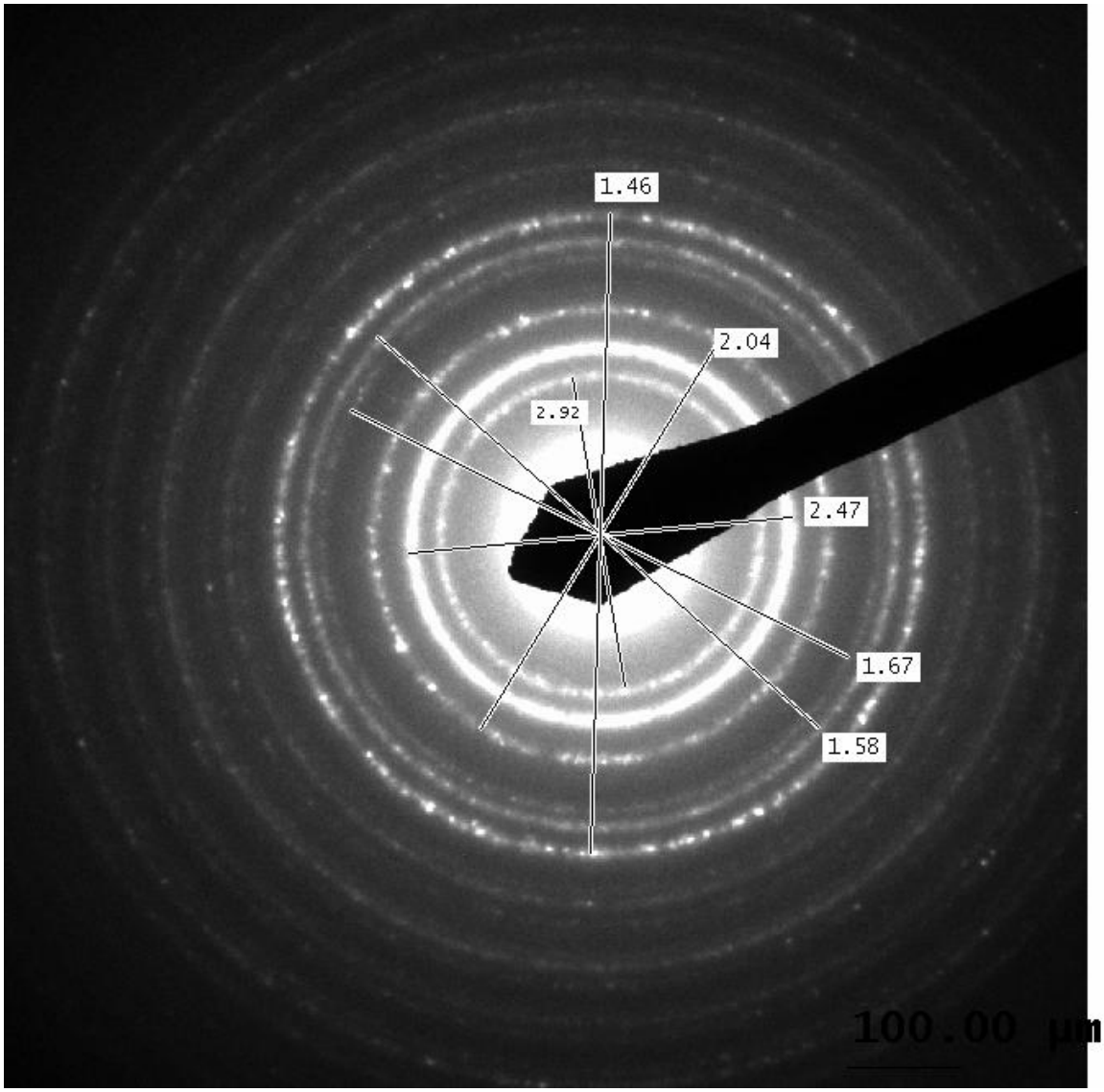

Figure 42. SAED of magnetite nanoparticles prepared using the coprecipitation method.

Table 2. SAED of magnetite sample prepared using coprecipitation.

Measured Spacing (Å)	Magnetite Standard (Å)	Hkl	Intensity
2.92	2.86	200	30
2.47	2.44	311	100
1.67	1.65	422	20
1.58	1.56	511	40
1.46	1.43	400	50

SQUID analysis was performed to elucidate the magnetic properties of these particles. In general we are looking for particles that exhibit a blocking temperature very near to the working temperature, that is to say somewhere near 298 K. It is clear from Figure 43 that the blocking temperature is somewhere above 280 K, the melting temperature of the Poly Ethylene Glycol used as a binder in this experiment. Also, we see some coercivity, 8 Oe, at 295 K indicating that there are 'blocked' particles in the sample (Figure 44). This slight coercivity could be explained by a small population of particles that are not within the superparamagnetic regime. In fact, several particles with diameters in the +20 nm range can be seen in the above TEM data (Figure 9), these could easily account for this slight hysteretic behavior at this temperature.

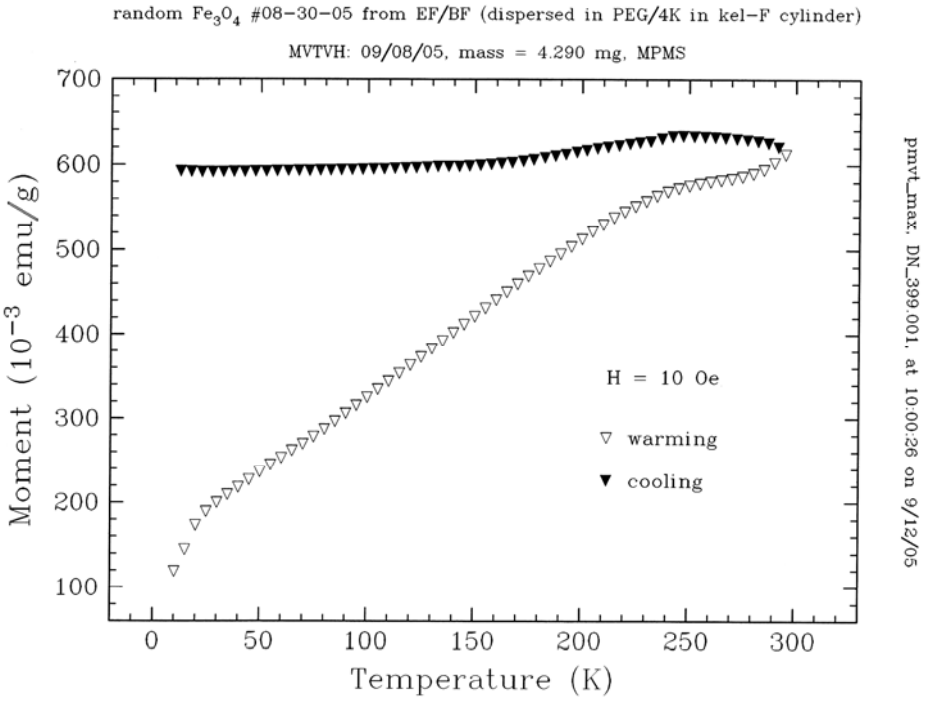

Figure 43. The blocking temperature of the coprecipitation magnetite sample.

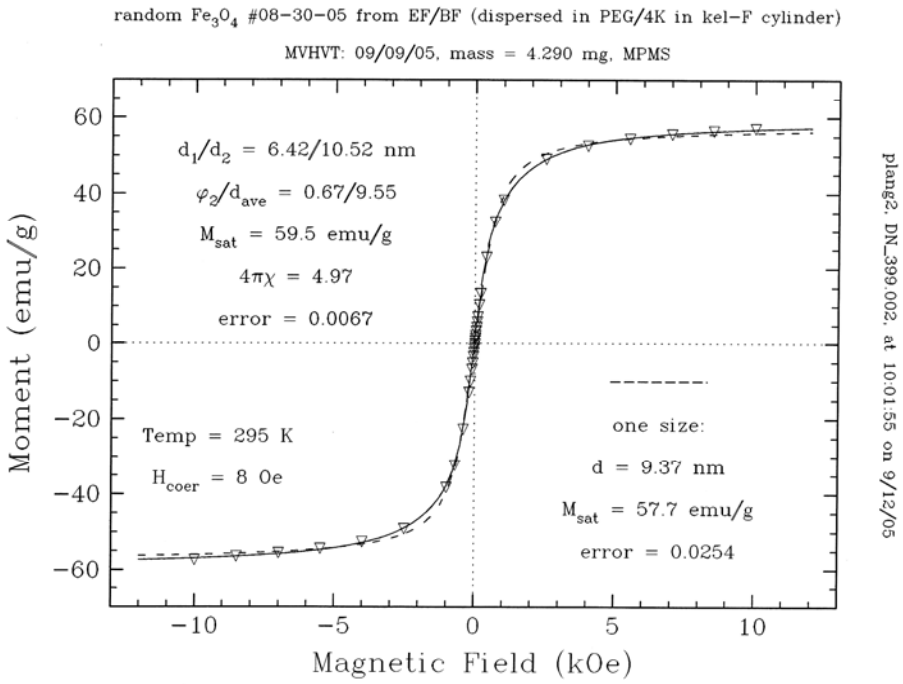

Figure 44. Hysteresis plot shows a slight coercivity at this temperature and a M_S close to the bulk value for magnetite.

A small portion of the hysterisis measurement was repeated over a range of temperatures and is plotted in Figure 45. As we would expect, the coercivity (H_C) steadily decreases inversely proportional to the rising temperature.

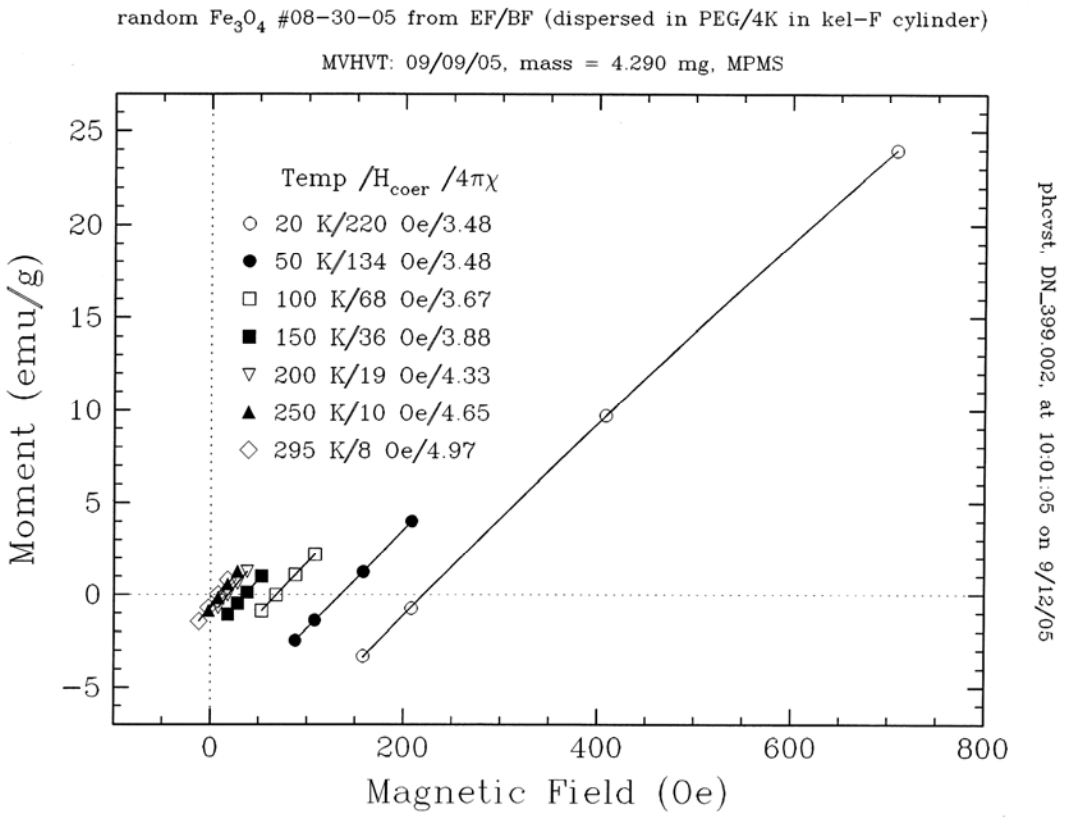

Figure 45. Comparison of the slope near the origin at various temperatures provides both coercivity and a scaled susceptibility.

Chapter 13

Huber, Frankamp

PREPARATION OF NANOPARTICLE CONTAINING MAGNETOSTRICTIVE ELASTOMERS

Preparation of Magnetostriction Samples

As stated earlier, the purpose of creating a sample of magnetite was to systematically manipulate the susceptibility of the matrix used to create magnetoresponsive materials. To that end, a series of samples were prepared with a constant volume percent of carbonyl iron, diameter 200-400 nm, using the magnetite nanoparticles to 'dope' the PDMS matrix. Samples with magnetite ratios of 0, 3, 5, 7, and 9 volume percent were mixed, degassed, and cured overnight at 60° C in a uniaxial field. Careful attention was given to vacuum degassing the slurries prior to heating to ensure that no voids were left in the body of the sample.

In general the molds required 0.500 mL total volume to be completely filled. Taking this into account we would prepare samples of ~ 0.150 mL excess volume to ensure proper filling of the mold area. The degassing process consisted of several cycles between vacuum (~ 100 mtorr) followed by rapid pressurization to collapse surface bubbles. This process was repeated 3 to 4 times until the dissolved gas, as evidenced by a limited number of bubbles, was negligible. Following these evacuation cycles the sample was repeatedly struck against the bench top to facilitate the migration of any remaining bubbles to the top of the sample and ultimately out into the atmosphere. If this vacuum degassing step was not performed numerous voids were present as seen in Figure

14. After curing the samples were carefully freed from the mold, measured to obtain physical dimensions, and analyzed using a home made magnetostriction apparatus.

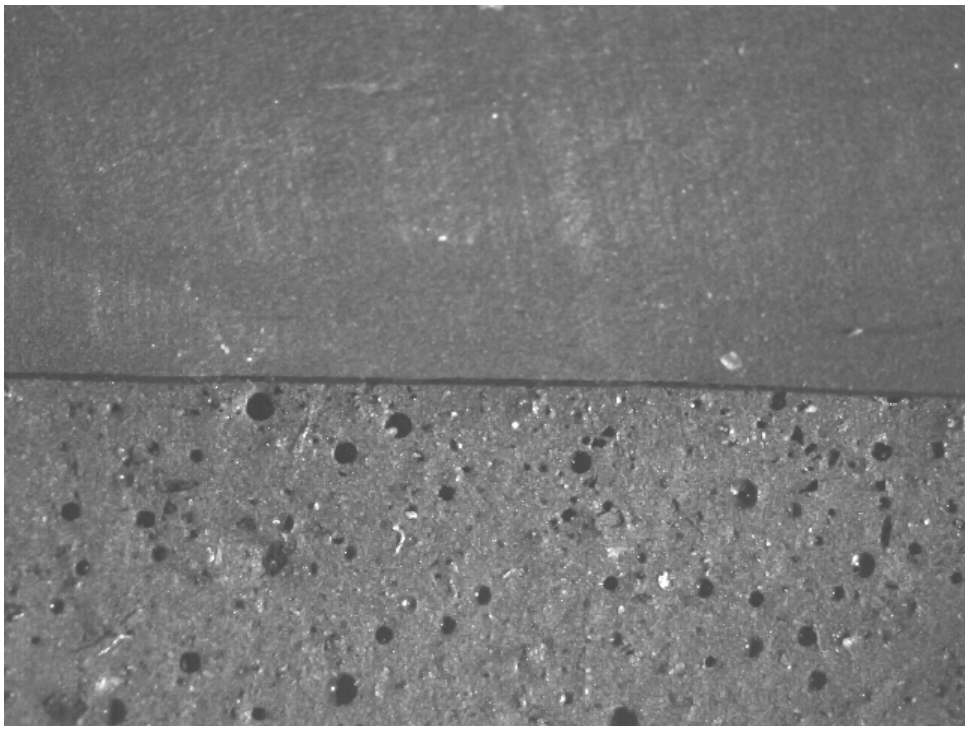

Figure 46. Fully degassed sample (top) is free of voids compared to a sample cured without careful vacuum treatment (bottom).

Chapter 14

Huber, Frankamp, Martin

MAGNETOSTRICTION MEASUREMENTS OF NANOPARTICLE CONTAINING MAGNETOSTRICTIVE ELASTOMERS

Introduction

We predicted that the addition of magnetic nanoparticles to micron scale magnetostrictive composites would yield an effective increase in the susceptibility of the matrix. Due to the large size difference between the two particles, and the lack of mobility in a cured matrix, it was anticipated that the individual susceptibility of the nanoparticles and matrix could be simply averaged. This would yield a matrix with a higher effective susceptibility, which would provide for a higher magnetostrictive response. It appears, however, the behavior is not this simple.

The first indication that the nanoparticle filler would not behave as expected was that the nanoparticles decreased the modulus of the composite. Typically, when rigid inclusions are place in an elastomeric matrix, the composite shows a higher modulus than the pure matrix. In most cases the modulus then increases with increasing loading. It was therefore surprising to see that the addition of nanoparticles to the magnetostrictive composites yielded a decrease in modulus (see figure 47).

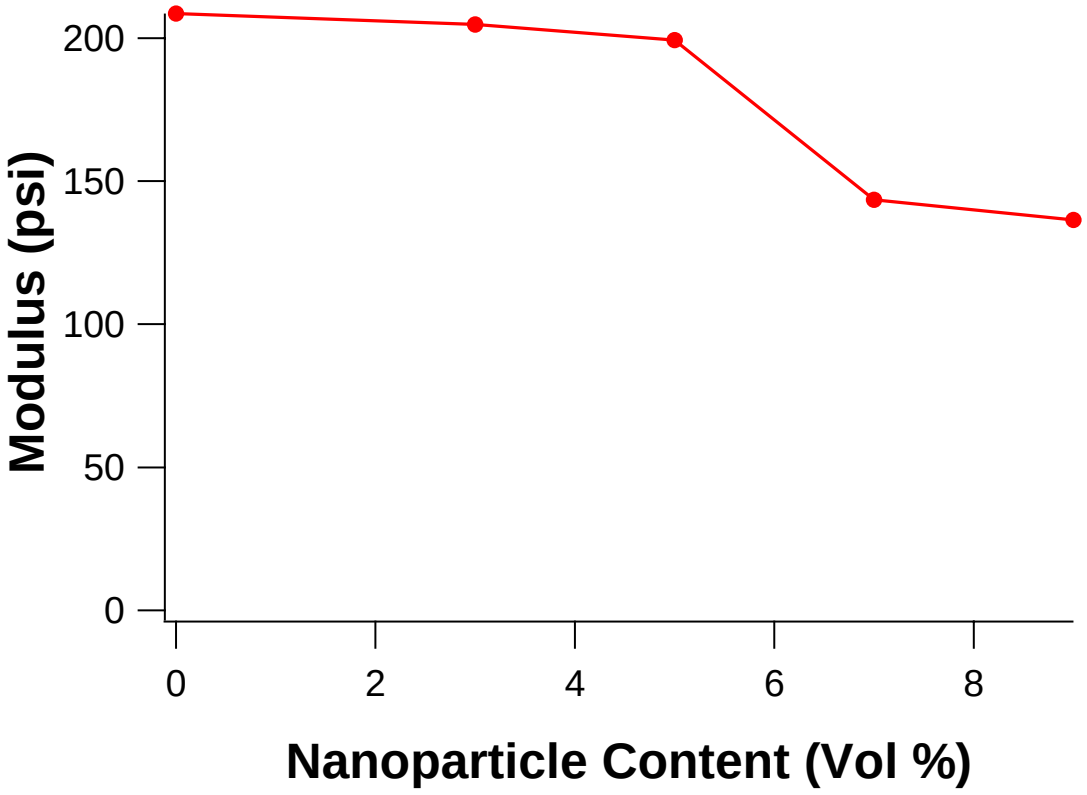

Figure 47. The modulus of the composite decreases slightly upon incorporation of larger volume fraction of nanoparticle.

There are a number of possible explanations for this decreasing modulus. The matrix may have weak adhesion to the nanoparticles, allowing the matrix to deform around them. The nanoparticles may phase separate in a manner that creates weaknesses, or they may associate with the micron particles in such a way as to negate their positive influence on the modulus.

Interestingly, the magnetic response was also opposite what we anticipated. The addition of nanoparticles weakens the magnetostriction of the composite, despite the increase in magnetic material (see figures 48 and 49). There appears to be something structural causing this unusual behavior, and a simple model with well dispersed nanoparticles will not explain it.

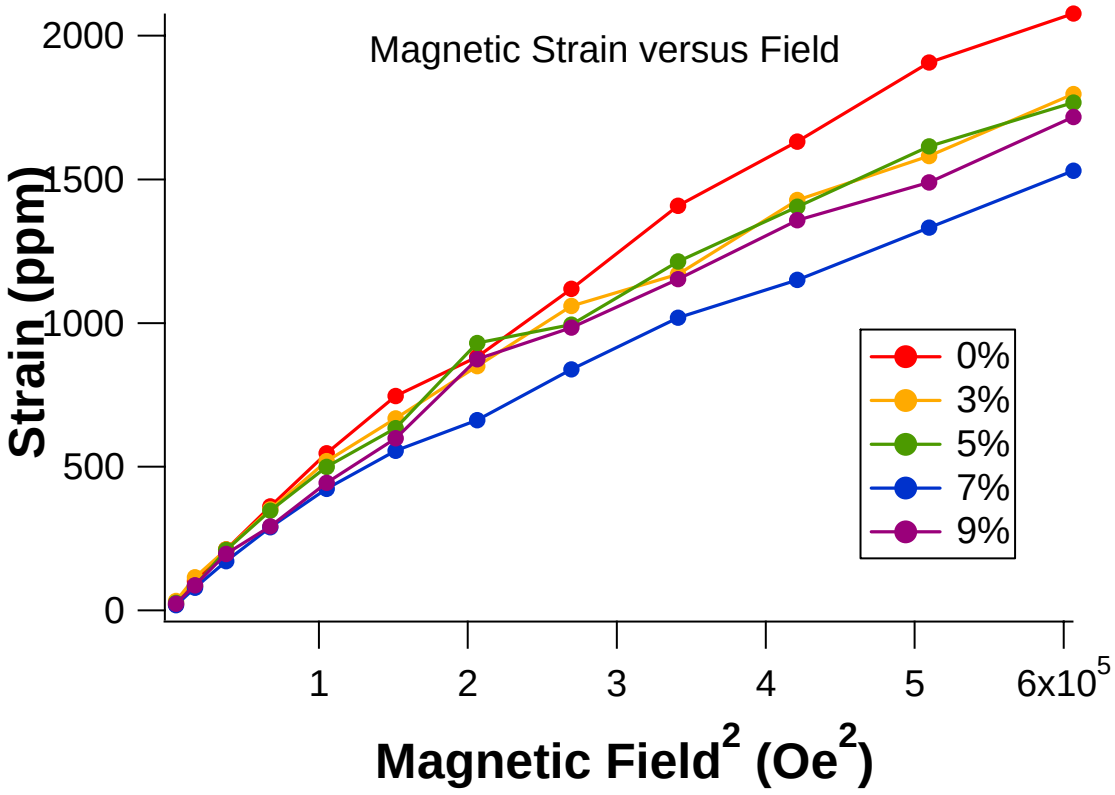

Figure 48. We observe an over all decrease in the magnetostrictive character upon magnetite doping.

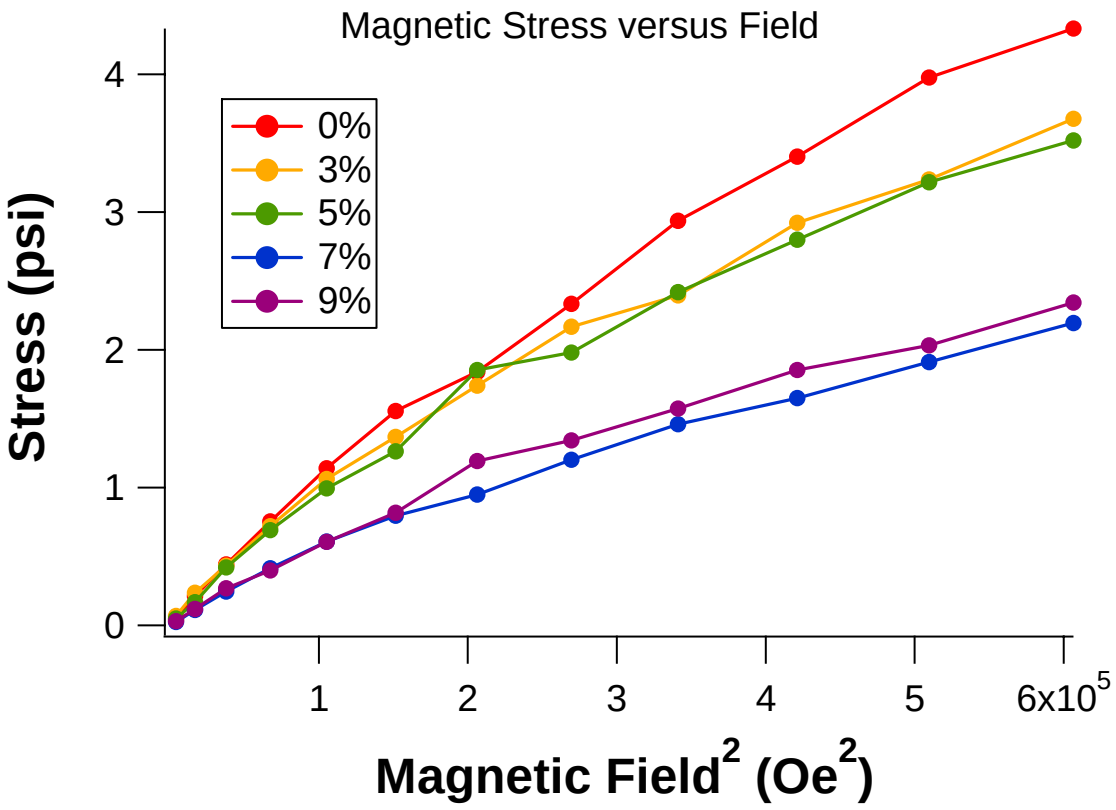

Figure 49. Plots of stress versus applied field clearly demonstrate the systems response to higher loadings of nanoparticles

Data

The nanoparticles themselves can be used to create a magnetostrictive composite, though its response is not as strong as the micron scale composites. This was expected due to the weaker magnetic properties of the magnetite nanoparticles compare to the iron particles, and is not necessarily due to the size of the particles. The magnetostrictive strain of a 9 volume percent nanocomposites is shown in figure 50. Though the magnitude of magnetostriction is about 30 times lower than in a 20% micro-composite, the magnetostriction is still well within the sensitivity of the instrument. It is worth noting that the modulus of the nanocomposite is calculated to be 146 psi, which is higher than both the 9% nanoparticle hybrid and the 7% nanoparticle hybrid, and substantially higher than the unfilled polymer. The nanoparticles therefore do not inherently lower the modulus of the composite, but do so only in conjunction with the micron scale particles.

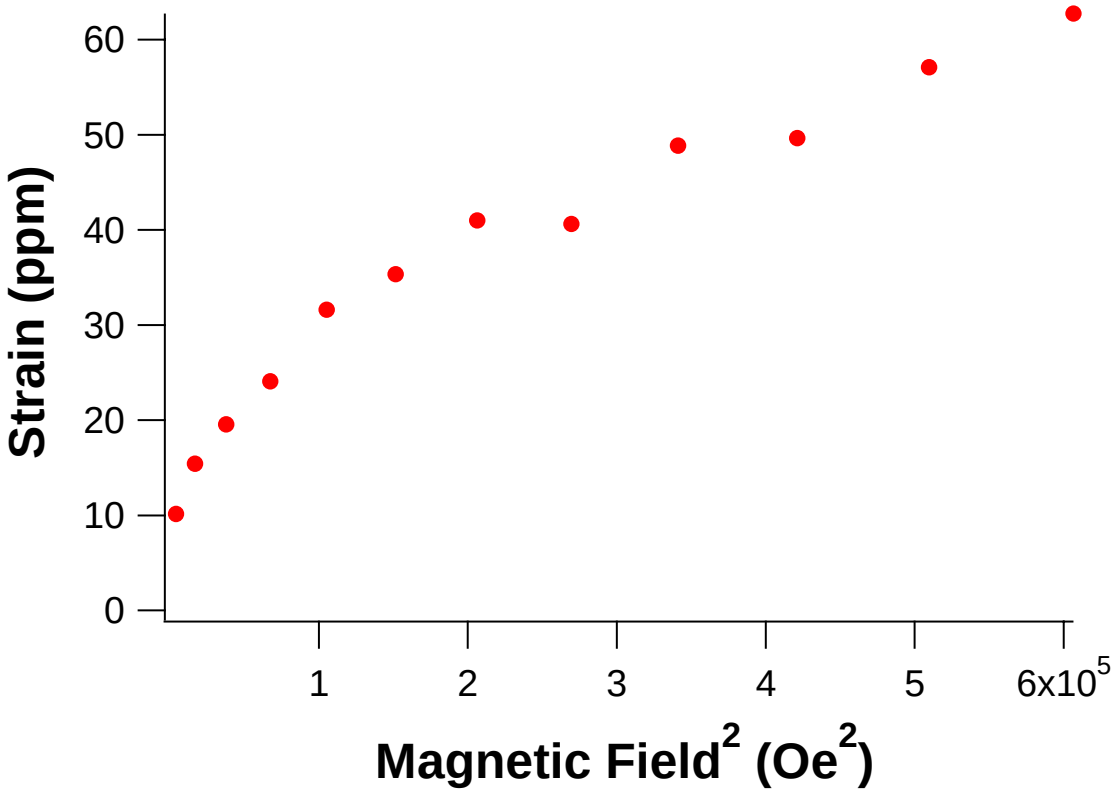

Figure 50. The initial slope of this line is much sharper for samples of nanosized magnetic particles based in part on their increased low field suseptability.

The shape of the data in figure 50 is also interesting. While the behavior of the micron scale composites could be crudely approximated as linear, this plot has a much stronger curve. This can be explained by the high low field response of superparamagnetic particles, which typically have a much higher susceptibility than micron scale particles. Going to a higher saturation magnetization material could yield very interesting magnetostrictive nanocomposites with excellent low field responses.

Still there remains the question of the decrease in modulus and magnetostriction when nanoparticles and micron particles are combined. Since we have established that the nanoparticles can be fashioned into magnetostrictive elastomers it is clearly not some inherent property of the nanoparticles, but a question of the structure of the hybrid composite. A reasonable explanation of both the modulus and magnetostriction depression would be the creation of a structure where nanoparticles are drawn into the gaps between micron scale particles, where the magnetic field is concentrated. High

concentrations of nanoparticles could lead to poor adhesion to the matrix. If adhesion is poor, then instead of acting as a high modulus inclusion, the nanoparticles could cause delamination where the delaminated area acts as a bubble (a low modulus inclusion). Predicting how this concentration of nanoparticles in the gaps would effect magnetostriction is not trivial, but it seems feasible that it would cause the noted decrease.

While we have some plausible theories as to what is causing the unexpected behavior of the hybrid micro-nano composites, more study is required to understand the physical underpinnings. We have a great deal of data on these system, shown in tables 3-8, and we will continue our attempts to understand this data.

Table 3. Measured strain in hybrid micro/nano magnetostrictive composites as a function of field and prestress. This composite contained 20% microparticles and 0% nanoparticles by volume.

Field^2 (Oe^2)	**0.28 psi prestress**	**1.25 psi prestress**	**3.38 psi prestress**	**7.35 psi prestress**	**13.70 psi prestress**
4212.01	9.4051	11.2861	21.8198	44.0159	19.9388
16848.04	18.0578	40.2538	93.6748	126.781	102.327
37908.09	46.2731	74.1122	191.864	267.481	211.803
67392.16	61.3213	101.575	291.182	431.506	361.908
105300.3	89.1604	129.038	368.303	604.184	547.377
151632.4	139.572	156.501	441.287	651.324	746.477
206388.5	230.237	210.674	600.422	1035.28	881.834
269568.6	317.817	221.208	649.328	1178.01	1119.04
341172.8	391.625	231.742	699.74	1326.77	1407.85
421201	499.223	246.414	704.918	1445.38	1631.66
509653.2	585.373	258.452	726.91	1612.23	1906.4
606529.4	670.396	284.786	790.032	1689.82	2077.27

Table 4. Measured strain in hybrid micro/nano magnetostrictive composites as a function of field and prestress. This composite contained 20% microparticles and 3% nanoparticles by volume.

Field^2 (Oe^2)	**0.28 psi prestress**	**1.25 psi prestress**	**3.38 psi prestress**	**7.35 psi prestress**	**13.70 psi prestress**
4212.01	0	7.90028	13.9195	15.4244	33.106
16848.04	13.9195	18.434	39.1252	45.1445	115.495
37908.09	23.3246	40.2538	81.2601	93.6748	211.803
67392.16	25.5819	68.8453	124.9	150.105	351.751

105300.3	42.8873	89.5366	167.787	236.256	519.538
151632.4	46.2731	108.723	221.584	303.597	668.138
206388.5	63.5785	129.038	267.481	425.487	849.67
269568.6	70.7264	149.353	312.249	498.094	1059.41
341172.8	79.3791	164.025	359.275	580.483	1169.97
421201	96.3082	179.073	404.796	672.653	1427.95
509653.2	116.999	192.616	439.783	907.297	1581.4
606529.4	141.829	208.041	476.651	948.843	1796.5

Table 5. Measured strain in hybrid micro/nano magnetostrictive composites as a function of field and prestress. This composite contained 20% microparticles and 5% nanoparticles by volume.

Field^2 (Oe^2)	**0.28 psi prestress**	**1.25 psi prestress**	**3.38 psi prestress**	**7.35 psi prestress**	**13.70 psi prestress**
4212.01	10.1575	10.9099	11.2861	15.0482	25.5819
16848.04	12.7909	21.0674	39.1252	49.2827	84.6459
37908.09	18.8102	38.3728	67.7167	94.051	210.674
67392.16	39.8776	59.4402	114.366	151.234	346.86
105300.3	49.6589	79.3791	168.916	216.317	499.599
151632.4	59.4402	101.199	197.883	283.658	634.656
206388.5	69.2215	125.652	240.394	360.78	930.751
269568.6	80.8839	137.691	293.439	445.802	994.409
341172.8	93.6748	158.382	333.317	525.557	1214.2
421201	105.337	170.044	369.809	623.37	1405.17
509653.2	112.109	185.469	420.596	676.039	1614.91
606529.4	116.623	196.379	445.049	874.463	1767.02

Table 6. Measured strain in hybrid micro/nano magnetostrictive composites as a function of field and prestress. This composite contained 20% microparticles and 7% nanoparticles by volume.

Field^2 (Oe^2)	**0.28 psi prestress**	**1.25 psi prestress**	**3.38 psi prestress**	**7.35 psi prestress**	**13.70 psi prestress**
4212.01	13.1671	4.89065	30.81	26.3343	18.0578
16848.04	19.1864	16.1768	91.79	82.3887	78.6266
37908.09	21.4436	29.7201	165.15	177.192	171.549
67392.16	33.8584	36.1156	225.72	288.172	288.925
105300.3	39.1252	50.7875	287.796	428.873	423.606
151632.4	49.6589	51.1637	358.899	529.697	555.277
206388.5	51.9162	101.575	395.767	671.9	662.119
269568.6	62.4499	115.118	442.792	731.735	838.279
341172.8	80.9779	124.147	495.084	897.179	1018.53
421201	83.5173	128.662	511.261	1001.71	1150.54

509653.2	110.228	138.819	533.834	1060.73	1332.13
606529.4	117.752	141.077	561.673	1138.48	1530.48

Table 7. Measured strain in hybrid micro/nano magnetostrictive composites as a function of field and prestress. This composite contained 20% microparticles and 9% nanoparticles by volume.

Field^2 (Oe^2)	**0.28 psi prestress**	**1.25 psi prestress**	**3.38 psi prestress**	**7.35 psi prestress**	**13.70 psi prestress**
4212.01	18.3964	15.8006	25.5819	31.6011	22.9484
16848.04	38.3728	49.2827	105.337	119.633	87.6555
37908.09	65.0833	81.6363	170.42	239.266	196.755
67392.16	86.5269	115.495	257.324	382.223	292.687
105300.3	116.247	143.334	345.355	509.004	443.921
151632.4	139.948	167.035	405.172	646.319	598.917
206388.5	152.739	187.35	486.056	832.248	873.793
269568.6	186.973	209.169	543.239	956.214	983.687
341172.8	208.417	226.475	586.502	1055.39	1153.22
421201	232.118	237.761	621.489	1157.91	1358.27
509653.2	259.957	257.324	652.338	1255.07	1489.6
606529.4	299.082	266.352	694.473	1454.09	1717.43

Table 8. Measured strain in hybrid micro/nano magnetostrictive composites as a function of field and prestress. This composite, prepared as a control, contained 0% microparticles and 9% nanoparticles by volume.

Field^2 (Oe^2)	**0.28 psi prestress**	**1.25 psi prestress**	**3.38 psi prestress**	**7.35 psi prestress**	**13.70 psi prestress**
4212.01	3.11	7.44884	11.9633	3.38584	10.1575
16848.04	9.03	10.533	14.2205	8.27645	15.42
37908.09	12.41	10.533	15.4246	12.4147	19.56
67392.16	15.8	14.672	19.1864	18.3964	24.07
105300.3	15.8	19.525	24.378	21.4436	31.6
151632.4	17.61	20.315	22.9108	21.8198	35.36
206388.5	22.57	23.2494	30.0211	25.2053	41
269568.6	18.9	24.378	27.7639	28.2153	40.63
341172.8	28.55	24.8295	33.0683	34.2342	48.8689
421201	30.02	30.0888	29.3439	36.4914	49.6589
509653.2	30.47	26.2967	29.7197	39.84	57.1078
606529.4	35.33	27.8383	30.4725	43.2258	62.7508

CONCLUSIONS

We have shown that the magnetostriction of field-structured magnetoelastomers is extremely dependent upon the structure of the particle agglomerates. In increasing order of response are biaxial composites, random composites, uniaxial composites, and triaxial composites formed by heterodyning with a field bias. Magnetostrictions of up to 10,000 ppm have been demonstrated, as have modulus enhancements of 2000 kPa. We have shown that even for high aspect ratio samples demagnetizing field corrections can be important, and have identified a torque instability in samples formed in biaxial fields. Finally, we have shown that there is a possibility of particle clumping transitions in these composites, and have shown how this transition depends on field, gel modulus, and sample strain. A future challenge is to understand precisely why the observed sample contraction increases linearly with sample prestrain.

ACKNOWLEDGEMENTS

Sandia is a multiprogram laboratory operated by Sandia Corporation, a Lockheed Martin Company for the United States Department of Energy's National Nuclear Security Administration under contract DE-AC04-94AL85000. This work supported by the Sandia National Laboratories Laboratory Directed Research and Development funds. The authors thank Todd Monson and Paula Provencio for the TEM images, Eugene Venturini for SQUID measurements, Brad Butler and Eric Fish for synthesis and magnetostriction data collection.

REFERENCES

1. M.R. Jolly, J.D. Carlson, B.C. Munoz and T.A. Bullions, *J. Intell. Mat. Sys. and Struc.* **7**, 613-622 (1996).
2. J. D. Carlson and M. R. Jolly, MR fluid, foam, and elastomer devices, *Mechatronics*, **10**, 555-569 (2000).
3. J. Ginder, S. Clark, W. Sclhotter, M. Nichols, Int. J. Mod. Phys. B **16**, 2412 (2002).
4. G. Bossis, E. Coquelle, and P. Kuzhir, Annales de Chimie (Science des Materiaux); Nov.-Dec. 2004; vol.29, no.6, p.43-54.
5. J. A. Osborn, Phys. Rev. **67**, 351 (1946).
6. Shape effect can be minimized by using elongated samples, incorporating the sample into a close-fitting solenoid, using the material to complete a reluctance circuit, etc.
7. This field enhancement can be computed in several ways. The simplest is to sum the field due to the dipoles in a needle-like cavity aligned with the field, which avoids cavity field issues.
8. A particle in a nonuniform field, perhaps created by vicinal particles, will also exhibit multipolar moments.
9. J. E. Martin and R. A. Anderson, *J. Chem. Phys.* **111**, 4273-4280 (1999). This paper is written in the language of electrostriction, an isomorphic problem.
10. J.E. Martin, R. A. Anderson and R. L. Williamson, *J. Chem. Phys.* **118** 1557 (2003).
11. J. E. Martin, E. Venturini, J. Odinek, and R. A. Anderson, *Phys. Rev. E* **61**, 2818-2830 (2000).
12. J. E. Martin, E. Venturini, G. Gulley, and J. Williamson, *Phys. Rev. E* **69**, 021508 (2004).
13. Divide by 4π to convert cgs or Gaussian units.
14. United States Patent #6,194,769 BI Issued "*Sensor devices comprising field structured composites*," J. E. Martin, R. C. Hughes, and R. A. Anderson, Feb. 27, 2001.
15. J. E. Martin, R. A. Anderson, J. Odinek, D. Adolf and J. Williamson, *Phys. Rev. B* **67** 94207-1 to 11 (2003).
16. T. Smith, D. Wychick, *J. Phys. Chem.* **1980**, *84*, 1621-1629.

17. C. Griffiths, M. Ohoro, T. Smith, *J. Appl. Phys.* **1979**, *50*,7108-7115.

18. Park, J.; An, K.; Hwang, Y.; Park, J-E.; Noh, H-J.; Kim, J-Y.; Park, J-H.; Hwang, N-M.; Hyeon, T. "Ultra large synthesis of monodisperse nanocrystals" *Nature Materials* **2004**, *3*, 891-895

19. Sahoo, Y.; Goodarzi, A.; Swihart, M. T.; Ohulchanskyy, T. Y.; Kaur, N.; Furlani, E. P.; Prasad, P. N. "Aqueous Ferrofluid of Magnetite Nanoparticles: Fluorescence Labeling and Magnetophoretic Control" *J. Phys. Chem. B.* **2005**, *109*, 3879-3885.

Distribution

2	MS1415	Dale L. Huber	01112
2	MS1415	Jim E. Martin	01112
2	MS0888	Robert A. Anderson	01821
1	MS1415	Douglas H. Read	01112
2	MS1415	Benjamin L. Frankamp	01112
1	MS1415	D. Peebles	01112
1	MS1427	J. Phillips	01100
2	MS9018	Central Technical Files	8945-1
2	MS0899	Technical Library	4536
2	MS0123	D. Chavez, LDRD Office	1011

Sandia National Laboratories